SYNTHESIS AND CHARACTERIZATION OF NOVEL-MIXED-METAL-ORTHOBORATES

ESRA GÜL

FEBRUARY 2013

SYNTHESIS AND CHARACTERIZATION OF NOVEL-MIXED-METAL-ORTHOBORATES

by
ESRA GÜL

THESIS SUBMITTED TO
THE GRADUATE SCHOOL OF NATURAL AND APPLIED SCIENCES
OF
THE ABANT İZZET BAYSAL UNIVERSITY
IN PARTIAL FULFILLMENT OF THE REQUIREMENTS FOR THE DEGREE
OF
MASTER OF SCIENCE
IN
THE DEPARTMENT OF CHEMISTRY

FEBRUARY 2013

Approval of the Graduate School of Natural and Applied Sciences

Prof. Dr. Yaşar DÜRÜST
Director

I certify that this thesis satisfies all the requirements as a thesis for the degree of Master of Science.

Prof. Dr. Çetin BOZKURT
Head of Department

This is to certify that we have read this thesis and that in our opinion it is fully adequate, in scope and quality, as a thesis for the degree of Master of Science.

Prof. Dr. Ayşe MORKAN
Supervisor

Examining Committee Members

1- Prof. Dr. Ceyhan KAYRAN .....

2- Prof. Dr. Nilgün ÖZPOZAN .....

3- Prof. Dr. Ayşe MORKAN .....

ABSTRACT

SYNTHESIS AND CHARACTERIZATION OF NOVEL-MIXED-METAL- ORTHOBORATES

GÜL, Esra
Master of Science, Department of Chemistry
Supervisor: Prof. Dr. Ayşe MORKAN

February 2013, 92 pages

In this study, magnesium orthoborate and novel-mixed-metal orthoborates were synthesized by high temperature solid state reaction method and the characterization of products were examined by powder X-ray Diffraction (XRD), Fourier Transform Infrared Spectroscopy (FTIR), Scanning Electron Microscopy (SEM), and Thermogravimetric/Differential Thermal Analysis (TG/DTA) methods.

In the first part of this study, magnesium orthoborate, $Mg_3(BO_3)_2$, was synthesized using different magnesium sources, MgO, $MgCO_3$, $MgSO_4$, by conventional ceramic method. It was found that the magnesium orthoborate with the highest purity was prepared from the $MgSO_4$.

In the second part of this study, different amounts of manganese (II) ion were doped to magnesium, cobalt and nickel orthoborate to obtain novel-mixed-metal

orthoborate compounds, at the formula $M_{3-x}Mn_x(BO_3)_2$ (M = Mg, Co, Ni; $0 \leq x \leq 0.10$).

All these compounds obtained were indexed in the orthorhombic crystal system and their unit cell parameters refined by Jana2006 are given as follows;

For magnesium manganese orthoborates, $Mg_{3-x}Mn_x(BO_3)_2$ ($0 \leq x \leq 0.10$),

$Mg_{2.99}Mn_{0.01}(BO_3)_2$: a= 5.406(3), b= 8.430(4), c= 4.508(4),

$Mg_{2.95}Mn_{0.05}(BO_3)_2$: a= 5.410(4), b= 8.436(2), c= 4.507(8),

$Mg_{2.90}Mn_{0.1}(BO_3)_2$: a= 5.144(4), b= 8.444(3), c= 4.512(0) Å;

For cobalt manganese orthoborates, $Co_{3-x}Mn_x(BO_3)_2$ ($0 \leq x \leq 0.10$),

$Co_{2.99}Mn_{0.01}(BO_3)_2$: a= 5.469(7), b= 8.451(2), c= 4.533(5),

$Co_{2.95}Mn_{0.05}(BO_3)_2$: a= 5.469(9), b= 8.452(8), c= 4.533(8),

$Co_{2.90}Mn_{0.1}(BO_3)_2$: a= 4.483(4), b= 8.476(4), c= 4.538(4) Å;

For nickel manganese orthoborates, $Ni_{3-x}Mn_x(BO_3)_2$ ($0 \leq x \leq 0.10$),

$Ni_{2.99}Mn_{0.01}(BO_3)_2$: a = 5.397(4), b= 8.301(8), c= 4.458(9),

$Ni_{2.95}Mn_{0.05}(BO_3)_2$: a= 5.403(6), b= 8.311(6), c= 4.463(3),

$Ni_{2.50}Mn_{0.50}(BO_3)_2$: a= 5.405(8),b= 8.313(3), c= 4.465(2) Å.

It was determined that all these compounds were found isostructural with kotoite type of borates, $M_3(BO_3)_2$ (M= Mg, Ni, Co).

The IR study showed that these borates have the BO_3 units in planar triangles. Besides, SEM images showed that these compounds were homogeneus. It was also detected that these orthoborates prepared were thermodynamically stable in the temperature range of 20-1200 ^oC by TG/DTA method.

Keywords: Mixed-Metal Orthoborate, Kotoite, Mn (II) doped borate, XRD, FTIR, TG/DTA, SEM.

ÖZET

YENİ KARMA-METAL-ORTOBORATLARIN SENTEZİ VE KARAKTERİZASYONU

GÜL, Esra
Yüksek Lisans, Kimya Bölümü
Tez danışmanı: Prof. Dr. Ayşe MORKAN

Şubat 2013, 92 sayfa

Bu çalışmada, magnezyum ortoborat ve karma metal ortoboratlar yüksek sıcaklık katı hal yöntemi ile sentezlenmiş ve bu ürünlerin karakterizasyonu X-ışını Kırınımı (XRD), Kızılötesi spekturumu (FTIR), Taramalı Elektron Microskopu (SEM), ve Termogravimetrik analiz-difransiyal ısısal analiz (TG/DTA) gibi yöntemlerle karşılaştırmalı olarak incelenmiştir.

Bu çalışmanın ilk bölümünde, magnezyum metal ortoboratı, $Mg_3(BO_3)_2$, MgO, $MgCO_3$, $MgSO_4$ gibi farklı magnezyum kaynakları kullanılarak sentezlenmiştir. Yüksek saflıkta magnezyum borat, magnezyum kaynağı olarak $MgSO_4$ kullanılmasıyla elde edildiği bulunmuştur.

Bu çalışmanın ikinci bölümünde, $M_{3-x}Mn_x(BO_3)_2$ (M = Ni, Mg, Co; $0 \leq x \leq 0.10$) formülünde yeni karma metal ortoboratlar elde etmek için magnezyum, nikel ve cobalt ortoborat'a değişik oranlarda mangan (II) katkılanmıştır.

Bu reaksiyonlardan elde edilen ürünlerin tamamı ortorombik kristal sistemde indekslenmiştir ve birim hücre boyutları Jana2006 kullanılarak aşağıda gösterildiği gibi hesaplanmıştır.

Magnezyum mangan ortoborat $Mg_{3-x}Mn_x(BO_3)_2$ ($0 \leq x \leq 0.10$), için,

$Mg_{2.99}Mn_{0.01}(BO_3)_2$: a= 5.406(3), b= 8.430(4), c= 4.508(4),

$Mg_{2.95}Mn_{0.05}(BO_3)_2$: a= 5.410(4), b= 8.436(2), c= 4.507(8),

$Mg_{2.90}Mn_{0.1}(BO_3)_2$: a= 5.144(4), b= 8.444(3), c= 4.512(0) Å;

Cobalt mangan ortoborat, $Co_{3-x}Mn_x(BO_3)_2$ ($0 \leq x \leq 0.10$), için,

$Co_{2.99}Mn_{0.01}(BO_3)_2$: a= 5.469(7), b= 8.451(2), c= 4.533(5),

$Co_{2.95}Mn_{0.05}(BO_3)_2$: a= 5.469(9), b= 8.452(8), c= 4.533(8),

$Co_{2.90}Mn_{0.1}(BO_3)_2$: a= 4.483(4), b= 8.476(4), c= 4.538(4) Å;

Nikel mangan ortoborat, $Ni_{3-x}Mn_x(BO_3)_2$ ($0 \leq x \leq 0.10$), için,

$Ni_{2.99}Mn_{0.01}(BO_3)_2$: a = 5.397(4), b= 8.301(8), c= 4.458(9),

$Ni_{2.95}Mn_{0.05}(BO_3)_2$: a= 5.403(6), b= 8.311(6), c= 4.463(3),

$Ni_{2.50}Mn_{0.50}(BO_3)_2$: a= 5.405(8),b= 8.313(3), c= 4.465(2) Å.

Bu elde edilen bileşiklerinin tamamının kotoit tipindeki boratlarla izomorf olduğu belirlenmiştir.

IR çalışmaları sentezlenen boratların üçgen düzlem BO_3 birimine sahip olduklarını göstermiştir. Ayrıca bileşiklerin homojen oldukları SEM analizi ile belirlendi. Ayrıca, Bu ortoboratların 20-1200^oC sıcaklıkları arasında termodinamik olarak kararlı oldukları TG/DTA yöntemyle belirlenmiştir.

Anahtar Kelimeler: Karma Metal Ortoborat, Kotoit, Boratlara Mn(II) katkılanması, XRD, FTIR, TG/DTA, SEM.

To My Family…

ACKNOWLEDGEMENT

I would like to express my deep gratitude to Professor Dr. Ayşe MORKAN, my research supervisor, for her professional guidance, enthusiastic encouragement useful critiques and constructive suggestions during the planning and development of this research work. Her willingness to give her time so generously has been very much appreciated.

I would also like to extend my thanks to Prof. Dr. İzzet MORKAN, moral support and encouragement all the time.

I would like thank to Prof. Dr. Ahmet VARİLCİ and Uzm. Nevin SOYLU for providing and informing SEM analysis.

Especially, I would like thank to Gülden ÖZEN KAHVECİ and Seda TANYILDIZI for their helps.

Finally, honorable mention goes to my parents Abdullah Sadettin GÜL and Melek GÜL, other members of my family, İlknur GÜL, İlker GÜL and Halime GÜL especially little member Mehmet Enes GÜL for their understandings and supports on me in completing this project. Without helps of the particular that mentioned above, I would face many difficulties while doing this. Also, I express a sense of gratitude and love to my friends Besra ÖZER and Nesibe AVAN for their manual support, strength, help and for everything.

LIST OF ABBREVATIONS

XRD	X-ray Diffraction Spectroscopy
FTIR	Foruier-Transform Infrared Spectroscopy
ICDD	International Centre For Diffraction Data
SEM	Scanning Electron Microscope
EDX	Energy Dispersive X-ray Analysis

TABLE OF CONTENTS

LIST OF TABLES

TABLE

LIST OF FIGURES

FIGURE

CHAPTER I

INTRODUCTION

1.1. BORON

Boron is a unique and exciting element. Over the years it has proved a constant challenge and stimulus not only to preparative chemists and theoreticians, but also to industrial chemists and technologists. Boron is found in Group 13 of the periodic table. The atomic number and relative atomic mass of boron are 5 and 10.81 amu, respectively. There are two stable isotopes of boron, which are ^{10}B and ^{11}B distiributed as 19.78% and 80.22%, respectively in nature. Elemental boron, which finds as a solid at room temperature, is black monoclinic crystal. If it is impure solid, it finds yellow or brown amourphous powder. Although boron crystals are too hard, they are easily broken. It is a metaloid (i.e., semimetal), in other words, it finds between metal and nonmetal elements. For this reason, it has some of characteristics properties like metal and nonmetal. For instance; it shows many similarities to its nonmetal neighbours, carbon and silicon, like a marked propensity to form covalent and molecular compounds, but it differs sharply from them in having one less valence electron. This situation sometimes has referred as "electron deficiency", which has a dominant effect on its chemistry. In addition to these, boron gives reaction with other chemicals, by heat treatments since

it is extremely stable at low temperatures [1-5].

1.1.1. History of Boron

Compounds of boron probably have been used for nearly sixty thousand years, eventhough pure boron was not discovered until 1808. At a lot of countries, such as Egypt, China, Tibet and Arabia, using of such compounds are established in their daily life in ancient times [6].

The first civilization in China and the Middle East used borax for different kinds of aims, despite of rare. Goldsmiths and Silversmiths melted borax used as a flux, which is a substance that removes unwanted impurities from metals. Civilization continued to use borax in the same way until end of eighteeth century. They discovered new resources of borax in the beginning of nineteenth century. As a consequence, borax became less expensive, and scientist started to study of the chemistry of boron compounds [5].

Also, French chemists, who are Joseph-Louis Gay-Lussac and Louis-Jacques Thénard, and English chemist, Humphry Davy, isolated independently elemental boron by reducing boron trioxide with potassium and by electrolysis with boric acid, but their compound was impure form (almost 50%) [7].

1.1.2. Boron Minerals and Reserves

Athough elemantal boron do not found in pure form on Earth, there are approximetly 250 different natural boron compounds, in the form of inorganic borates called as mineral. Table 1.1 gives commonly used some boron minerals

worldwide. These minerals are commercially important, though more than 200 minerals contain boron.

Common minerals, such as tourmaline which is the most abundant boron mineral, also contain boron, but have no economic potential because the boron content is usually very small about 10%.

Table 1.1 Commonly Used Boron Minerals Worldwide [8]

Mineral	**Formula**	**B_2O_3 (%)**	**Regions of mineral**
Kernite (Rasortie)	$Na_2B_4O_7.4H_2O$	51.0	Kırka, USA, and Argentina
Pandermite (Priceite)	$CaB_{10}O_{19}.7H_2O$	49.8	Sultançayır and Bigadiç
Ulexite (Boronatrocalcite)	$NaCa\ B_5O_9.8H_2O$	43.0	Kırka, Bigadiç, Emet, and Argentina
Colemanite	$Ca_2B_6O_{11}.5H_2O$	50.8	Emet, Bigadiç, Küçükler, and USA
Probertite (Kramerite)	$NaCaB_5O_9.5H_2O$	49.6	Kestelek, Emet, and USA
Szaibelyite (Ascharite)	$MgBO_2.2H_2O$	41.4	Russia
Boraxs (Tincal)	$Na_2B_4O_7.10H_2O$	36.6	Kırka, Emet, Bigadiç, and USA
Boracite (Stassfurite)	$Mg_6B_{14}O_{26}C_{12}$	62.2	Germany
Hydroboracite	$CaMgB_6O_{11}.6H_2O$	50.5	Emet

Boron is a commonly existing element in the earth, in soil, rocks and water. Boron minerals occur mostly as borates which are deposited from volcanic gases or hot springs near volcanic activities, and current borates reserves of world are given Figure 1.1. Boron reserves having high concentration and economical extent are found mostly in Turkey and in arid, volcanic and high hydrothermal activity regions of U.S. as compounds of boron attached to oxygen. The largest boron reserves in the world are located in Emet, Kırka, Bigadiç regions of Turkey and in California, USA [10]. World boron reserves are given Table 1.2 and Turkey boron reserves are given Table 1.2.

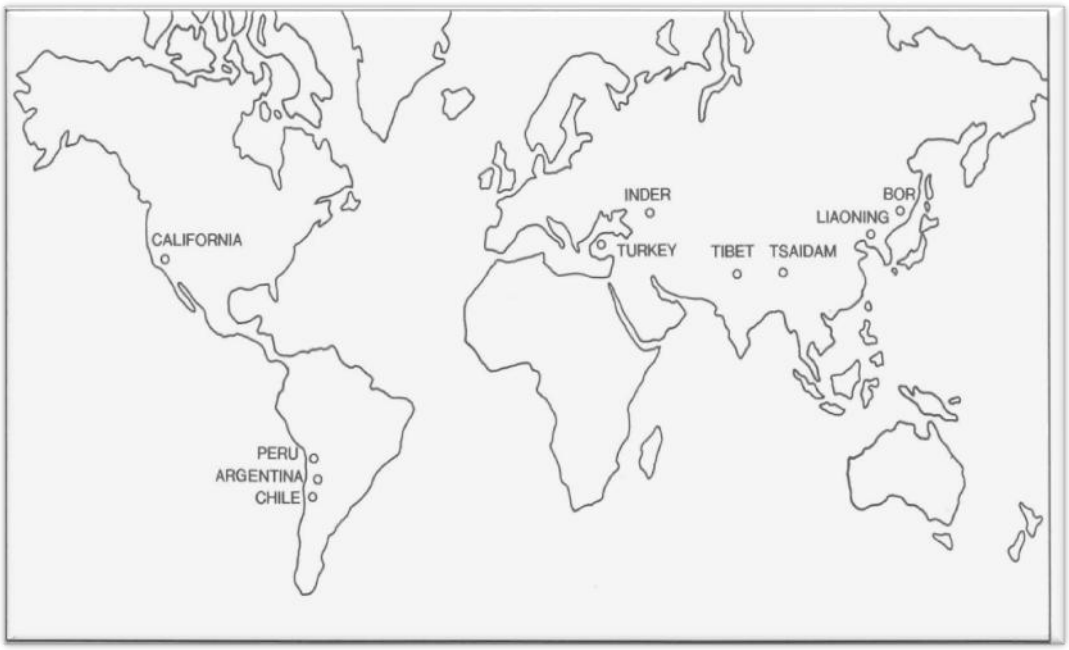

Figure 1.1 Current world sources of borates. [9]

Table 1.2 The world boron reserves (million metric tons) [11]

County Name	**Region and type**	**Total Ore**	**Contained B_2O_3**	**B_2O_3 Reserve**	**B_2O_3 Reserve Base**	**B_2O_3 Total Reserve**
Turkey	Bigadiç-Balikesir (Ca-NaCa types)	935	330	(1030-360)	624	851
	Emet-Kütahya (Ca-type)	545	200	(890-310)		
	Kestelek (Ca-type)	7	3	(8-3)		
	Kırka (Na-type)	520	140	(519-130)		
	Subtotal	2007	673	227		
USA	Boron-(Na-type)	113	26			
	(Ca-type)	198	20			
	Subtotal	311	46			
	Searles Lake, Death Valley, Hector, Owens Lake, Salton Sea, Four Corners, Muddy Mountains, etc.	255	77	40	40	80
	Subtotal	566	123			
Russia	Dalnegorsk, etc.	700	64	40	60	100
China	Liaoning, etc.	480	65	27	9	36
Mexico	Mesa del Amo, Vitro,Tubutama, etc.	140	13.5	-	-	-
Argentina	Loma Blanca, Sijes, Tincalayu, Salars, etc.	100	20.5	2	7	9

Table 1.2 The world boron reserves (million metric tons) (continue)

Chile	Surire, Atacama, etc.	60	76	8	33	41
Serbia	Jarandol, Raska, etc.	40	8	3	-	3
Kazakhstan	Inder, Satimola, etc.	77	5	14	1	15
Bolivia	Salars, Uyuni, etc.	20	15	4	15	19
Peru	Salars de Salinas, etc.	20	5	4	18	22
Others	Iran, Germany, etc.	100	10			
General	Total	4310	1078	369	807	1176

1.1.3. Utilization Area of Boron

As boron compounds have been used for thousands of years for different purposes, there are very range application area of compounds of boron; glass [12], ceramic [13], cleaning and bleaching [14], flame retardant [15], agriculture [16], metallurgy [17], nuclear applications [18], boron fibers [19], aerospace [20], energy [21], health [22], cement [23]. Table 1.3 gives important boron products and their utilization areas.

Table 1.3 Important boron products and their utilization areas [24]

Product	**Utilization Areas**
Colemanite	Textile quality fiberglass, Boron alloys, metallurgical slag formation agent
Ulexite and Probertite	Isolation fiberglass, Borosilicate glass, antiseptics, boron alloys,nuclear reactors, fire retarder, nylone, photography, textile, fertilizer, catalyst, glass, fiber glass, enamel, glaze
Anhydrous Borax	Fertilizer, glass, fiberglass, metallurgical slag former, enamel glaze, fire retarder
Sodium Perborate	Detergent and whiteness, textile
Sodium Metaborate	Detergent, agricultural medicine, photography, textile
Sodium Pentaborate	Fire retarder, fertilizer
Boric Acid	Glass, ceramic, glass fibre, as industrial and antiseptic use
Amorphous and Cyrstalline Boron Element	Military purpose, nuclear weapons and protector in nuclear reactors
Sodium Boron Hydride	Cleaning of metal surfaces, paper whitener and special chemical refining
Boron Alloys	Surface hardening of nucleus
Boron Nitride	Cubical boron nitride cutting tools in place of diamond
Boron Carbide	Abrasive material, manufacture of special hard protecting material and nuclear reactors
Boron Flammable	Composites for Aerospace, composites for sporting material
Boron Halides	Medicine Industry, catalysts, electronic pieces, boron filaments and fiber optics
Boron Esthers	Catalysts for polymerization reactions, fire retarder
Special Sodium Borates	Chemicals for photography, adhesives, textile, “finishing” compounds, materials of detergency and cleaning, fire retarder, fertilizer and agricultural medicines

1.2. BORATES

Borates are defined as minerals containing boric oxide or boron-oxygen molecules. These can generally be expressed on the basis of B_2O_3 in combination with a major cation [25]. According to Carpeni, borates are classified in three group: ortho- or metaborates, tetraborates and pentaborates, shown in Fig.1.2. The classification was made according to the number of boron atoms in the anion and according to the basicity of the anion [26].

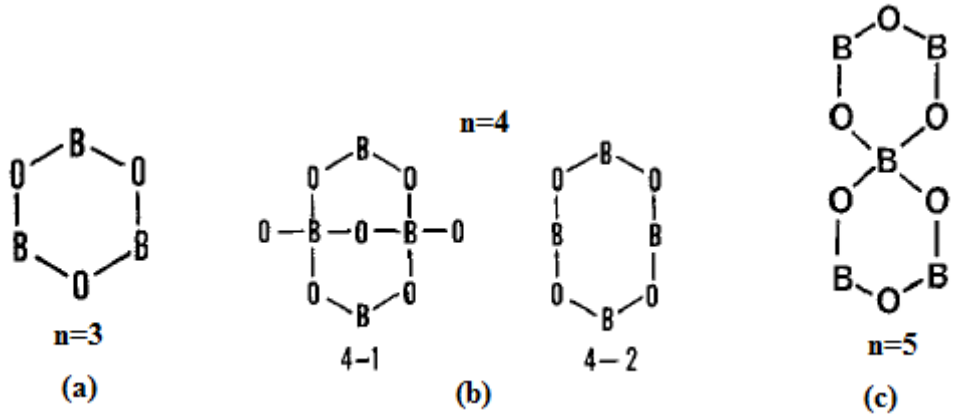

Figure 1.2 Structure of a) metaborate, b) tetraborate, c) pentaborate [27]

Borates are known in which the structural unit is mononuclear (1 B atom), bi-, tri-, tetra- or pentanuclear, or in which there are polydimensional networks including glasses. The main structural principles underlying the bonding in crystalline metal borates are as follows [1]:

1. Boron can link either three oxygens to form a triangle, BO_3, or four oxygens to form a tetrahedron, BO_4.

2. Polynuclear anions are formed by cornersharing only of boron-oxygen triangles and tetrahedra in such a manner that a compact insular group results.
3. In the hydrated borates, protonatable oxygen atoms will be protonated in the following sequence: available protons are first assigned to free O^{2-} ions to convert these to free OH^- ions; additional protons are assigned to tetrahedral oxygens in the borate ion, and then to triangular oxygens in the borate ion; finally any remaining protons are assigned to free OH^- ions to form H_2O molecules.
4. The hydrated insular groups may polymerize in various ways by splitting out water; this process may be accompanied by the breaking of boron-oxygen bonds within the poly anion framework.
5. Complex borate polyanions may be modified by attachment of an individual side group, such as (but not limited to) an extra borate tetrahedron, an extra borate triangle, 2 linked triangles, an arsenate tetrahedron, and so on.
6. Isolated $B(OH)_3$ groups, or polymers of these, may exist in the presence of other anions.

Examples of minerals and compounds containing monomeric triangular, BO_3^{3-} units are the rare-earth orthoborates $M^{III}BO_3$, the minerals $CaSn^{IV}(BO_3)_2$, kotoite $Mg_3(BO_3)_2$, hambergite and orthoborates, shown in Fig.1.2.a. Binuclear trigonal planar units, $B_2O_5^{4-}$, are found in the pyroborates $Mg_2B_2O_5$, ThB_2O_5, $Co^{II}{}_2B_2O_5$ and $Fe^{II}{}_2B_2O_5$, shown in Fig.1.2.b. Trinuclear chain units, $B_3O_6^{3-}$, are present in $NaBO_2$, KBO_2, metaboric acid, shown in Fig.1.2.c [1].

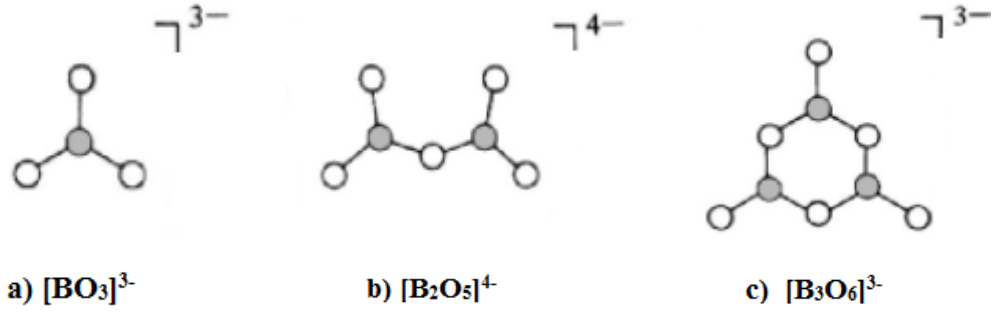

Figure 1.3 Different structure of boron oxygen compounds a) orthoborates, b)pyroborates, c) metaborates

B-O bond distances show wide diversity in different structures like shown in Fig. 1.3, the distance increases with increase in coordination:

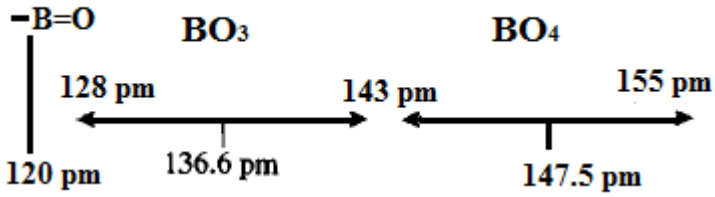

Figure 1.4 The change of bond distances of borates

1.2.1. Orthoborates

The salts in which isolated BO_3^{3-} and BO_4^{-5} ion known as orthoborates, and boron:oxygen ratio is 1:3. Structure of orthoborate resembles with nitrates and carbonates. Generally, orthoborates have MBO_3 molecule structure. At 1968, the structure of some orthoborates like $ScBO_3$, $InBO_3$, $GaBO_3$, $CrBO_3$, $TiBO_3$, VBO_3, which are isostructural with mineral calcite, were described by Waugh [28]. Similarly, rare earth orthoborates, $LnBO_3$, are isomorphous with $CaCO_3$. $LaBO_3$,

dBO_3, $YbBO_3$, $SmBO_3$ crystallize in aragonite, vaterite and calcite forms similar to that of $CaCO_3$ [29].

1.2.2. Metal Orthoborates

Various metal borates, such as lithium borate, beryllium borate, aluminum borate, calcium borate, nickel borate, copper borate, zinc borate, strontium borate, lead borate, barium borate, and magnesium borate have attracted much attention in recent years, due to their potential applications as reinforcements in electronic ceramics, wide band gap semiconductors, antiwear additive, plastics or aluminum/magnesium matrix alloys, luminescent materials, nonlinear optical and laser devices [30]. Owing to unique properties of metal borates, which are their light weight, high strength, high heat resistance, corrosion-resistance etc., metal borates provides distinctive opportunities with discovery and identification of new compounds [31].

Metal orthoborates with the general formula of $M_3B_2O_6$ (M = Ca, Sr, Ni, Mg, Mn, Ba, Cd ,Co, etc.) have been synthesized as an interesting subject of study by many workers (e.g. Weir and Schroeder, 1964; Van der Voort et al., 1992). Among these borates group, to date only $Mg_3B_2O_6$ (kotoite) and $Mn_3B_2O_6$ (jimboite) have been identified in nature, shown in Fig. 1.5 [32].

Ebelmen (1851), Mallard (1887), Le Chatelier (1891), Ouvrard (1901), Guertler (1904) and Hofmann Höschele (1914) have described cobalt and magnesium orthoborate crystals. They pointed out that magnesium and cobalt orthoborates are isomorphous with each other and orthorhombic with a rather perfect cleavage paralel to 110 [33].

Magnesium orthoborate, $Mg_3(BO_3)_2$, which was also discovered by Watanabe (1938), is an uncomon mineral, which included 62.78% of MgO and 35.20% of B_2O_5, typically formed in the contact zone of magnesium rich skarn borate deposites [34]. The mineral is orthorombic with point group: 2/m 2/m 2/m, and the cell data is space group: Pnmn, a = 5.401, b = 8.422, c = 4.507 Å and Z =2 [35].

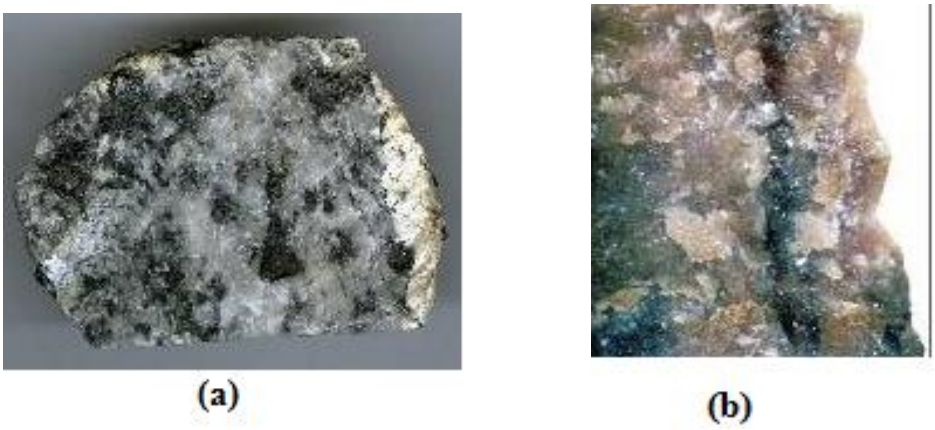

Figure 1.5 a) Kotoite and **b)** Jimboite mineral [34]

The crystal structure of kotoite was simultaneously determined by Sadanga (1948) and Berger (1949). Berger reported that the crystal structure of the isomorphous cobalt and magnesium orthoborates is found with $2Me_3(BO_3)_2$ formula in the orthorhombic system, and BO_3^{3-} triangles unit is the nearly equilateral and $(MeO_6)^{10-}$ is octahedron. As a result of evidence of the existance of BO_3^{3-}, Berger pointed out that the formula must be written as $Me_3(BO_3)_2$ [33].

In the crystal structure of Kotoite, $Mg_3(BO_3)_2$, the Mg atoms are surrounded by an octahedron of oxygen atoms in each crystal, shown in Figure 1.6. Boron atoms

are always surrounded by three oxygens, BO_3, in a triangular configuration and single links BO_3 chains of oxygen octahedra [36].

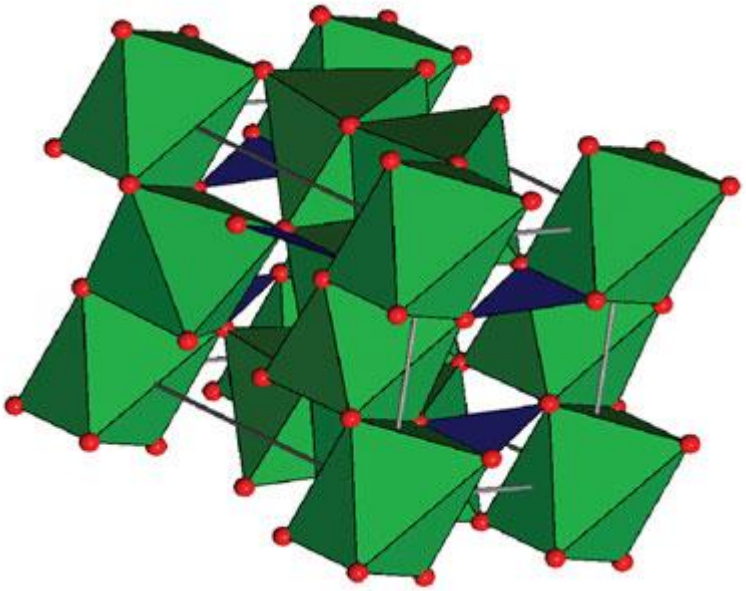

Figure 1.6 The Crystal Structure of Kotoite

Various synthesis methods for the preparation of magnesium borates have been reported thus far, but recent studies focus on nanoscale structure of magnesium borates. Jiang Zhang et al. have synthesized orthorhombic magnesium borate nanobelt, $Mg_3B_2O_6$, by heating mixed powders of boron and MgO under flowing Ar/H_2O gases at 1100 $^{\circ}$C. Typical widths with the nanobelts are in the range of 100–300 nm and lengths are up to tens of micrometers. [37].

Afterwards, magnesium orthoborate, $Mg_3(BO_3)_2$, has been prepared by solid state reactions using microwave and thermal energy at above 600^{o}C for 3hrs [38].

Single-phase $Mg_3B_2O_6$ has been synthesized from using the starting chemials which are stoichiometric MgO and excess of 11 wt.% and 14 wt.% B_2O_3 by high temperature solid state reaction techniques. The mixed starting materials have been

heated 10 hours at 600, 900, 1000, 1100, 1200 ^{o}C, respectively. The ceramic compound, $Mg_3B_2O_6$, has been characterized structurally and dielectrically [39].

Recently, magnesium borate compound, $Mg_3B_2O_6$, has been synthesized from B_2O_3/MgO powder blends by mechanically activated annealing under air. The effects of B_2O_3/MgO mole ratios, milling durations (30 minutes and 1 and 2 hours), annealing durations (2 and 5 hours), and annealing temperatures (973, 1173, and 1273 K (700, 900, and 1000 ^{o}C) on the formation and microstructure of magnesium borate have also been investigated [40].

The mean time, Ray L. Frost and Yunfei Xi have characterised a natural kotoite, obtained from The Mineralogical Research Company, using vibrational specroscopy and assess the structure of the mineral with Raman spectra. They reported that vibration of symmetric stretching mode of tetrahedral boron dominated by very intense band 835 cm^{-1} in raman spectrum. Raman bands of antisymmetric stretching modes of tetrahedral boron were observed at 919, 985 and 1015 cm^{-1} [35].

Manganese orthoborate, $Mn_3(BO_3)_2$, jimboite, also discovered by Watanabe et al. (1963). In 1965, Sadanaga et al. have determined the crystal structure of jimboite, $Mn_3(BO_3)_2$, with the aid of three-dimensional least squares and Fourier syntheses. Manganese orthoborate consists of BO_3^{3-} groups and octahedral coordinations of oxygen ions around manganese ions and is almost isostructural with kotoite having been reported. Aside from the obvious differences between Mn-O and Mg-O distances, the basic features of these two structures are markedly similar to each other as in Fig. 1.7 [41].

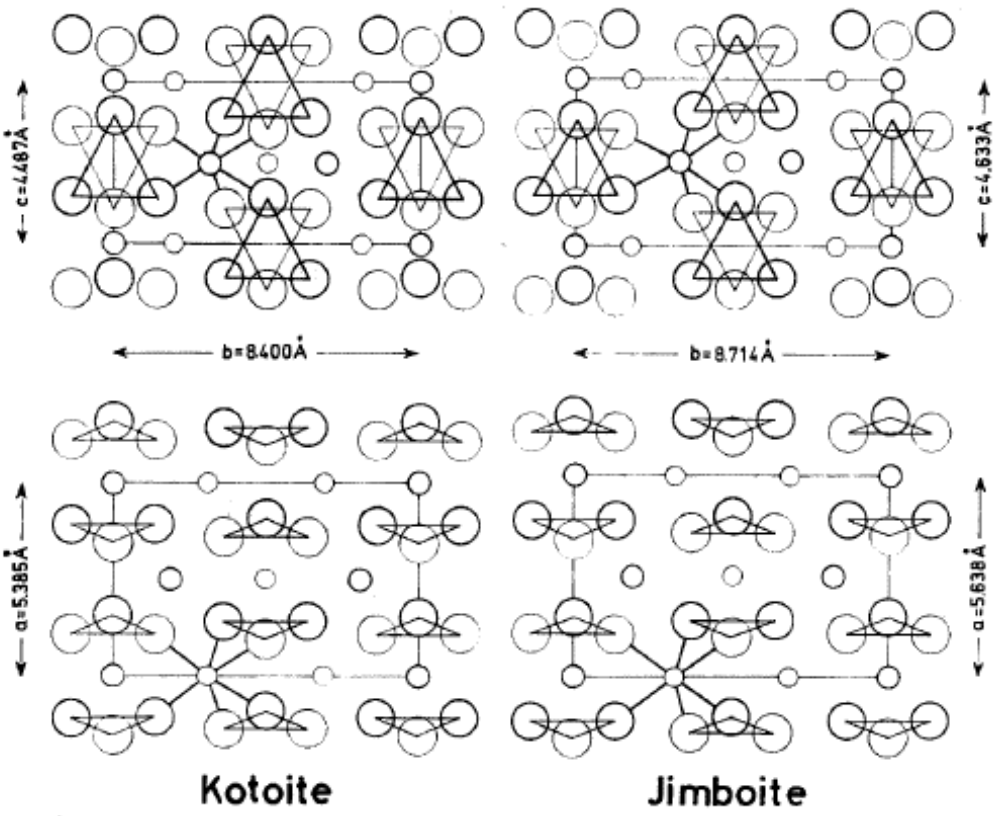

Figure 1.7 Structures of kotoite and jimboite compared [41]

Another metal orthoborate, $Ni_3(BO_3)_2$ has been synthesized with formula $3NiO.B_2O_3$ by Weir & Schroeder. Later, at 1963, Götz has reported that nickel orthoborate, $Ni_3(BO_3)_2$, is isomorphous with cobalt and magnesium orthoborates, but its crystal structure has been clarified with three dimensional Patterson synthesis and, Pardo et al. reported that nickel orthoborate was crystallized in the orthorhombic system with Pnnm space group. Lattice parameters of nickel orthoborates have been found as a=5.396±0.001, b=4.459±0.001 and c=8.297±0.002 Aº from the Weissenberg photograps [42].

Efenberger and Pertlik have determined crytal structure of kotoite type of borates, $M_3(BO_3)_2$ (M= Mg, Co, and Ni), which synthesized from melts, with single

crystal X-ray data and structure of $Mn_3(BO_3)_2$ has been compared with these orthoborates and decided in kotoite type too. [43].

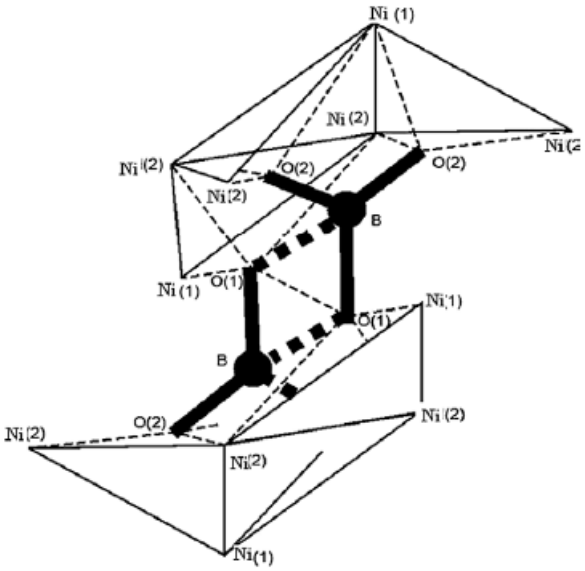

Figure 1.8 Structures of kotoite type $Ni_3(BO_3)_2$ [44]

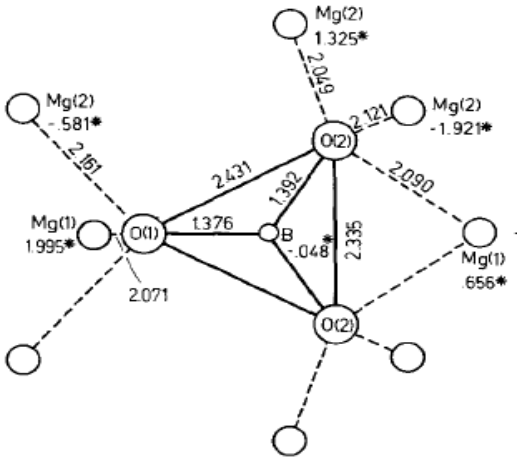

Figure 1.9 Crystal Structure of $Mg_3(BO_3)_2$

The recent studies focuses on the development of a new route for the synthesis of more pure metal borates at low temperatures and in short reaction periods. Menaka et al. reported new route for the synthesis method of $Ni_3(BO_3)_2$.

Monophasic and uniform spherical nanoparticles of nickel borate, $Ni_3(BO_3)_2$, have been obtained with 25 nm size by thermal decomposition of nickel-boron precursor at 800 ^oC from the reverse micellar route. The magnetic property of nickel orthoborate has been investigated and found an antiferromagnetic behavior with a Néel temperature of 47 K [44].

Anisotropic nanostructures of nickel borate, $Ni_3(BO_3)_2$, with controlled size and morphology have been synthesized by a precursor-mediated route. The nickel boron precursor has been prepared through the microemulsions using Tergitol as a surfactant [45]. Recently, nickel borate has been synthesized by sol-gel method using nickel nitrate and boric acid as reactants, citric acid as the foaming agent. Nanorod nickel borates have also been prepared and diameters of nanorods controlled by adjusting the molar ratio of $Ni(NO_3)_2/H_3BO_3$ [46].

The mean time, pure phase of rod-like micron nickel borate particles, $Ni_3(BO_3)_2$, have been prepared via a facile flux NaCl by means of following reaction and surfactant poly(oxyethylene)$_9$nonylphenol ether (NP-9) assisted thermal conversion route at 750–800 °C for 2.0 h.

$$3NiCl_2 \cdot 6H_2O + Na_2B_4O_7 \cdot 10H_2O \rightarrow Ni_3(BO_3)_2 + 2H_3BO_3 + 4HCl + 2NaCl + 11H_2O$$

The effects of molar ratio of reactants, NaCl and NP-9 have been investigated on the formation of nickel borate, $Ni_3(BO_3)_2$. The introduction of NaCl have favorable for the formation of rod like nickel borate particles, while NP-9 cause the smaller size of nickel borate particles [30].

Binary orthoborate, $Sr_2Cu(BO_3)_2$, which is α-form at the low-temperature and β-form at the high-temperature, has been synthesized by solid state reaction.

Structures of binary compounds have been established, the α-phase of $Sr_2Cu(BO_3)_2$ crystallizes in a monoclinic cell of dimensions *a* = 5.707(1), *b* = 8.796(2), *c* = 6.027(1) Å, and β = 116.98(1)° with *Z* = 2; the space group is P21/c and the β-phase crystallizes in an orthorhombic cell of dimensions *a* = 7.612(3), *b* = 10.854(7), *c* = 13.503(4) Å with *Z* = 8; the space group is Pnma [47].

It was found that $SrCu_2(BO_3)_2$ crystallized in tetragonal crystal structure with the unit cell dimensions *a* = 8.995(1), *c* = 6.649(1) Å, and *V* = 537.9(1) $Å^3$ with *Z* = 4 and with the space group $I\bar{4}2m$ [48].

Later on, Smith and Kezsler have reported the structure of the new orthoborate compound, $BaZn_2(BO_3)_2$. crystallized in orthorhombic cell with dimensions *a* = 9.305(3), *b* = 12.128(1), and *c* = 4.9255(8) Å; the space group is $P2_12_12_1$ [49].

Single crystal structure of another binary orthoborate, $Ba_2Zn(BO_3)_2$, has been solved and found that the compound was crystallized in orthorhombic system with *a* = 15.068(2), *b* = 8.720(2), and c = 10.128(3) A^o and space group: $Pca2_1$ and Z =8 [50].

Manganese containing single crystal binary pyroborates, $MnCo(B_2O_5)$ and $MnMg(B_2O_5)$ have been prepared by using B_2O_3 flux techniques in an argon atmosphere. These pyroborates crystallize in triclinic system with space group C_2-P_1, I: a=320.94(10), b=619.20(11), c=939.0(2) pm, α=104.38(2)^o, β=90.76(2)^o, δ=92.046^o. Their structures are isotypic with $Co_2B_2O_5$, and all metal ions are octahedrally coordinated by six oxygen atoms [51].

Later on, low-temperature magnetization, ac susceptibility, and specific heat of powdered $MnMgB_2O_5$ have been measured and the susceptibility has been found down to 2 K. Moreover, the magnetic and specific-heat measurements have been

reported that, below 600 mK, the $MnMgB_2O_5$ pyroborate freezes in a glassy state [52].

Single crystal $Pb_2CuB_2O_6$ has been reported in mononoclinic crystal system from a $PbO/CuO/B_2O_3$ flux by means of following reaction. Crystal structure and magnetic properties of $Pb_2CuB_2O_6$ have been described, which is the first of a new family of lead copper borates in the ternary system, $PbO–CuO–B_2O_3$ [53].

$$2PbO + CuO + B_2O_3 \rightarrow Pb_2CuB_2O_6$$

$Co_2Ni(BO_3)_2$ and $CoNi_2(BO_3)_2$ have been synthesized by thermally included solid state chemical reaction at 900 ^oC from $Co(NO_3)_2 \cdot 6H_2O$, $Ni(NO_3)_2 \cdot 6H_2O$ and H_3BO_3 with the mol ratio 2:1:2 and 1:2:2 respectively. It was found that the crystal structure of these borates is kotoite type like previously reported kotoite type compounds, $M_3(BO_3)_2$ (M= Mg, Co and Ni). The syntesized compounds are indexed in the orthorhombic system and cell parameters found with refinement a = 5.444(8), b = 8.404(0), c = 4.504(1) A° , Z = 2; a = 5.419(9), b= 8.352(0), c = 4.478(8) Å and Z= 2, respectively. Space group of both binary compounds has been determined as Pnmn [28-54].

Zahng and coworkers have been reported the synthesis by standard solid state reaction, growth, crystal structure of a novel barium cadmium diborate, $Ba_2Cd(BO_3)_2$ and explained optical properties. $Ba_2Cd(BO_3)_2$ crystallizes in the monoclinic system with space group C2/m with a = 9.6305(4), b = 5.3626(3), c = 6.5236(2) A$^\circ$, β = 118.079(3)$^\circ$, Z = 2. The crystal structure is composed of isolated $[BO_3]$ triangles, $[CdO_6]$ octahedra and $[BaO_9]$ polyhedra, shown in Fig.1.10 [55].

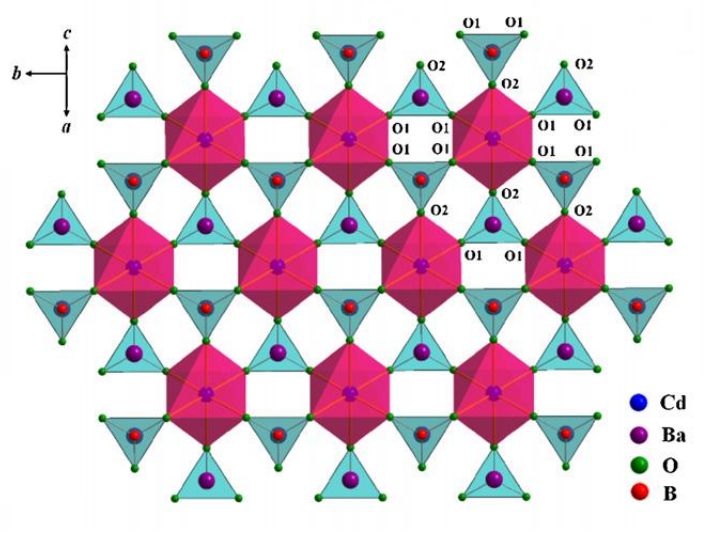

Figure 1.10 Crystal Structure of $Ba_2Cd(BO_3)_2$

Scientists pointed out that metal orthoborates are good host lattices for rare earths, which are of great interest since they are found to be superior in non- linear optical applications [56]. These kind of studies are found in literature from 1974 to today. The difference spectrum the Eu^{2+} luminescence in the borates $X_2Z(BO_3)_2$ has been explained in 1995. Structure of the mixed alkaline earth orthoborate, $Ba_2Cd(BO_3)_2$, a buetschliite derivative, have been established; crystal data: a = 5.343(2), c = 16.520(3) A^o, V = 406.4(2) A^3, Z = 3, space group = R3m. Eu^{3+} doped powder exhibits a luminescence peak at 606 nm and a Stokes shift of 11.000cm^{1-} [57].

Synthesis and thermoluminescence properties of $Sr_2Mg(BO_3)_2$ phosphors doped respectively with Tm^{3+}, Tb^{3+} and Dy^{3+} as an activator from high temperature solid state method has been explained [58]. Later on, Wang et al. has reported the properties of magnesium borate, $Mg_3B_2O_6$, doped with Co^{2+} by means of following reaction by the Czochralski technique.

$$(3\text{-}3x)\ MgCO_3 + 2\ H_3BO_3 + 3x\ CoCl_2.6H_2O \rightarrow (Mg_{1-x}Co_x)_3B_2O_6 + (3\text{-}3x)\ CO_2 + (6+30x)H_2O + 6x\ HCl$$

The crystal-field parameter of Co^{2+} doped $Mg_3B_2O_6$ has been found as Dq = 943.3 cm^{-1}, the Racah parameter B = 821.6 cm^{-1}, and Dq/B = 1.15. The luminescence life time of Co^{2+}:$Mg_3B_2O_6$ corresponding to the transition $^4T_1(^4P) \rightarrow {}^4T_2$ centered at 717 nm has been measured [59].

$Ba_2Mg(BO_3)_2$:Eu^{2+} has been prepared by combustion-assisted method used stiochiometrically $Ba(NO_3)_2$, $Mg(NO_3)_2.6H_2O$, Eu_2O_3, H_3BO_3 as starting material and NH_2CONH_2 as a fuel. It was found that these phosphors are suitable to be excited by an NUV-emitting LED chip due to their broad excita- tion band from 250 to 400 nm and intense yellow emission [60].

$Sr_2Mg(BO_3)_2$: Ce^{3+}, Li^+ and $Sr_2Mg(BO_3)_2$: Ce^{3+}, Li^+, Mn^{2+} phosphors have been synthesized by conventional solid state reaction technique at 900 ^oC for 12 hours in reducing atmosphere and the phase purity, photoluminescence properties, thermal stability, energy transfer and luminescent decay curves of these compounds have also been examined [61].

In addition to these, similar type of various metal borates have been reported in literature such as; $Ba_2Ca(BO_3)_2$: Ce^{3+} [62]; $Ba_2Mg(BO_3)_2$: Eu^{3+} [63]; $Ba_2Mg(BO_3)_2$: Eu^{2+} [64]; $Sr_2Mg(BO_3)_2$: Tb^{3+} [65]; $Sr_2Mg(BO_3)_2$: Ce^{3+} and $Sr_2Mg(BO_3)_2$: Ce^{3+} [66]; $Ba_2Mg(BO_3)_2$: Ce^{3+}, $Ba_2Ca(BO_3)_2$: Ce^{3+} and $Sr_2Mg(BO_3)_2$: Ce^{3+} [67].

$Cu_{1-x}Ni_xB_2O_4$, $Cu_{1-x}CoxB_2O_4$, $Cu_{1-x}MnxB_2O_4$ compounds (x = 0, 0.10, 0.50) prepared by flux method. These compounds crystallize in tetragonal system with space group I42d [68].

Mn^{2+} doped magnesium pyroborates, $(Mg_{1-x}Mn_x)_2B_2O_5$ ($0 \leq x \leq 0.30$), have been prepared using solid state reaction method and the crystal structure was found as triclinic system and space group: $P\bar{I}$ [69].

Recently, single crystal $LiMg_{1-x}Mn_xBO_3$ prepared through the solid state technique at 800 ^oC and has been reported that these compounds crystalized in monoclinic system with the refined cell parameters of a = 5.1820(2) , b = 8.9241(4), c = 10.1529(6) A˚ , β = 91.5824(18) [70].

1.3. SYNTHESIS METHODS OF BORATES

Various synthesis techniques have been developed to prepare high quality borate compound, such as precipitation, hydrothermal, combustion, microwave synthesis, conventional solid state reaction, co-precipitation technique, spray drying technique, sol-gel method, flux method, solid state combustion synthesis, solution combustion synthesis, mechanochemical methods and etc. All these synthesis methods of powder ceramics are mainly classified in three catagories: (i) solid state synthesis methods (ii) solution methods (iii) vapour phase methods [71].

In a solid state reaction, powder solid reactants are mixed and heated to produce new solid compound. Carbonates, nitrates, hydroxides, sulfates, acetates, oxalates, alkoxides, and other metal salts are commonly used as reactants of solid state reactions. Further reaction involves the transport of an atoms, molecules or ions. In powder systems, solid state reaction depend on several parameters which contain the chemical nature of reactants and the products; the size, size distribution, and shape of particles; the uniformity of mixing; the reaction atmosphere; the temperature; and time [72]. Solid state synthesis methods are catagorized as conventional ceramic process, metallurgical routes, microwave synthesis method, solid state combustion method, mechanochemical methods.

In scientific area, conventional ceramic process is the most widely used method of solid state synthesis which is the direct reaction of mixture of solid starting

materials. The procedure is to take stoichiometric amounts of the binary oxides, grind them in a pestle and mortar, shown in Fig. 1.5.a to give a uniform small particle size. Reaction between powders occur at elevated temperatures (1000-1500 ^{o}C). In this method, platinium, alumina, and silica containers, shown in Fig. 1.4.b are usually used for metal oxides, while graphite containers are suitable for sulphides and other chalcogenides [71-74].

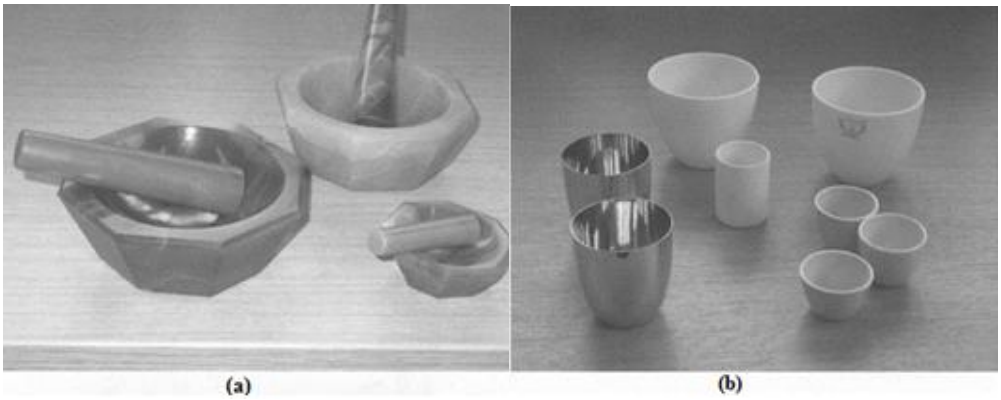

Figure 1.11 (a) Pestles and mortars **(b)** Platinum, alumina and porcelein crucibles[75]

The advantages of solid-state reactions are the ready availability of oxide precursors and the low cost for powder production on the industrial scale. These reactions are also convenient for laboratory-scale preparations [75].

1.4. PURPOSE OF THE WORK

The importance and the aim of this thesis is the preparation and characterization of some new novel-mixed-metal orthoborates as $M_{3-x}Mn_x(BO_3)_2$ (M = Ni, Mg, Co) by high temperature solid state method and pure $Mg_3(BO_3)_2$ from different starting reagents.

In the first part of this work, the kotoite type of compound, $Mg_3(BO_3)_2$, was prepared from different starting materials by conventional ceramic process and characterise by X-ray diffraction (XRD) and Infrared spectroscopy (IR).

In the second part of this study, the aim is

- to prepare the novel-mixed-metal orthoborates by doping manganase (II) ion to magnesium, nickel and cobalt orthoborates, with the formula of $M_{3-x}Mn_x(BO_3)_2$ (M = Mg, Co, Ni; $0 \leq x \leq 0.10$),
- to examine their crystal structures by X-ray diffraction (XRD),
- to refine their unit cell parameters with the aid computer programs,
- to investigate the vibrational motions of B-O bonds in triangular BO_3 units by IR technique,
- to study the thermal behaviors using TG/DTA
- to observe the morphology of prepared orthoborates by SEM.

The proposed reactions are given as follows:

$$(3-x)MgSO_{4(s)} + xMnSO_4.H_2O_{(s)} + 2H_3BO_{3(s)} \rightarrow Mg_{(3-x)}Mn_x(BO_3)_{2(s)} + 3SO_{2(g)} + (3+x)\,H_2O_{(g)} + 4.5O_{2(g)}$$

(x = 0, 0.01, 0.05, 0.10)

$$(3-x)M(NO_3)_2.6H_2O_{(s)} + xMnSO_4.H_2O_{(s)} + 2H_3BO_{3(s)} \rightarrow M_{(3-x)}Mn_x(BO_3)_{2(s)} + (6-2x)NO_{2(g)} + xSO_{2(g)} + (21-5x)H_2O_{(g)} + 1.5O_{2(g)}$$

(M = Co, Ni; x = 0, 0.01, 0.05, 0.10)

CHAPTER II

EXPERIMENTAL TECHNIQUES

2.1. CHEMICALS

The following chemicals were used in the synthesis of the products:

$MnSO_4.H_2O$: Lachema (pure %99.00)

MgO: Merck (pure %99.00)

$MgCO_3$: Merck (pure %99.00)

$MgSO_4$: Lachema (pure %99.00)

$Ni(NO_3)_2.6H_2O$: Aldrich

$Co(NO_3)_2.6H_2O$: Lachema (pure %99.00)

H_3BO_3: Fluka (pure 99.5%)

Gd_2O_3:Merck (pure 99.9%)

KBr: Spectroscopic grade and it was used for making IR pellets.

It was dried at 180^oC about 2 hours before using.

2.2. INSTRUMENTATION

i.) X-Ray Powder Diffractometer

X-ray powder diffraction patterns (XRD) were recorded on Rigaku miniflex, BD127412, and CuKα (30-40 kV, 10-20 mA, λ=1.54056 Å) radiation. Indexing of

the XRD pattern was accomplished by a program developed in our laboratory and checked by the POWD program. The least square refiment procedure of the unit cell parameters was done by Jana2006.

ii.) Infrared Spectrophotometer

Shimadzu Fourier Transform Infrared (FTIR) Spectrophotometer was used to obtain the spectra of the products in the region of the 4000-400 cm^{-1}. Spectra of solid samples were taken from KBr pellets using 0.0003:0.00050 (wt/wt) product to KBr ratio.

iii.) Thermogravimetric-Differential Thermal Analyzer (TG / DTA)

TG /DTA 6300, SII EXSTAR 6000 Differential Thermal Analyser was used to investigate the thermal properties of products in the range of 20^{o}C to 1400^{o}C.

iv.) Scanning Electron Microscope (SEM)- Energy Dispersive X-ray (EDX)

SEM-EDX photographs were taken using Jeol JSM 6390LV. The samples used for SEM were coated with carbon.

v.) Furnaces

All the reactions have been carried out in air with the aid of Nuve MF 1400, Nuve 1200 and Protherm 1600 furnaces. Heating ranges were 450-900 ^{o}C.

2.3. EXPERIMENTAL PROCEDURE

2.3.1. Synthesis of $Mg_3(BO_3)_2$ from MgO

Stoichiometric amount of MgO and H_3BO_3 were mixed and grinded together in an agate mortar. Homogenized mixtures was transfered into a convenient porcelain crucible and placed into the furnace. The main products were obtained in four steps;

Firstly, the temperature was raised up to 450 ^oC with an increase of 15^oC per minute. After being held for 4 hours at 450 ^oC, the mixture was taken out from the oven and cooled down and placed to the oven back again after crushing and blending well.

Secondly, the temperature was raised up to 600 ^oC with an increase of 1^oC per min and the mixture was held for 3 hours at 600 ^oC. In the third stage, the specimen was heated four times to 900 ^oC with an increase of 1^oC per min and was held for 12 hours.

Finally, the product was cooled down to the room temperature with a decrease of 1^oC per min [28,77,78].

At the end of each heating period, the mixtures were weighed, ground well and subjected to X-ray and IR analysis. The following reaction is predicted:

$$3MgO_{(s)} + 2H_3BO_{3(s)} \rightarrow Mg_3(BO_3)_{2(s)} + 3\,H_2O_{(g)}$$

2.3.2. Synthesis of $Mg_3(BO_3)_2$ from $MgCO_3$

The reaction mixture was prepared by weighing the stoichiometric amounts of reactants, $MgCO_3$ and H_3BO_3, separately and grinding together in an agate mortar, then heating by means of section 2.3.1. The expected reaction is:

$$3MgCO_{3(s)} + 2H_3BO_{3(s)} \rightarrow Mg_3(BO_3)_{2(s)} + 3\,CO_{2(g)} + 3\,H_2O_{(g)}$$

2.3.3. Synthesis of $Mg_3(BO_3)_2$ from $MgSO_4$

$MgSO_4$ and H_3BO_3 were used as magnesium and boron sources, respectively and the same procedure was followed in weighing, grinding and heating as mentioned in section 2.3.1. The desired reaction is;

$$3MgSO_{4(s)} + 2H_3BO_{3(s)} \rightarrow Mg_3(BO_3)_{2(s)} + 3\,SO_{2(g)} + 3\,H_2O_{(g)} + 1.5\,O_{2(g)}$$

2.3.4. Solid State Reactions of $(3\text{-}x)MgSO_4 + xMnSO_4.H_2O + 2H_3BO_3$

The reaction mixtures were prepared for every x values (x = 0, 0.01, 0.05, 0.10) by weighing separately the stoichiometric amounts of reactants, $MgSO_4$, $MnSO_4.H_2O$, H_3BO_3, and grinding homogeneously together in an agate mortar then each of them transferred into porcelain crucibles and placed into the furnace, then heating same procedure in section 2.3.1. The following reactions are expected:

For x=0;

$$3MgSO_{4(s)} + 2H_3BO_{3(s)} \rightarrow Mg_3(BO_3)_{2(s)} + 3SO_{2(g)} + 3\,H_2O_{(g)} + 1.5\,O_{2(g)}$$

For x=0.01;

$$2.99MgSO_{4(s)} + 0.01MnSO_4.H_2O_{(s)} + 2H_3BO_{3(s)} \rightarrow Mg_{2.99}Mn_{0.01}(BO_3)_{2(s)} + 3SO_{2(g)} + 3.01\,H_2O_{(g)} + 4.5O_{2(g)}$$

For x=0.05;

$$2.95MgSO_{4(s)} + 0.05MnSO_4.H_2O_{(s)} + 2H_3BO_{3(s)} \rightarrow Mg_{2.95}Mn_{0.05}(BO_3)_{2(s)} + 3SO_{2(g)} + 3.05H_2O_{(g)} + 4.5O_{2(g)}$$

For x=0.10;

$$2.90MgSO_{4(s)} + 0.10MnSO_4.H_2O_{(s)} + 2H_3BO_{3(s)} \rightarrow Mg_{2.90}Mn_{0.10}(BO_3)_{2(s)} + 3SO_{2(g)} + 3.10\ H_2O_{(g)} + 4.5O_{2(g)}$$

2.3.5. Solid State Reactions of $(3-x)Co(NO_3)_2.6H_2O + xMnSO_4.H_2O + 2H_3BO_3$

Stoichiometric amounts of $Ni(NO_3)_2.6H_2O$, $MnSO_4.H_2O$ and H_3BO_3 were used as a starting materials for each x values (x = 0, 0.01, 0.05, 0.10) and grinding homogeneously together in an agate mortar then each of them transfferred into the porcelain crucibles and placed into the furnace, then heating same procedure in section 2.3.1. The following reactions are predicted:

For x= 0,

$$3Co(NO_3)_2.6H_2O_{(s)} + 2H_3BO_{3(s)} \rightarrow Co_3(BO_3)_{2(s)} + 6NO_{2(g)} + 21H_2O_{(g)} + 1.5O_{2(g)}$$

For x= 0.01,

$$2.99Co(NO_3)_2.6H_2O_{(s)} + 0.01MnSO_4.H_2O_{(s)} + 2H_3BO_{3(s)} \rightarrow Co_{2.99}Mn_{0.01}(BO_3)_{2(s)} + 5.98NO_{2(g)} + 0.01SO_{2(g)} + 20.95H_2O_{(g)} + 1.5O_{2(g)}$$

For x= 0.05,

$$2.95Co(NO_3)_2.6H_2O_{(s)} + 0.05MnSO_4.H_2O_{(s)} + 2H_3BO_{3(s)} \rightarrow Co_{2.95}Mn_{0.05}(BO_3)_{2(s)} + 5.9NO_{2(g)} + 0.05SO_{2(g)} + 20.75H_2O_{(g)} + 1.5O_{2(g)}$$

For x= 0.10,

$$2.90Co(NO_3)_2.6H_2O_{(s)} + 0.1MnSO_4.H_2O_{(s)} + 2H_3BO_{3(s)} \rightarrow Co_{2.90}Mn_{0.10}(BO_3)_{2(s)} + 5.8NO_{2(g)} + 0.1SO_{2(g)} + 20.5H_2O_{(g)} + 1.5O_{2(g)}$$

2.3.6. Solid State Reactions of $(3-x)Ni(NO_3)_2.6H_2O + xMnSO_4.H_2O + 2H_3BO_3$

The amounts of starting materials calculated with the molar ratios changing x values, $Ni(NO_3)_2.6H_2O:MnSO_4.H_2O:H_3BO_3 = 3\text{-}x:x:2$ (x=0, 0.01, 0.05, 0.10). Taken stoichiometric amounts of these powders were weighted separately and homogeneously mixed in an agate mortar with a pestle. Each homogenized mixtures was transffered into a convenient porcelain crucible and placed into the furnace. The main products were obtained with four periods in section 2.3.1. The following reactions are predicted:

For x= 0,

$$3Ni(NO_3)_2.6H_2O_{(s)} + 2H_3BO_{3(s)} \rightarrow Ni_3(BO_3)_{2(s)} + 6NO_{2(g)} + 21H_2O_{(g)} + 1.5O_{2(g)}$$

For x= 0.01,

$$2.99Ni(NO_3)_2.6H_2O_{(s)} + 0.01MnSO_4.H_2O_{(s)} + 2H_3BO_{3(s)} \rightarrow Ni_{2.99}Mn_{0.01}(BO_3)_{2(s)} + 5.98NO_{2(g)} + 0.01SO_{2(g)} + 20.95H_2O_{(g)} + 1.5O_{2(g)}$$

For x= 0.05,

$$2.95Ni(NO_3)_2.6H_2O_{(s)} + 0.05MnSO_4.H_2O_{(s)} + 2H_3BO_{3(s)} \rightarrow Ni_{2.95}Mn_{0.05}(BO_3)_{2(s)} + 5.9NO_{2(g)} + 0.05SO_{2(g)} + 20.75H_2O_{(g)} + 1.5O_{2(g)}$$

For x= 0.10,

$$2.90Ni(NO_3)_2.6H_2O_{(s)} + 0.1MnSO_4.H_2O_{(s)} + 2H_3BO_{3(s)} \rightarrow Ni_{2.90}Mn_{0.10}(BO_3)_{2(s)} + 5.8NO_{2(g)} + 0.1SO_{2(g)} + 20.5H_2O_{(g)} + 1.5O_{2(g)}$$

CHAPTER III

RESULTS AND DISCUSSION

3.1. Synthesis of Magnesium Orthoborate, $Mg_3(BO_3)_2$

Various magnesium sources, MgO, $MgCO_3$, and $MgSO_4$, were used to prepare magnesium orthoborate, $Mg_3(BO_3)_2$ in pure form. Mg/B ratio was used in 3/2 mol ratios and heated at 450 ^oC for 4 hours, at 600 ^oC for 3 hours, and four times at 900 ^oC for 12hours. Then, Mg/B ratio was chaged to 3/3 and heated in the same procedure for the reaction of H_3BO_3 with $MgSO_4$. The following reactions were predicted;

$$3MgO_{(s)} + 2H_3BO_{3(s)} \rightarrow \mathbf{Mg_3(BO_3)_{2(s)}} + 3H_2O_{(g)}$$

$$3MgCO_{3(s)} + 2H_3BO_{3(s)} \rightarrow \mathbf{Mg_3(BO_3)_{2(s)}} + 3CO_{2(g)} + 3H_2O_{(g)}$$

$$3MgSO_{4(s)} + 2H_3BO_{3(s)} \rightarrow \mathbf{Mg_3(BO_3)_{2(s)}} + 3SO_{2(g)} + 3H_2O_{(g)} + 1.5O_{2(g)}$$

$$3MgSO_{4(s)} + 3H_3BO_{3(s)} \rightarrow \mathbf{Mg_3(BO_3)_{2(s)}} + 3SO_{2(g)} + 0.5B_2O_{3(g)} + 4.5H_2O_{(g)} + 1.5O_{2(g)}$$

3.1.1. X-ray Powder Diffraction (XRD) Studies

Figure 3.1 shows X-ray powder diffraction patterns of magnesium orthoborates having kotoite type structure synthesized from different magnesium sources.

Examination of XRD patterns revals that the products obtained by the reaction of MgO and $MgCO_3$ with H_3BO_3 were kotoite, $Mg_3B_2O_6$, and suanite, $Mg_2B_2O_5$. The assignments of the characteristic reflections are made by comparing the patterns with the available data in ICDD cards 75–1807 for kotoite type magnesium orthoborate and 83–0625 for suanite type magnesium pyroborate.

However, in the XRD pattern of product prepared through the reaction of $3MgSO_4 + 2H_3BO_3$, the lines belong to kotoite type of $Mg_3(BO_3)_2$ as single phase was observed.

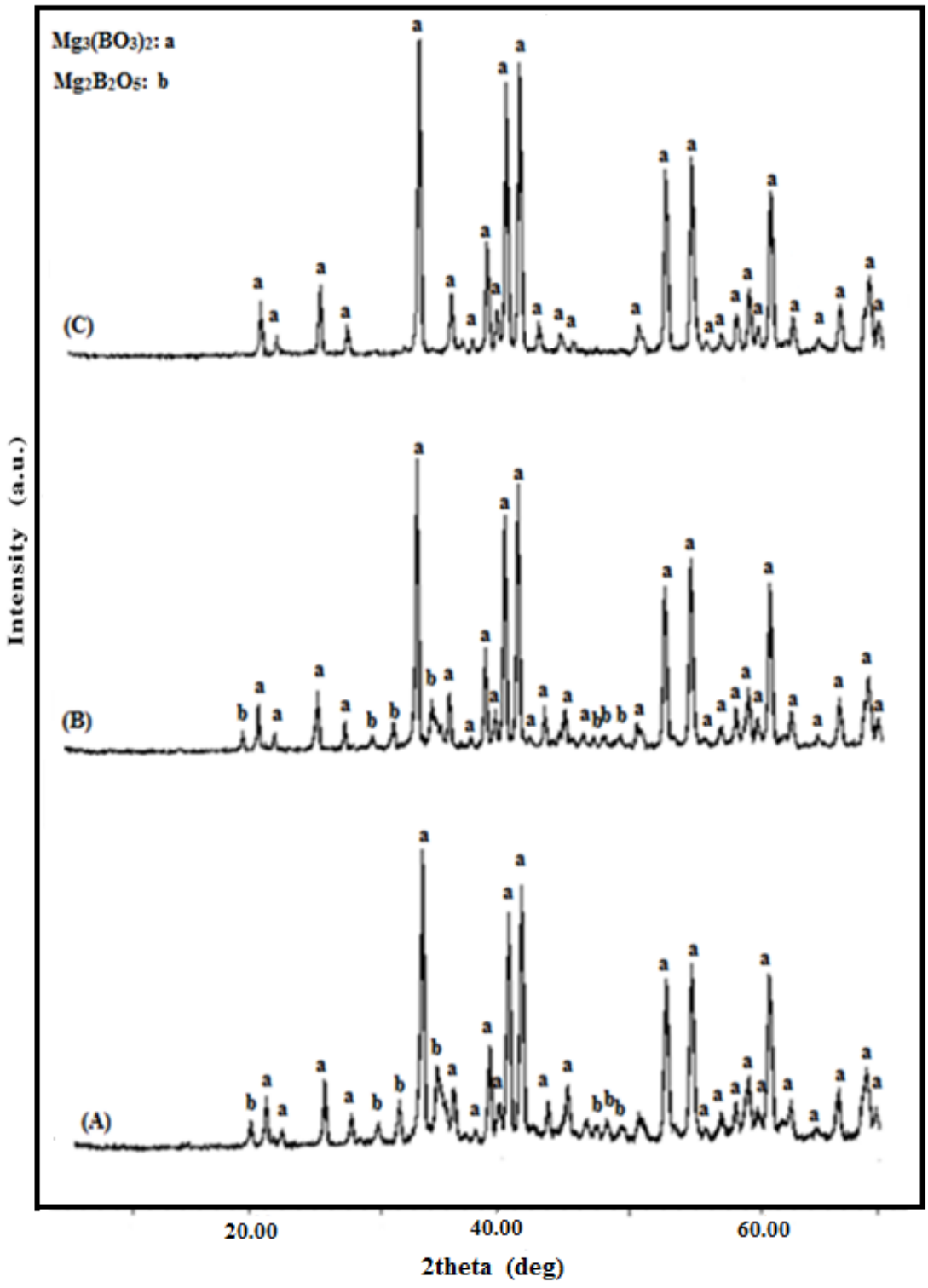

Figure 3.1 XRD Patterns of synthesized $Mg_3(BO_3)_2$ from (**A)** MgO, **(B)** $MgCO_3$, **(C)**$MgSO_4$ as starting materials

3.1.2. Infrared Spectroscopy Studies

The infrared spectra of kotoite type magnesium orthoborates are given Figure 3.2. In the FTIR spectrum of borates, the vibrational bands concentrated on the wave number range of 2000–500 cm^{-1}, and vibrational modes of the borate network have three region. The 1200-1600 cm^{-1} band is the first region, which is due to asymmetric stretching relaxation of the B-O bond of trigonal BO_3 units. The second region is located between 800 and 1200 cm^{-1}, and is due to the B-O bond stretching of tetrahedral BO_4 units and the last band around 700 cm^{-1} is due to the bending of B-O-B linkages in the borate network [78-82].

The structure of the B_2O_5 group consists of two nonidentical BO_3 triangles with one common oxygen atom. For this reason, the infrared spectrum of $Mg_2B_2O_5$ can be interpreted on the basis of these two, non-identical joined triangles[83].

The FTIR spectrum of magnesium borate obtained from reaction of excess boric acid with magnesium sulphate are presented in Figure 3.2.a, the vibrational bands are observed at 1496, 1288, 1271, 1172, 1024, 837, 711, 660, 609, 496 and 449 cm^{-1} which showed the existence of two different phases, kotoite, $Mg_3B_2O_6$, and synthetic suanite, $Mg_2B_2O_5$ [83,84].

The band around 1293 and 1203 cm^{-1} are due to B-O stretching vibrations of BO_3^{3-} unit in orthoborates, other peaks appeared at 736, 661, 610, 486 and 420 cm^{-1} are due to the product synthesized from MgO. In addition to these, the vibration modes of magnesium pyroborates are shown as second phase at 1448, 1497, and 1028 cm^{-1} [83,84].

In the FTIR spectrum of synthesized from $MgCO_3$, the asymmetric stretching, out of plane and in plane bending modes of B-O at 1290, 1205, 746, 664,

611, 462, and 430 cm^{-1}. Also, second phase magnesium pyroborate vibrational bands are observed at 1502, 1455, and 1028 cm^{-1} [83,84].

1278, 1196, 724, 664, 611, 496 and 420 cm^{-1} vibrational bands, assigned as kotoite type borates, were observed in the infrared spectrum of magnesium orthoborate, synthesized from $MgSO_4$. It is obtained as single phase orthoborate in the form of kotoite, shown in Fig.3.2.d.

Similarly, the band in the region of 3200–3600 cm^{-1} is ascribed to the vibrational motions of water groups. The absorption band at 3421cm^{-1} is attributed to symmetric OH stretching mode [80].

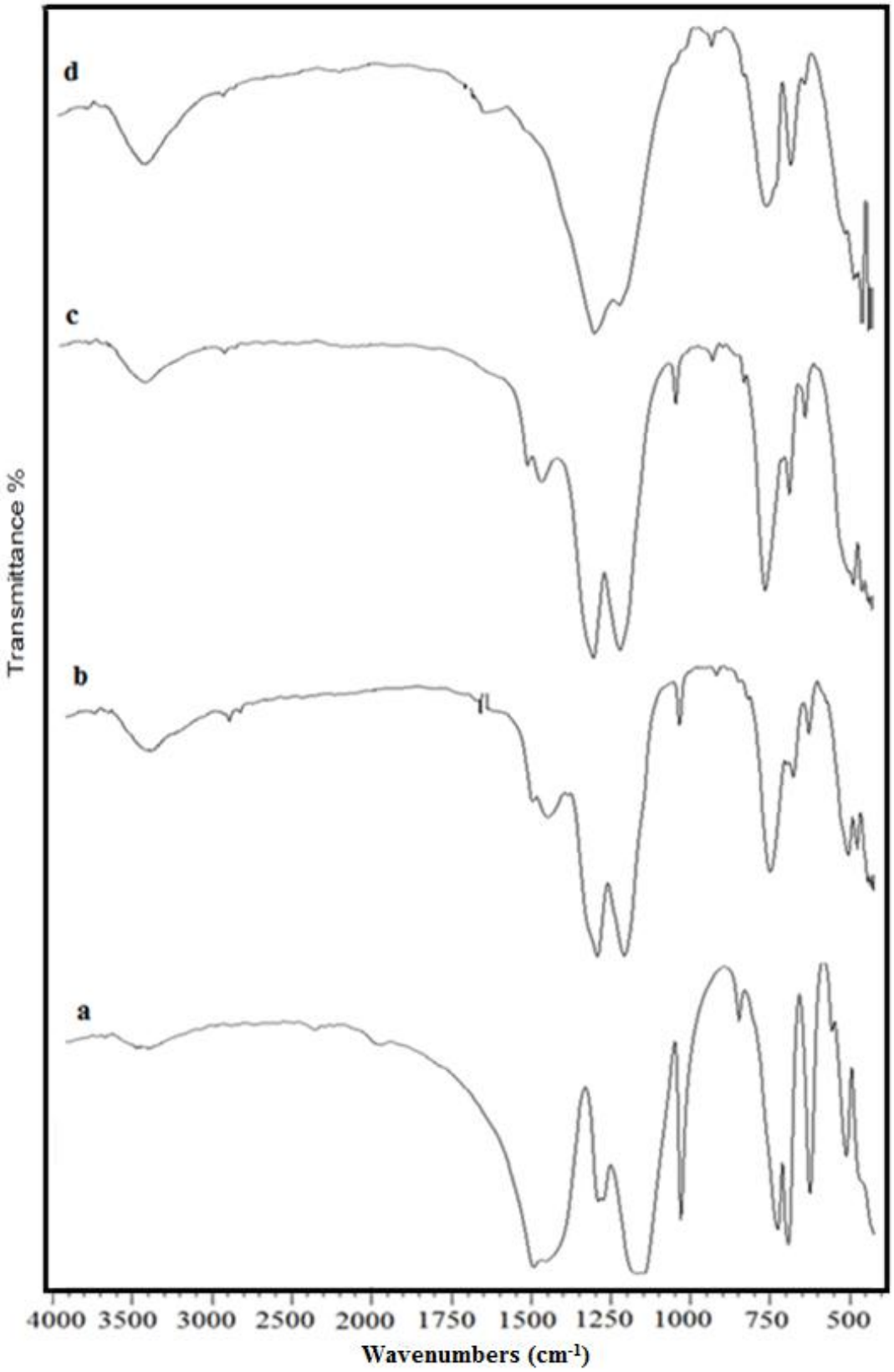

Figure 3.2 IR Spectra of synthesized $Mg_3(BO_3)_2$ from **a)** excess amount of H_3BO_3 + $MgSO_4$ **b)** MgO, **c)** $MgCO_3$, **d)** $MgSO_4$

3.2. Synthesis of $Mg_{3-x}Mn_x(BO_3)_2$ (x = 0, 0.01, 0.05, and 0.10)

The stoichiometric mixture of reactants, $MgSO_4$, $MnSO_4.H_2O$ and H_3BO_3, were heated at 450 ^oC for 4hours, 600 ^oC for 3 hours, and 4 times at 900 ^oC for 12 hours, to form of the compounds, $Mg_{3-x}Mn_x(BO_3)_2$ (x = 0, 0.01, 0.05, and 0.10). The following reaction is expected;

$$(3\text{-}x)MgSO_{4(s)} + xMnSO_4.H_2O_{(s)} + 2H_3BO_{3(s)} \rightarrow \mathbf{Mg_{(3-x)}Mn_x(BO_3)_{2(s)}} + 3SO_{2(g)} + (3+x)\,H_2O_{(g)} + 4.5O_{2(g)}$$

(x = 0, 0.01, 0.05, 0.10)

3.2.1. X-ray Power Diffraction (XRD) Studies

The X-ray powder diffraction patterns of the each products, $Mg_3(BO_3)_2$, $Mg_{2.99}Mn_{0.01}(BO_3)_2$, $Mg_{2.95}Mn_{0.05}(BO_3)_2$, and $Mg_{2.90}Mn_{0.10}(BO_3)_2$, were shown in Figure 3.5. The color of products became darker from white to brown with increasing doping amount of manganese (II) (Fig. 3.3.).

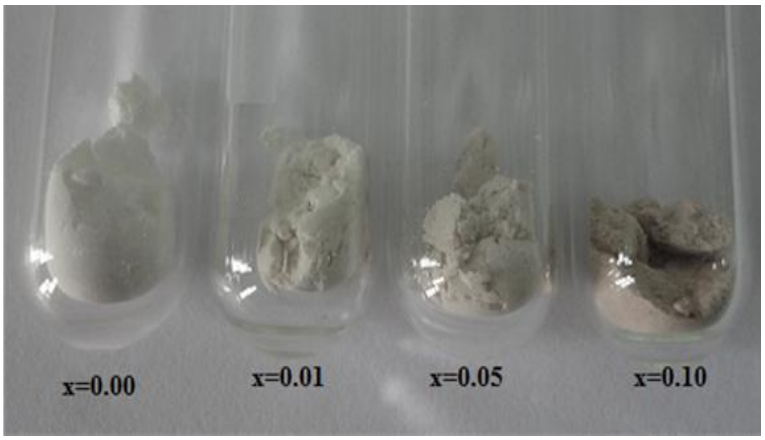

Figure 3.3 Digital photos of $Mg_{3-x}Mn_x(BO_3)_2$ (x= 0, 0.01, 0.05 and 0.10)

In the XRD patterns, all lines of the kotoite type of $Mg_{2.99}Mn_{0.01}(BO_3)_2$, $Mg_{2.95}Mn_{0.05}(BO_3)_2$, and $Mg_{2.90}Mn_{0.10}(BO_3)_2$ were indexed in the orthorhombic crystal system. The observed and calculated d values were given in Table 3.1 to 3.3. The refined unit cell parameters were found as a= 5.406(3), b= 8.430(4), c= 4.508(4) Å; a= 5.410(4), b= 8.436(2), c= 4.507(8) Å and a= 5.144(4), b= 8.444(3), c=4.512(0) Å, respectively, in good agreement with the unit cell parameters of previously reported kotoite type magnesium orthoborate, so these compounds are isostructural each other [33,43].

Figure 3.4 shows the variation of the lattice parameters of $Mg_{3-x}Mn_x(BO_3)_2$ with the different values of x. It is observed that the cell parameters linearly increase with increasing of manganese ion concentration because of the larger ionic radius of manganese ion, $r_{Mn(II)}$ = 0.97 ˚A, than that of magnesium ion $r_{Mg(II)}$ = 0.86 ˚A [85].

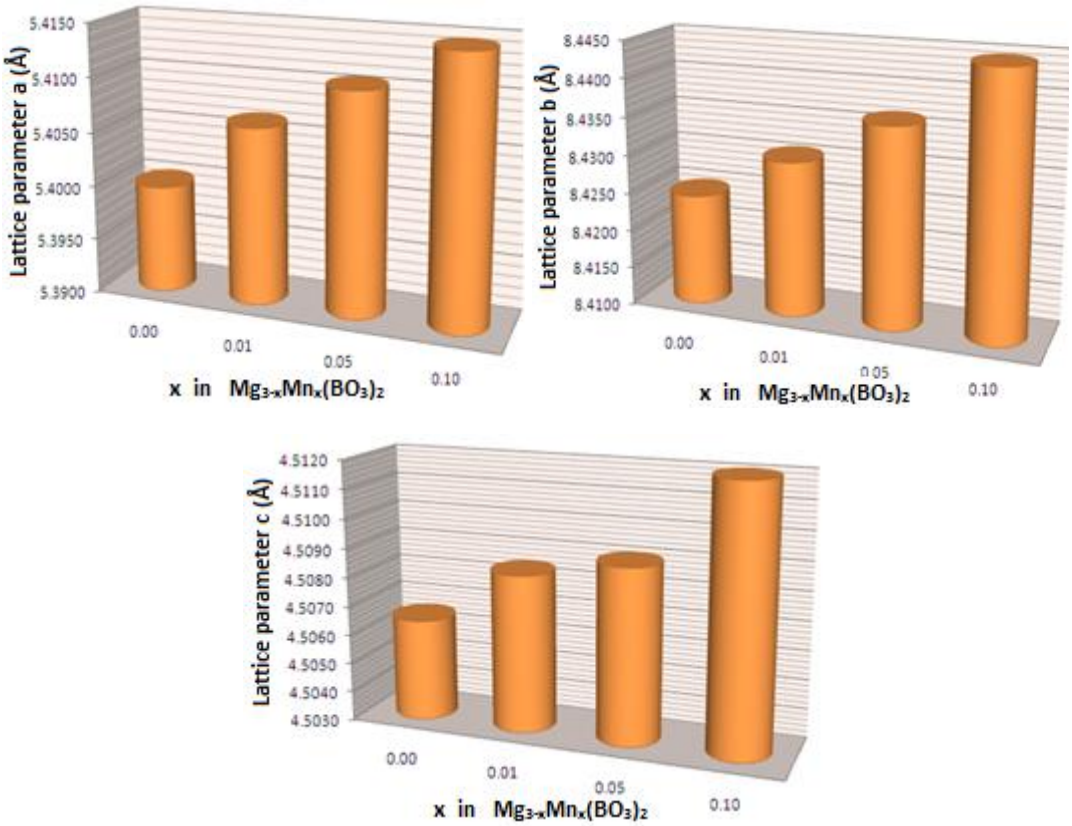

Figure 3.4 Lattice parameters of $Mg_{(3-x)}Mn_x(BO_3)_2$ as a function of substitution Mn content

The XRD patterns of the compounds are very similar to that of kotoite form of magnesium orthoborate, ICDD card No. 75-1807. However, through these patterns, small impurity lines were observed, these lines belong to suanite types of borate, $Mg_2B_2O_5$ (ICDD card no. 83–0625)

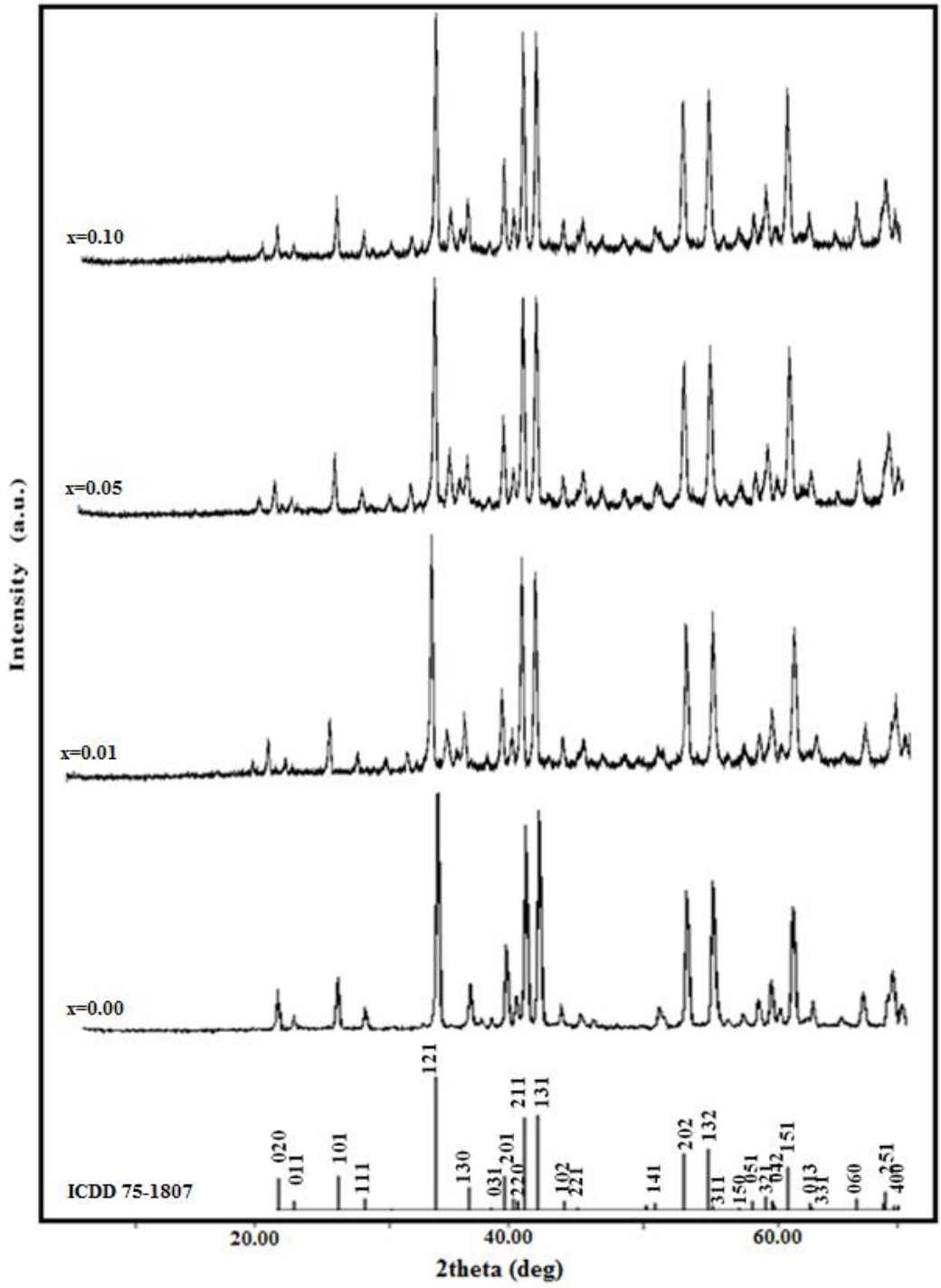

.

Figure 3.5 XRD Patterns of $Mg_{3-x}Mn_x(BO_3)_2$ (x= 0, 0.01, 0.05 and 0.10) and ICDD 75-1807

Table 3.1 The X-ray Powder Diffraction Data of $Mg_{2.99}Mn_{0.01}(BO_3)_2$; orthorhombic with a= 5.406(3), b= 8.430(4), c= 4.508(4) Å

No	hkl	I/I_0	$\sin^2(\theta)_{obs}$	$\sin^2(\theta)_{cal}$	d_{obs} (Å)	d_{cal} (Å)	XRD data of $Mg_3(BO_3)_2$ (ICDD 75-1807)	
							d values	I/I_0
1	020	18	0.0340	0.0336	4.176	4.202	4.208	25
2	011	7	0.0380	0.0380	3.952	3.951	3.966	9
3	101	24	0.0503	0.0500	3.435	3.445	3.455	27
4	111	12	0.0588	0.0584	3.181	3.187	3.196	10
5	121	100	0.0838	0.0836	2.660	2.664	2.670	100
6	130	22	0.0967	0.0961	2.476	2.485	2.489	19
7	031	7	0.1052	0.1052	2.375	2.374	2.380	4
8	201	41	0.1115	0.1113	2.307	2.309	2.314	27
9	220	18	0.1159	0.1154	2.263	2.267	2.272	11
10	211	88	0.1200	01197	2.223	2.226	2.231	70
11	131	95	0.1259	0.1256	2.171	2.174	2.178	71
12	102	17	0.1382	0.1386	2.072	2.069	2.076	9
13	221	10	0.1455	0.1449	2.018	2.024	2.028	4
14	112	14	0.1476	0.1471	2.005	2.008	2.015	2
15	141	13	0.1847	0.1844	1.792	1.794	1.797	7
16	202	63	0.1995	0.1999	1.724	1.723	1.728	43
17	132	64	0.2136	0.2140	1.667	1.665	1.669	46
18	311	8	0.2221	0.2219	1.635	1.635	1.639	2
19	150	9	0.2307	0.2304	1.604	1.605	1.607	4
20	051	16	0.2397	0.2396	1.573	1.574	1.576	9
21	321	26	0.2467	0.2470	1.551	1.550	1.553	13
22	042	12	0.2522	0.2526	1.534	1.533	1.536	5
23	151	61	0.2595	0.2599	1.512	1.511	1.515	33
24	330	61	0.2595	0.2595	1.512	1.512	1.515	33
25	013	15	0.2724	0.2743	1.476	1.471	1.476	7
26	331	7	0.2897	0.2892	1.431	1.432	1.435	3
27	060	21	0.3019	0.3023	1.402	1.401	1.403	10
28	251	29	0.3208	0.3213	1.360	1.359	1.361	15
29	400	17	0.3270	0.3270	1.347	1.347	1.349	6

Table 3.2 The X-ray Powder Diffraction Data of $Mg_{2.95}Mn_{0.05}(BO_3)_2$; orthorhombic with a= 5.410(4), b= 8.436(2), c= 4.508(8) Å

No	hkl	I/I_0	$\sin^2(\theta)_{obs}$	$\sin^2(\theta)_{cal}$	d_{obs} (Å)	d_{cal} (Å)	XRD data of $Mg_3(BO_3)_2$ (ICDD 75-1807)	
							d values	I/I_0
1	020	17	0.0341	0.0341	4.174	4.171	4.208	25
2	011	10	0.0383	0.0383	3.936	3.936	3.966	9
3	101	28	0.0504	0.0502	3.432	3.438	3.455	27
4	111	13	0.0586	0.0587	3.181	3.179	3.196	10
5	121	100	0.0839	0.0842	2.659	2.654	2.670	100
6	130	27	0.0967	0.0971	2.477	2.472	2.489	19
7	031	10	0.1054	0.1058	2.373	2.368	2.380	4
8	201	42	0.1116	0.1115	2.306	2.307	2.314	27
9	220	22	0.1157	0.1158	2.264	2.264	2.272	11
10	211	88	0.1198	0.1199	2.225	2.224	2.231	70
11	131	89	0.1256	0.1260	2.173	2.170	2.178	71
12	102	18	0.1382	0.1388	2.072	2.068	2.076	9
13	112	11	0.1513	0.1517	1.980	1.978	2.015	2
14	141	14	0.1847	0.1851	1.792	1.790	1.797	7
15	202	63	0.1995	0.2000	1.724	1.722	1.728	43
16	132	69	0.2136	0.2140	1.667	1.665	1.669	46
17	311	12	0.2215	0.2219	1.637	1.635	1.639	2
18	150	17	0.2310	0.2312	1.603	1.602	1.607	4
29	051	19	0.2393	0.2394	1.574	1.574	1.576	9
20	321	29	0.2465	0.2461	1.551	1.552	1.553	13
21	042	17	0.2517	0.2519	1.535	1.535	1.536	5
22	151	69	0.2594	0.2597	1.512	1.512	1.515	33
23	330	69	0.2594	0.2598	1.512	1.512	1.515	33
24	013	20	0.2722	0.2726	1.476	1.475	1.476	7
25	331	11	0.2881	0.2890	1.435	1.433	1.435	3
26	060	24	0.3022	0.3032	1.401	1.398	1.403	10
27	251	36	0.3202	0.3206	1.361	1.360	1.361	15
28	400	22	0.3262	0.3262	1.349	1.349	1.349	6

Table 3.3 The X-ray Powder Diffraction Data of $Mg_{2.90}Mn_{0.10}(BO_3)_2$; orthorhombic: with a= 5.144(4), b= 8.436(2), c= 4.512(0) Å

No	hkl	I/I_0	$\sin^2(\theta)_{obs}$	$\sin^2(\theta)_{cal}$	d_{obs} (Å)	d_{cal} (Å)	XRD data of $Mg_3(BO_3)_2$ (ICDD 75-1807)	
							d values	I/I_0
1	020	17	0.0342	0.0341	4.166	4.171	4.208	25
2	011	10	0.0383	0.0382	3.938	3.941	3.966	9
3	101	28	0.0504	0.0502	3.431	3.437	3.455	27
4	111	15	0.0589	0.0587	3.173	3.179	3.196	10
5	121	100	0.0840	0.0843	2.657	2.653	2.670	100
6	130	26	0.0965	0.0970	2.479	2.473	2.489	19
7	031	11	0.1052	0.1056	2.374	2.370	2.380	4
8	201	43	0.1117	0.1113	2.304	2.308	2.314	27
9	220	24	0.1159	0.1155	2.262	2.266	2.272	11
10	211	90	0.1199	0.1197	2.224	2.226	2.231	70
11	131	90	0.1259	0.1261	2.170	2.169	2.178	71
12	102	18	0.1382	0.1386	2.072	2.069	2.076	9
13	221	15	0.1452	0.1450	2.022	2.023	2.028	4
14	112	20	0.1479	0.1474	2.003	2.007	2.015	2
15	141	17	0.1847	0.1851	1.793	1.790	1.797	7
16	202	64	0.1995	0.2000	1.723	1.722	1.728	43
17	132	66	0.2139	0.2144	1.666	1.666	1.669	46
18	311	14	0.2221	0.2220	1.635	1.635	1.639	2
19	150	16	0.2313	0.2316	1.602	1.601	1.607	4
20	051	19	0.2393	0.2401	1.575	1.572	1.576	9
21	321	33	0.2467	0.2471	1.551	1.550	1.553	13
22	042	12	0.2522	0.2528	1.534	1.532	1.536	5
23	151	69	0.2594	0.2596	1.512	1.512	1.515	33
24	330	69	0.2594	0.2598	1.512	1.211	1.515	33
25	013	22	0.2722	0.2730	1.476	1.474	1.476	7
26	331	14	0.2885	0.2889	1.434	1.433	1.435	3
27	060	26	0.3017	0.3042	1.402	1.397	1.403	10
28	251	33	0.3199	0.3203	1.362	1.361	1.361	15
29	400	23	0.3271	0.3272	1.349	1.346	1.349	6

Refinement are made by using the program Jana2006 and the refinement patterns of compounds are shown in Figure 3.6 to 3.9

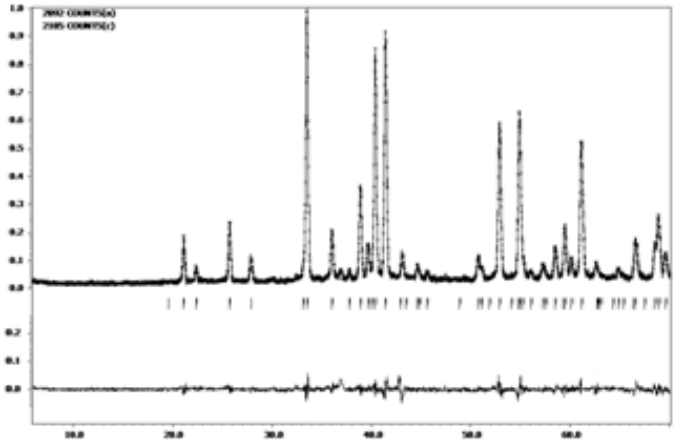

Figure 3.6 Jana2006 refinement pattern of $Mg_3(BO_3)_2$

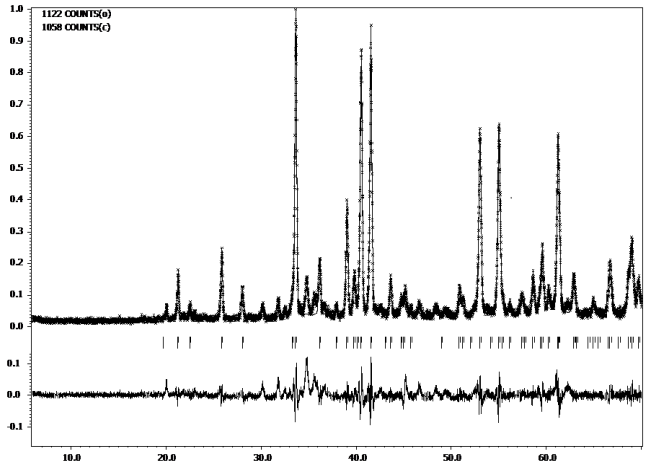

Figure 3.7 Jana2006 refinement pattern of $Mg_{2.99}Mn_{0.01}(BO_3)_2$

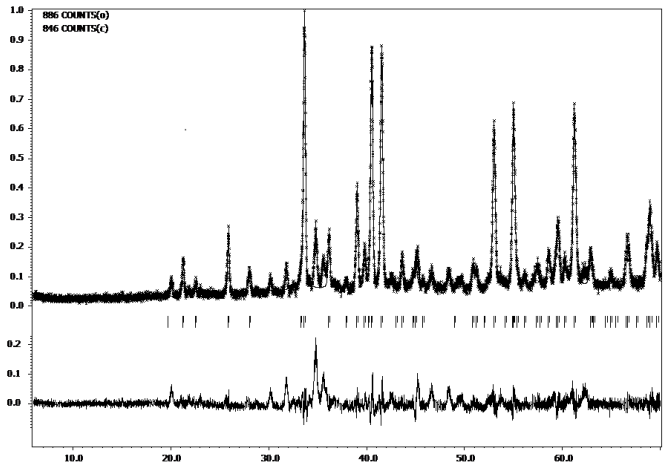

Figure 3.8 Jana2006 refinement pattern of $Mg_{2.95}Mn_{0.05}(BO_3)_2$

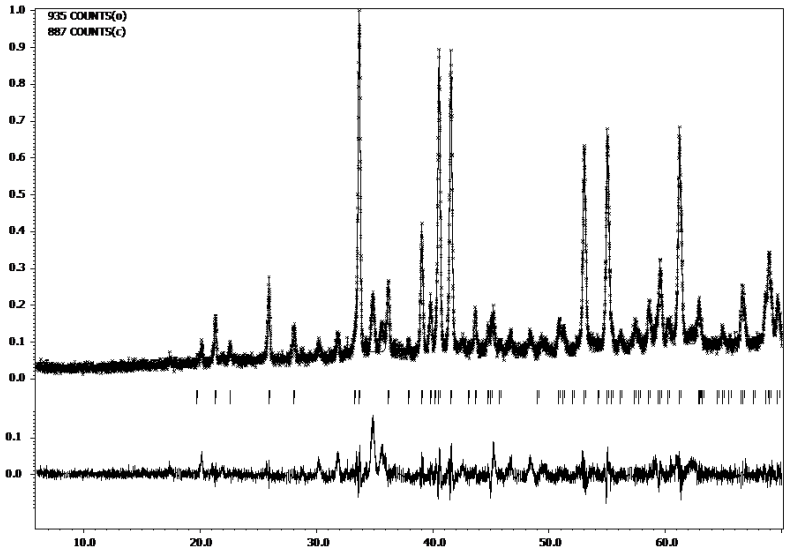

Figure 3.9 Jana2006 refinement pattern of $Mg_{2.90}Mn_{0.10}(BO_3)_2$

The XRD data enable to investigate the effect of doped manganese (II) ion on structural parameters such as crystallite size (t), density (d), specific surface area (S) of orthoborates. These parameters and details of Jana2006 refinement data and are given Table 3.4. It can be seen from the table that the value of crystallite size increases with increasing 'x' values of the formula; $Mg_{(3-x)}Mn_x(BO_3)_2$ (x= 0, 0.01, 0.05, and 0.10). Obviously, it proves that doping of manganese (II) ion affect crystallite size of compounds.

Table 3.4 Details of Jana2006 refinement and structural parameters of $Mg_{(3-x)}Mn_x(BO_3)_2$ (x= 0, 0.01, 0.05, and 0.10)

Samples	***x = 0.00***	***x = 0.01***	***x = 0.05***	***x = 0.10***
Diffractometer	Rigaku	Rigaku	Rigaku	Rigaku
Radiation type	Cu Kα	Cu Kα	Cu Kα	Cu Kα
Monochromator	Graphite	Graphite	Graphite	Graphite
Wavelength (Å)	1.5405	1.5405	1.5405	1.5405
Refined profile range(^{o}2θ)	6.00-70.00	6.00-70.00	6.00-70.00	6.00-70.00
Step size (^{o}2θ)	0.02	0.02	0.02	0.02
GOF	1.90	1.69	1.73	1.51
R_P	8.92	10.2	12.64	10.93
R_{WP}	15.35	13.29	15.35	15.41
Symmetry	orthorhombic	orthorhombic	Orthorhombic	orthorhombic
Space Group	Pnnm	Pnnm	Pnnm	Pnnm
a (Å)	5.399(9)	5.406(3)	5.410(4)	5.414(4)
b (Å)	8.424(6)	8.430(4)	8.436(2)	8.444(3)
c (Å)	4.506(5)	4.508(4)	4.508(8)	4.512(0)
α (^{o} degree)	90.000	90.000	90.000	90.000
β (^{o} degree)	90.000	90.000	90.000	90.000
δ (^{o} degree)	90.000	90.000	90.000	90.000
V ($Å^3$)	205.0	205.5	205.7	206.3
d (g/cm^3)	12.35	12.36	12.40	12.56
t (nm)	30.29	32.14	36.16	39.94
S (m^2/g)	16.04	15.05	13.45	11.96

GOF, R_P, R_{WP}: *agreement factors,* ***a, b, and c:*** *latice constants,* ***V:*** *volume,* ***t:*** *crystallite size,* ***d:*** *density and* ***S:*** *specific surface area*

3.2.2. Infrared Spectoscopy Studies

The IR spectra of borate were investigated in literature [78-82] and the characteristic vibration bands are dominated by six strong peaks, situated at 1000 and 1300 cm^{-1}; at 900 and 1000 cm^{-1} and at 710 and 450 cm^{-1} assigned to the antisymmetric stretching (ν_3), the symmetric bending (ν_1) and out/in of plane bend (ν_2) vibrational modes of the B-O ions, respectively.

The IR spectra of products were given in Figure 3.10 and the comparison of IR data of $Mg_{(3-x)}Mn_x(BO_3)_2$ (x= 0.01, 0.05, and 0.10) with kotoite type of magnesium orthoborate prove that all compounds have similiar kotoite vibrational bands, and an additinal peak of relatively small intensity around 1020 cm^{-1}. This band belongs to BO_3 group of impurity phase, $Mg_2B_2O_5$. Our results are summarized in Table 3.5.

In the IR region between 2800cm^{-1}-3800cm^{-1}, the broad bands correspond to the streching vibration of water molecules [80].

Table 3.5 Infrared band wave numbers (cm^{-1}) and Assigments for $Mg_{(3-x)}Mn_x(BO_3)_2$ (x= 0, 0.01, 0.05, and 0.10)

Assignment	**x= 0.00**	**x= 0.01**	**x= 0.05**	**x= 0.10**
ν_2 (BO_3)	733, 657	727, 657	721, 667	723,660
ν_1 (BO_3)	910	908	908	908
ν_3 (BO_3)	1285, 1202	1285, 1194	1285, 1180	1283, 1182
ν_{OH}	3379	3419	3373	3443

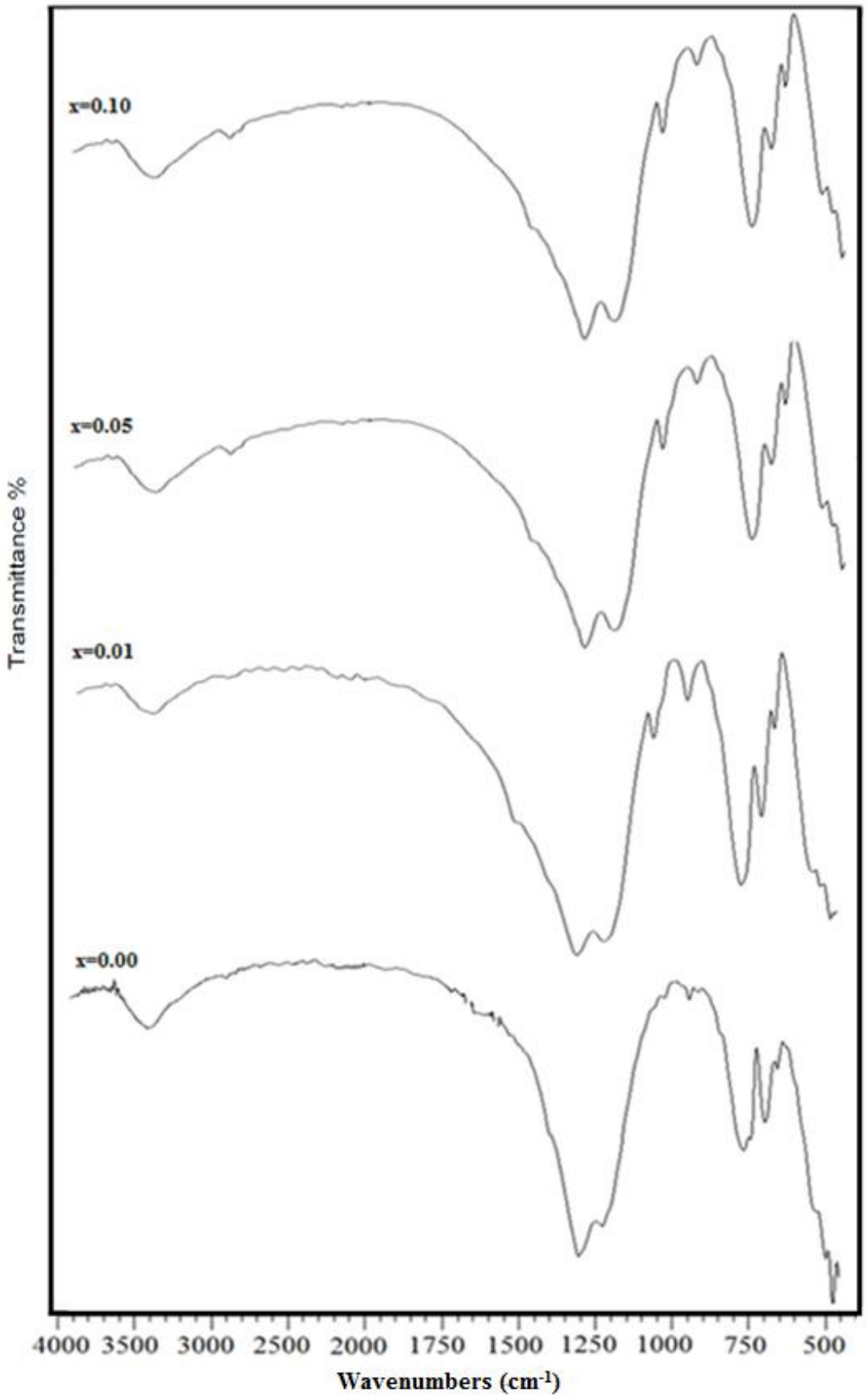

Figure 3.10 IR Spectra of $Mg_{3-x}Mn_x(BO_3)_2$ (x= 0.00, 0.01, 0.05 and 0.10)

3.2.3. SEM and EDX Analysis of $Mg_{3-x}Mn_x(BO_3)_2$

The SEM images of samples, $Mg_{2.99}Mn_{0.01}(BO_3)_2$ and $Mg_{2.90}Mn_{0.10}(BO_3)_2$ are shown in Figure 3.11. The images give information about the particle size and the morphology of products. It can be clearly seen that the uniformity of specimens, regularly grained powder, and the images of $Mg_{2.99}Mn_{0.01}(BO_3)_2$ and $Mg_{2.90}Mn_{0.10}(BO_3)$ are very similar with each other.

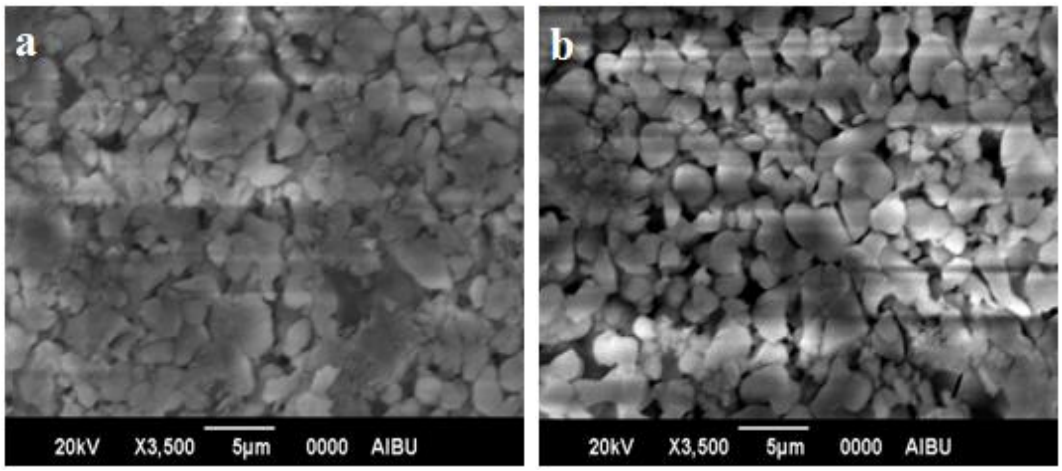

Figure 3.11 SEM images of a) $Mg_{2.99}Mn_{0.01}(BO_3)_2$ and b) $Mg_{2.90}Mn_{0.10}(BO_3)_2$

Through EDX analysis, shown in Figure 3.12 to 3.14, it was determined that the intensities of peaks attributed to manganese increase with increasing 'x' values at formula, $Mg_{(3-x)}Mnx(BO_3)_2$ as 0.01, 0.05, and 0.10 as expected.

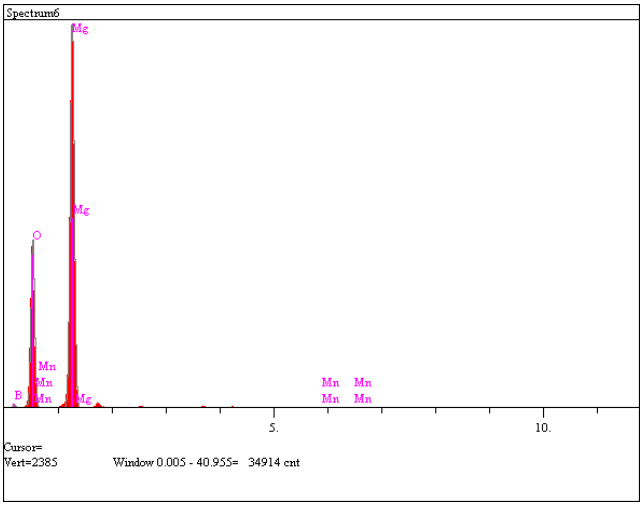

Figure 3.12 EDX spectrum of $Mg_{2.99}Mn_{0.01}(BO_3)_2$

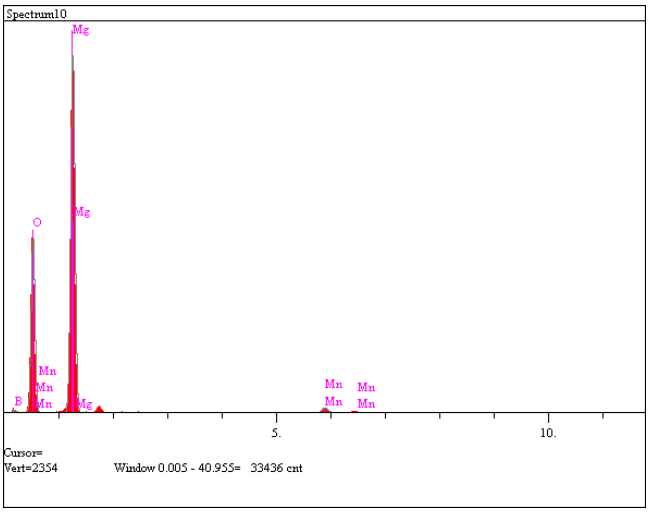

Figure 3.13 EDX spectrum of $Mg_{2.95}Mn_{0.05}(BO_3)_2$

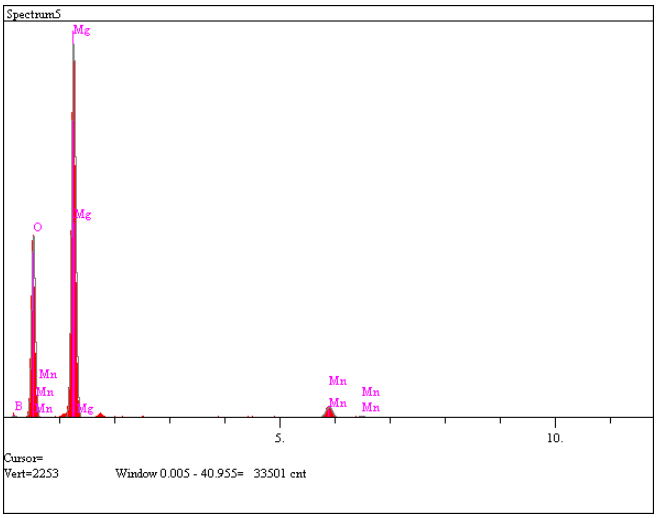

Figure 3.14 EDX spectrum of $Mg_{2.90}Mn_{0.10}(BO_3)_2$

3.2.4. Thermal Studies (DTA-TG) of $Mg_{3-x}Mn_x(BO_3)_2$ (x = 0, 0.01, 0.05,and 0.10)

The DTA/TG curves of the magnesium orthoborate with manganese(II), $Mg_{(3-x)}Mn_x(BO_3)_2$ (x = 0, 0.01, 0.05, and 0.10) are given from Figure 3.15 to Figure 3.18, respectively. The heating rate was 10^oC/min in temperature range from room temperature to 1400^oC. The curves indicate that these doped coumpounds are thermodynamically stable up to 1380 ^oC and there are very small amount of weight loss in these temperature ranges. In addition to these, as amount of manganase increases, the melting point of doped samples changes. It proves that manganase presences in kotoite type of magnesium orthoborate.

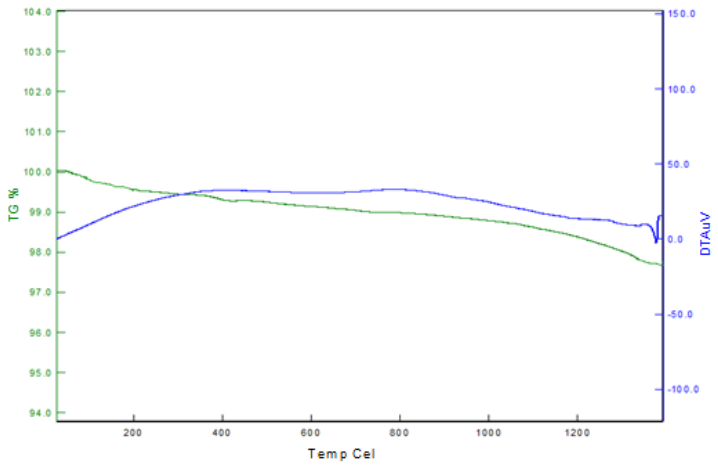

Figure 3.15 DTA/TG of $Mg_3(BO_3)_2$

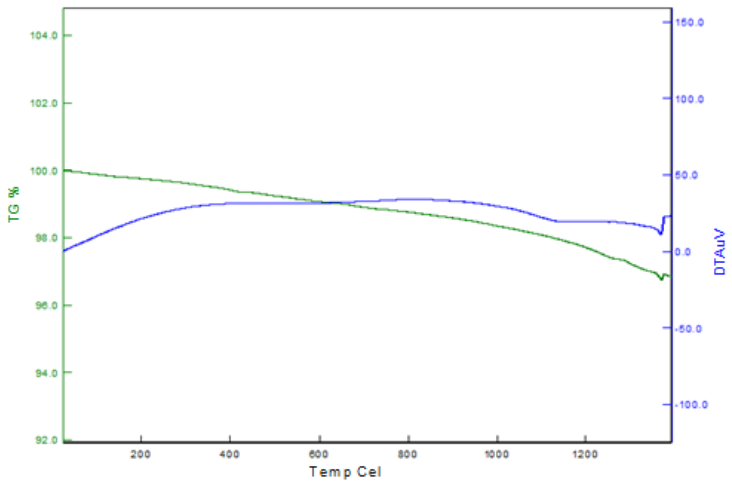

Figure 3.16 DTA/TG of $Mg_{2.99}Mn_{0.01}(BO_3)_2$

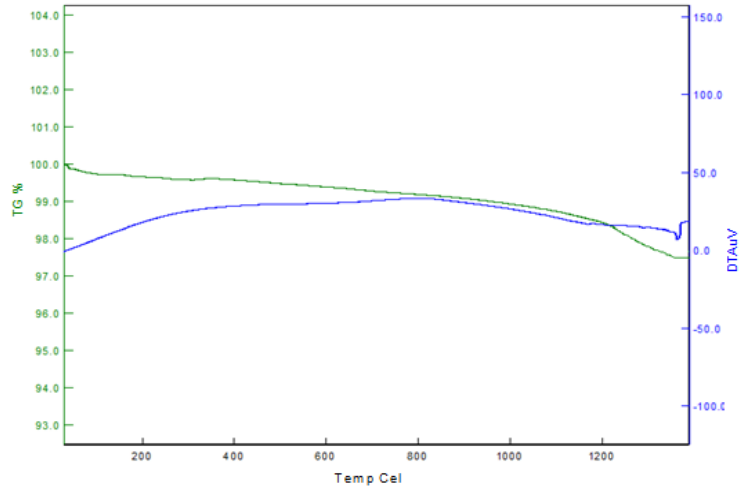

Figure 3.17 DTA/TG of $Mg_{2.95}Mn_{0.05}(BO_3)_2$

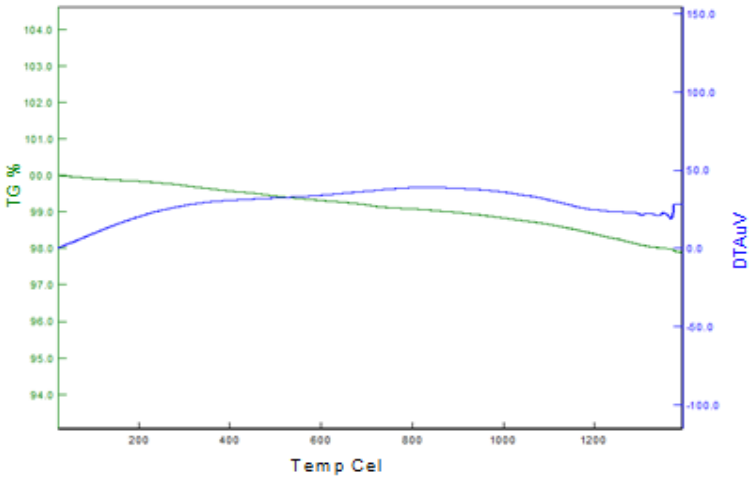

Figure 3.18 DTA/TG of $Mg_{2.90}Mn_{0.10}(BO_3)_2$

3.3. Synthesis of $Co_{3-x}Mn_x(BO_3)_2$ (x = 0, 0.01, 0.05, and 0.10)

The chemical reactions for the solid state synthesis of manganase (II) ion doped to cobalt orthoborate to obtain the $Co_{3-x}Mn_x(BO_3)_2$ (x = 0, 0.01, 0.05, 0.10) compounds, not reported in the literature, could be predicted as below;

$$(3-x)Co(NO_3)_2.6H_2O_{(s)} + xMnSO_4.H_2O_{(s)} + 2H_3BO_{3(s)} \rightarrow \mathbf{Co_{(3-x)}Mn_x(BO_3)_{2(s)}} + (18-6x)NO_{2(g)} + xSO_{2(g)} + (21-5x)H_2O_{(g)} + 1.5O_{2(g)}$$

(x = 0, 0.01, 0.05, 0.10)

3.3.1. X-ray Power Diffraction (XRD) Studies

The products obtained from different doped amount of magnesium (II) ions to cobalt orthoborate were subjected to X-ray powder diffraction analysis. The diffraction patterns observed for the each products $Co_3(BO_3)_2$, $Co_{2.99}Mn_{0.01}(BO_3)_2$, $Co_{2.95}Mn_{0.05}(BO_3)_2$, and $Co_{2.90}Mn_{0.10}(BO_3)_2$ were found to be similar (Figure 3.20). The color of products became darker from purple to dark purple with increasing doping amount of manganese (II), digital photo of $Co_{3-x}Mn_x(BO_3)_2$ (x= 0, 0.01, 0.05 and 0.10) were given in Figure 3.19.

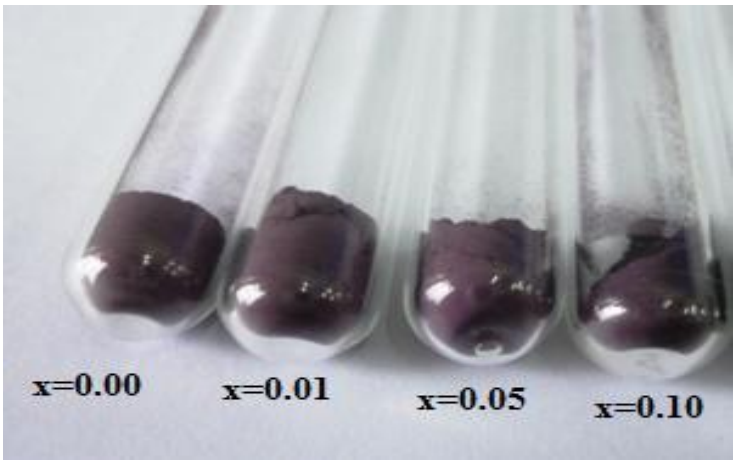

Figure 3.19 Digital photo of $Co_{3-x}Mn_x(BO_3)_2$ (x= 0, 0.01, 0.05 and 0.10)

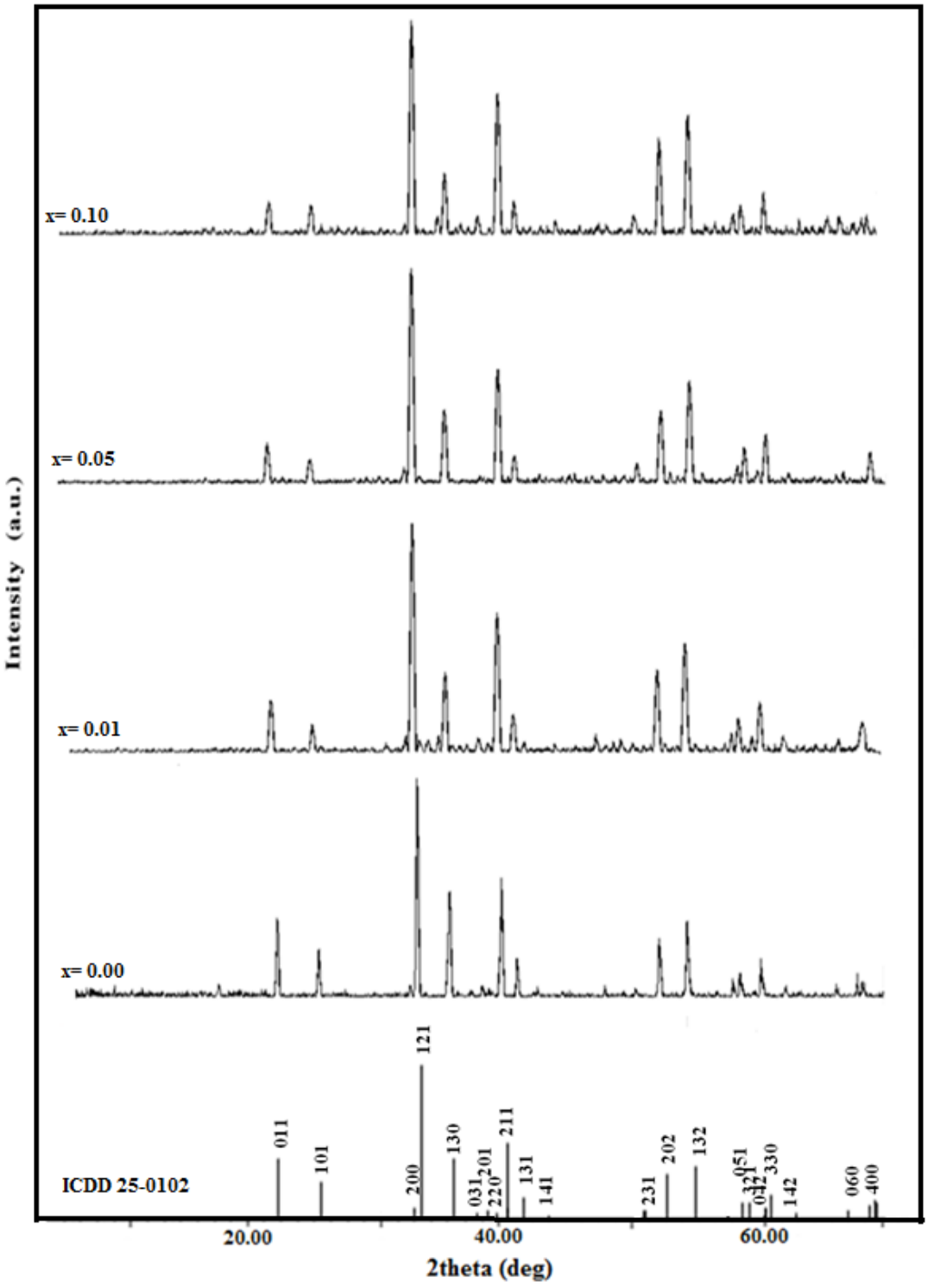

Figure 3.20 XRD Patterns of $Co_{3-x}Mn_x(BO_3)_2$ (x= 0, 0.01, 0.05 and 0.10) and ICDD 25-0102

In the analysis of the XRD patterns of the products, $Co_{3-x}Mn_x(BO_3)_2$ (x = 0.01, 0.05, 0.10), kotoite form of cobalt orthoborate lines (ICDD card No. 25-0102) were clearly observed and all lines in the XRD patterns were indexed in the orthorhombic crystal system, and details of indexes were given in Table 3.6 to 3.8, sequentially.

The refined unit cell parameters were calculated as a= 5.469(7), b= 8.451(2), c= 4.533(5) Å for $Co_{2.99}Mn_{0.01}(BO_3)_2$; a= 5.469(9), b= 8.452(8), c= 4.533(8) Å for $Co_{2.95}Mn_{0.05}(BO_3)_2$ and a= 4.483(4), b= 8.476(4), c= 4.538(4) Å for $Co_{2.90}Mn_{0.10}(BO_3)_2$. It is clearly seen that the powder data of products were found to be almost identical with previously reported kotoite type of $Co_3(BO_3)_2$ [33,43]. Change of lattice parameters with increasing Mn content x is shown in Fig. 3.21. The probable reason can be related that manganese ion, $r_{Mn(II)}$ = 0.97 ˚A, has the larger ionic radius than cobalt ion, $r_{Co(II)}$ = 0.88 ˚A [85].

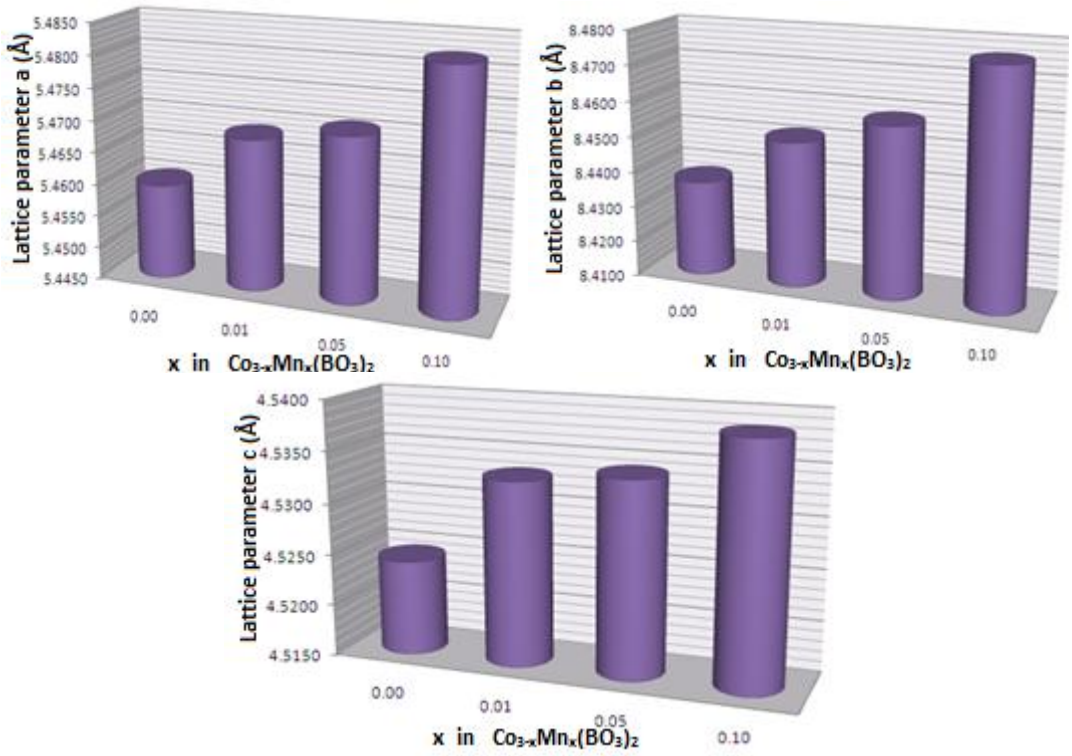

Figure 3.21 Lattice parameters of $Co_{(3-x)}Mn_x(BO_3)_2$ as a function of substitution Mn content

Table 3.6 The X-ray Powder Diffraction Data of $Co_{2.99}Mn_{0.01}(BO_3)_2$ with refined cell parameters, a= 5.469(7), b= 8.451(2), c= 4.533(5) Å

No	**hkl**	**I/I_0**	**$\sin^2(\theta)_{obs}$**	**$\sin^2(\theta)_{cal}$**	**d_{obs} (Å)**	**d_{cal} (Å)**	**XRD data of $Co_3(BO_3)_2$ (ICDD 25-0102)**	
							d values	**I/I_0**
1	011	23	0.0377	0.0374	3.969	3.988	3.994	40
2	101	11	0.0494	0.0491	3.465	3.476	3.489	25
3	200	7	0.0805	0.0802	2.715	2.719	2.734	9
4	121	100	0.0828	0.0827	2.677	2.678	2.689	100
5	130	34	0.0955	0.0956	2.492	2.491	2.503	40
6	031	4	0.1044	0.1046	2.384	2.381	2.391	6
7	201	6	0.1095	0.1092	2.328	2.331	2.341	8
8	220	3	0.1133	0.1137	2.288	2.284	2.295	6
9	211	60	0.1174	0.1176	2.248	2.246	2.255	50
10	131	17	0.1246	0.1247	2.182	2.181	2.190	16
11	231	4	0.1836	0.1841	1.798	1.795	1.800	8
12	202	35	0.1961	0.1962	1.739	1.739	1.744	30
13	132	48	0.2118	0.2113	1.674	1.675	1.678	35
14	051	6	0.2378	0.2377	1.579	1.580	1.582	12
15	321	14	0.2425	0.2425	1.564	1.564	1.569	13
16	042	6	0.2506	0.2497	1.539	1.541	1.544	4
17	330	21	0.2546	0.2550	1.526	1.525	1.529	18
18	142	7	0.2687	0.2695	1.486	1.484	1.486	6
19	060	6	0.3031	0.3005	1.398	1.405	1.376	10
20	400	13	0.3180	0.3201	1.366	1.361	1.366	12

Table 3.7 The X-ray Powder Diffraction Data of $Co_{2.95}Mn_{0.05}(BO_3)_2$ with refined cell parameters, a= 5.469(9), b= 8.452(8), c= 4.533(8) Å

No	hkl	I/I_0	$\sin^2(\theta)_{obs}$	$\sin^2(\theta)_{cal}$	d_{obs} (Å)	d_{cal} (Å)	XRD data of $Co_3(BO_3)_2$ (ICDD 25-0102)	
							d values	I/I_0
1	011	19	0.0378	0.0375	3.959	3.978	3.994	40
2	101	11	0.0494	0.0492	3.465	3.473	3.489	25
3	200	7	0.0892	0.0802	2.719	2.719	2.734	9
4	121	100	0.0831	0.0827	2.672	2.678	2.689	100
5	130	34	0.0955	0.0954	2.492	2.494	2.503	40
6	201	3	0.1102	0.1096	2.320	2.326	2.341	8
7	220	2	0.1135	0.1136	2.288	2.285	2.295	6
8	211	53	0.1175	0.1177	2.246	2.245	2.255	50
9	131	13	0.1248	0.1246	2.180	2.182	2.190	16
10	141	3	0.1776	0.1832	1.827	1.800	1.805	7
11	231	9	0.1841	0.1846	1.795	1.793	1.800	8
12	202	34	0.1966	0.1967	1.737	1.737	1.744	30
13	132	47	0.2118	0.2120	1.673	1.673	1.678	35
14	051	7	0.2384	0.2386	1.577	1.577	1.582	12
15	321	16	0.2431	0.2430	1.562	1.562	1.569	13
16	042	5	0.2513	0.2506	1.536	1.538	1.544	4
17	330	23	0.2552	0.2557	1.524	1.523	1.529	18
18	142	5	0.2687	0.2706	1.485	1.481	1.486	6
19	060	5	0.3019	0.3016	1.401	1.402	1.376	10
20	400	14	0.3183	0.3191	1.365	1.364	1.366	12

Table 3.8 The X-ray Powder Diffraction Data of $Co_{2.90}Mn_{0.10}(BO_3)_2$ with refined cell parameters, a= 4.483(4), b= 8.476(4), c= 4.538(4) Å

No	hkl	I/I_0	$\sin^2(\theta)_{obs}$	$\sin^2(\theta)_{cal}$	d_{obs} (Å)	d_{cal} (Å)	XRD data of $Co_3(BO_3)_2$ (ICDD 25-0102)	
							d values	I/I_0
1	011	16	0.0383	0.0381	3.934	3.948	3.994	40
2	101	14	0.0501	0.0498	3.441	3.451	3.489	25
3	200	4	0.0809	0.0810	2.707	2.706	2.734	9
4	121	100	0.0836	0.0838	2.663	2.661	2.689	100
5	130	29	0.0964	0.0967	2.481	2.476	2.503	40
6	031	6	0.1027	0.1060	2.403	2.365	2.391	6
7	201	9	0.1099	0.1101	2.324	2.312	2.341	8
8	220	3	0.1147	0.1150	2.274	2.271	2.295	6
9	211	67	0.1183	0.1188	2.240	2.234	2.255	50
10	131	16	0.1256	0.1259	2.174	2.171	2.190	16
11	231	9	0.1837	0.1870	1.798	1.781	1.800	8
12	202	44	0.1972	0.1982	1.734	1.730	1.744	30
13	132	55	0.2124	0.2129	1.672	1.669	1.678	35
14	051	8	0.2379	0.2381	1.579	1.578	1.582	12
15	321	13	0.2423	0.2427	1.565	1.563	1.569	13
16	330	20	0.2561	0.2563	1.522	1.521	1.529	18
17	142	6	0.2774	0.2775	1.462	1.462	1.486	6
18	060	7	0.2942	0.2946	1.420	1.419	1.407	7
19	123	8	0.3013	0.3015	1.403	1.403	1.376	10
20	251	7	0.3157	0.3152	1.370	1.363	1.369	14
21	400	10	0.3186	0.3191	1.364	1.364	1.366	12

Refined unit cell parameters are found using the program Jana2006, refinement details of Jana2006 and calculated structural parameters of $Co_{3-x}Mn_x(BO_3)_2$ (x = 0.01, 0.05, 0.10) such as crystallite size (t), density (d) and specific surface area (S) to observe the effect of doping of manganese (II) to orthoborate are given in Table 3.9. The measurements show that these compounds have slightly greater crystallite size than $Co_3(BO_3)_2$, and as doping amount of manganese (II) increases, linearly increasing of the crystallite size of these compounds was observed.

Table 3.9 Details of Jana2006 refinement and structural parameters of $Co_{(3-x)}Mn_x(BO_3)_2$ (x= 0, 0.01, 0.05, and 0.10)

Samples	***x = 0.00***	***x = 0.01***	***x = 0.05***	***x = 0.10***
Diffractometer	Rigaku	Rigaku	Rigaku	Rigaku
Radiation type	Cu Kα	Cu Kα	Cu Kα	Cu Kα
Monochromator	Graphite	Graphite	Graphite	Graphite
Wavelength (Å)	1.5405	1.5405	1.5405	1.5405
Refined profile range(^{o}2θ)	6.00-70.00	6.00-70.00	6.00-70.00	6.00-70.00
Step size (^{o}2θ)	0.02	0.02	0.02	0.02
GOF	1.29	1.01	1.02	1.03
R_P	2.26	2.83	2.83	3.00
R_{WP}	3.21	3.67	3.65	3.90
Symmetry	orthorhombic	orthorhombic	orthorhombic	orthorhombic
Space Group	Pnnm	Pnnm	Pnnm	Pnnm
a (Å)	5.459(8)	5.469(7)	5.469(9)	5.483(4)
b (Å)	8.434(9)	8.451(2)	8.452(8)	8.476(4)
c (Å)	4.524(3)	4.533(5)	4.533(8)	4.538(4)
α (^{o} degree)	90.000	90.000	90.000	90.000
β (^{o} degree)	90.000	90.000	90.000	90.000
δ (^{o} degree)	90.000	90.000	90.000	90.000
V ($Å^3$)	208.4	209.6	209.6	210.9
d (g/cm^3)	18.77	18.66	18.64	18.51
t (nm)	38.85	39.42	41.30	43.38
S (m^2/g)	8.23	8.15	7.79	7.47

GOF, R_P, R_{WP}: *agreement factors,* ***a, b, and c:*** *latice constants,* ***V:*** *volume,* ***t:*** *crystallite size,* ***d:*** *density and* ***S:*** *specific surface area*

3.3.2. Infrared Spectoscopy Studies

Infrared spectra of the kotoite type cobalt orthoborate compounds doped with different amount of manganese (II) ion are shown in Fig. 3.22, where the bands at around 1250 cm^{-1} may be assigned as the BO_3 antisymmetric stretching vibrations (ν_3); the bands in the frequency range 900 cm^{-1} owing to symmetric stretching vibrations; the bands in the frequency range 624.9–705.9 cm^{-1} caused by the out-of-plane bending vibrations (ν_2); the bands at about 540.0 cm^{-1} due to the in plane bending modes (ν_1), and those below 500 cm^{-1} attributed to lattice vibrations [28-54].

The characteristic strectching and bending vibration modes of assigned as the BO_3^{3-} in $Co_{2.99}Mn_{0.01}(BO_3)_2$ are at ν_3: 1251, 1175 cm^{-1}; ν_2: 705, 682, 623 cm^{-1}; ν_1: 546 cm^{-1}.

1252, 1171 cm^{-1} (ν_3); 708, 681, 625 cm^{-1} (ν_2); and 547 cm^{-1} (ν_1) vibration bands were observed in the IR spectrum of $Co_{2.95}Mn_{0.05}(BO_3)_2$.

The absoption bands of $Co_{2.90}Mn_{0.10}(BO_3)_2$ were observed at 1252, 1167 cm^{-1} (ν_3); 682, 621 cm^{-1} (ν_2); 553 cm^{-1} (ν_1).

It is clearly shown that IR vibration bands of products are in good agreement with that of $Co_3(BO_3)_2$. As a summary, the IR spectra for $Co_{(3-x)}Mn_x(BO_3)_2$ (x= 0, 0.01, 0.05, and 0.10) compounds confirm the existence of the $(BO_3)^{3-}$ groups.

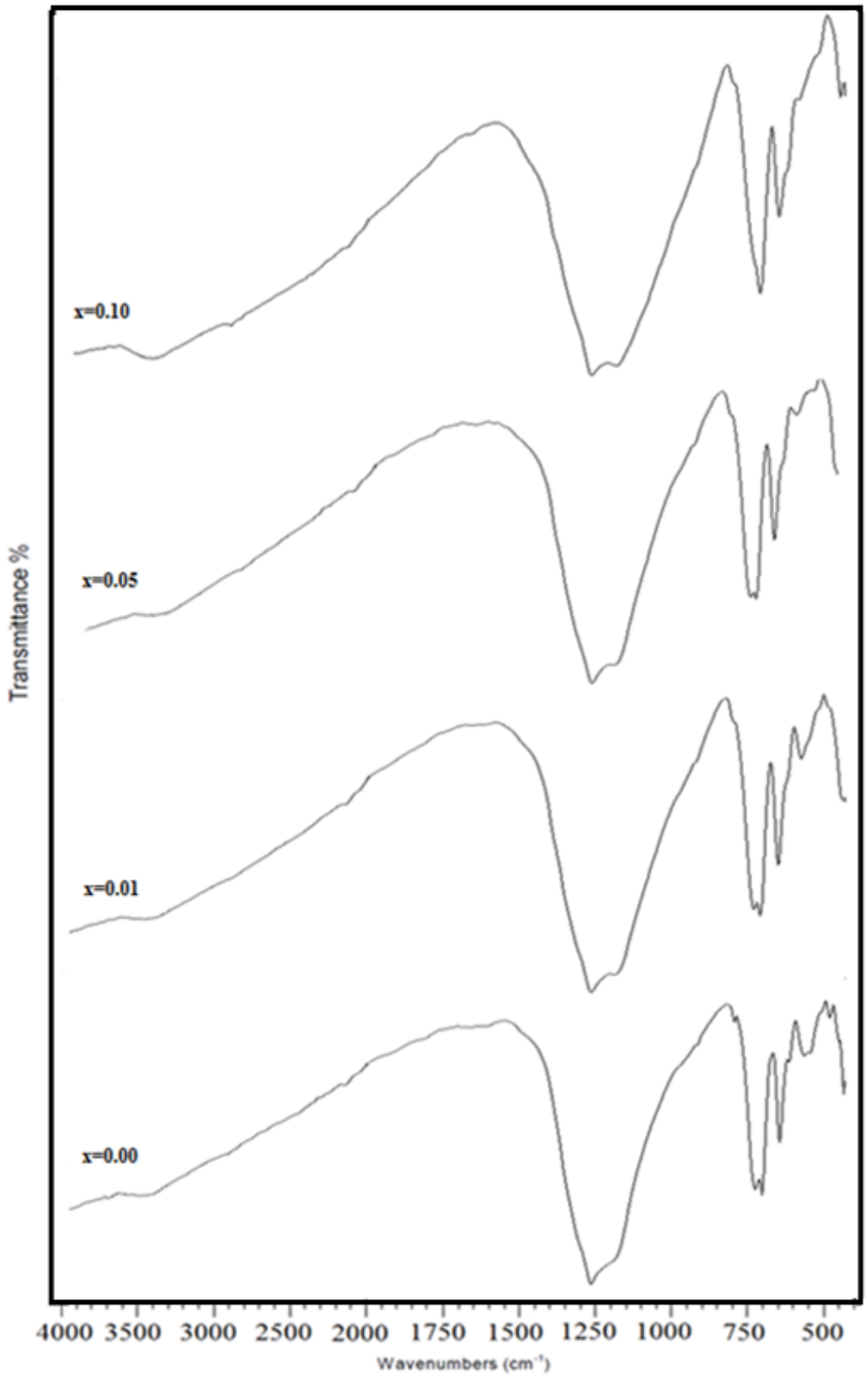

Figure 3.22 IR Spectra of $Co_{3-x}Mn_x(BO_3)_2$ (x= 0.00, 0.01, 0.05 and 0.10)

3.3.3. SEM and EDX Analysis of $Co_{3-x}Mn_x(BO_3)_2$ (x = 0, 0.01, 0.05, and 0.10)

The SEM images of products, $Co_{2.99}Mn_{0.01}(BO_3)_2$, $Co_{2.95}Mn_{0.05}(BO_3)_2$, and $Co_{2.90}Mn_{0.10}(BO_3)_2$ are shown in Figure 3.23.

It can be seen from the images that particle size of $Co_{2.99}Mn_{0.01}(BO_3)_2$ is smaller and agglomerated together to form larger particles than the others. Moreover, for having more amount of doping manganese (II) samples, its surface is smooth and have fine particles. This indicates that the increasing doping amount of manganese (II) inhibits the particle growth.

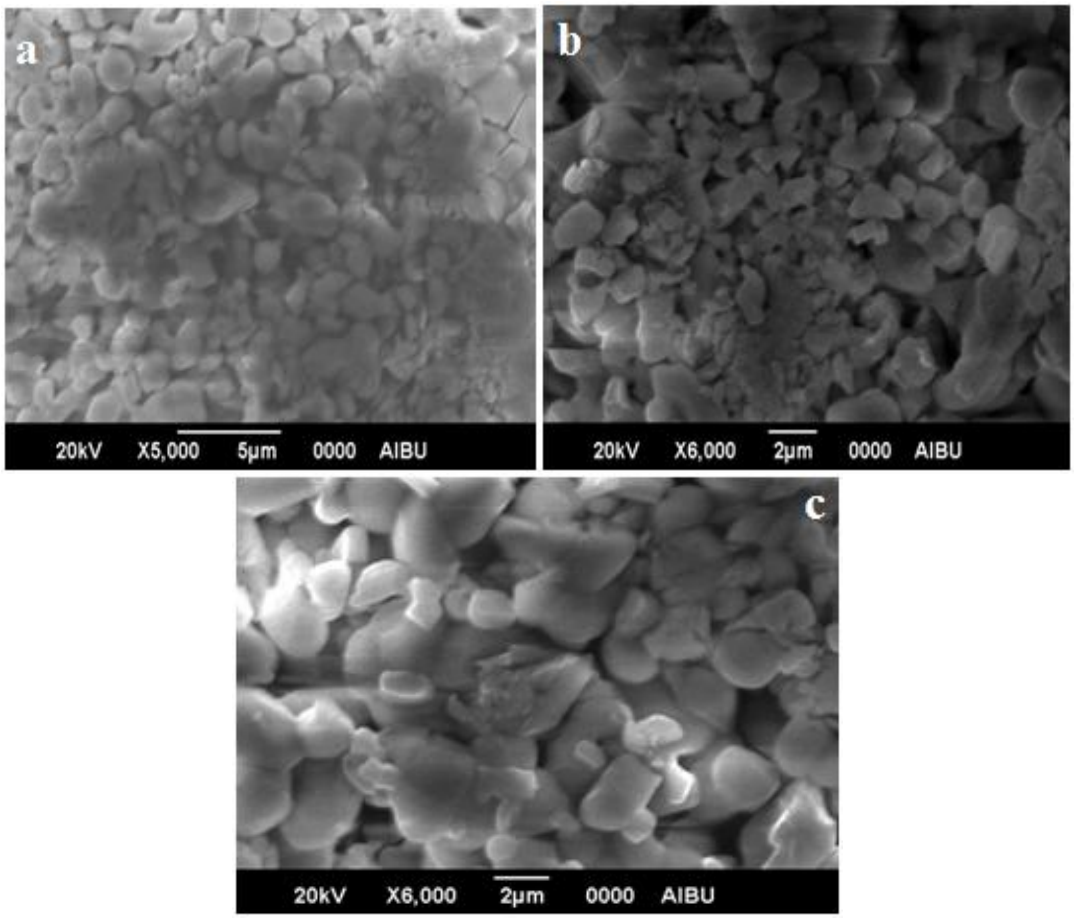

Figure 3.23 SEM images of a) $Co_{2.99}Mn_{0.01}(BO_3)_2$, b) $Co_{2.95}Mn_{0.05}(BO_3)_2$ and c) $Co_{2.90}Mn_{0.10}(BO_3)_2$

The presence of Co, Mn, B, and O elements in $Co_{(3-x)}Mnx(BO_3)_2$ (x=0.01, 0.05, 0.10) were determined through the EDX analysis of the products, shown in Figure 3.24 to 3.26. The analysis shows that the intensities of peaks attirubuted to manganese (II) increase as increasing the doping amount of manganese, as expected.

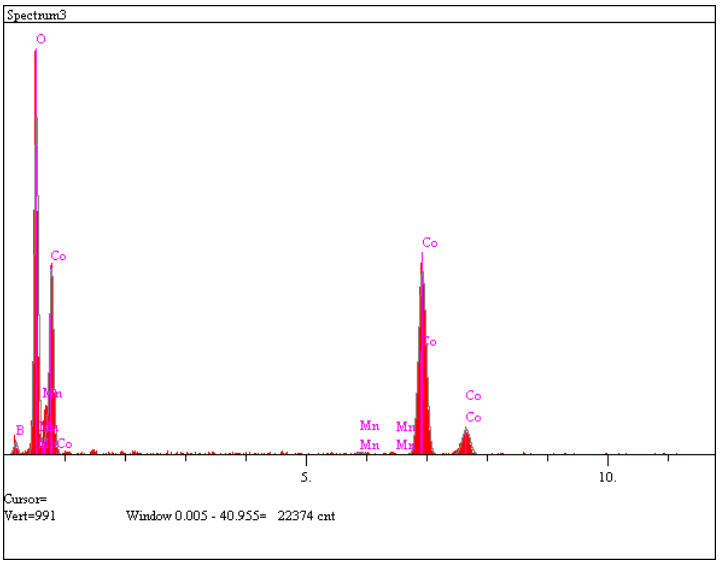

Figure 3.24 EDX spectrum of $Co_{2.99}Mn_{0.01}(BO_3)_2$

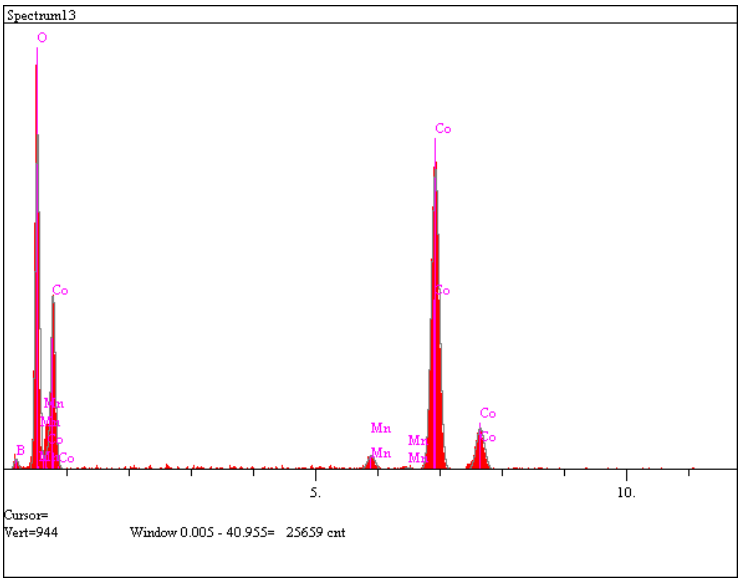

Figure 3.25 EDX spectrum of $Co_{2.95}Mn_{0.05}(BO_3)_2$

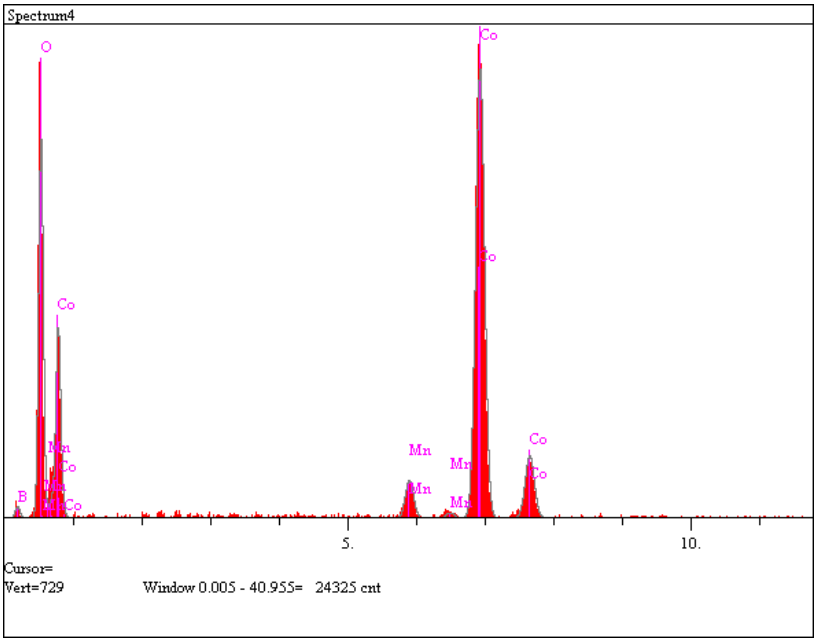

Figure 3.26 EDX spectrum of $Co_{2.90}Mn_{0.10}(BO_3)_2$

3.3.4. Thermal Studies (DTA-TG) of $Co_{3-x}Mn_x(BO_3)_2$ (x = 0, 0.01, 0.05,and 0.10)

The DTA/TG curves of the cobalt orthoborate with manganese(II), $Co_{(3-x)}Mn_x(BO_3)_2$ (x = 0, 0.01, 0.05, and 0.10) are given in Figure 3.27 to Figure 3.30, respectively. The curves indicate that there is no weight loss from 20 to 1170 ^oC. Morover, it shows that these compounds are thermally stable within these temperature ranges. In addition to these, as amount of manganase increases, the melting point of doped samples changes. These changes exhibit that manganase existences in kotoite type of cobalt orthoborate.

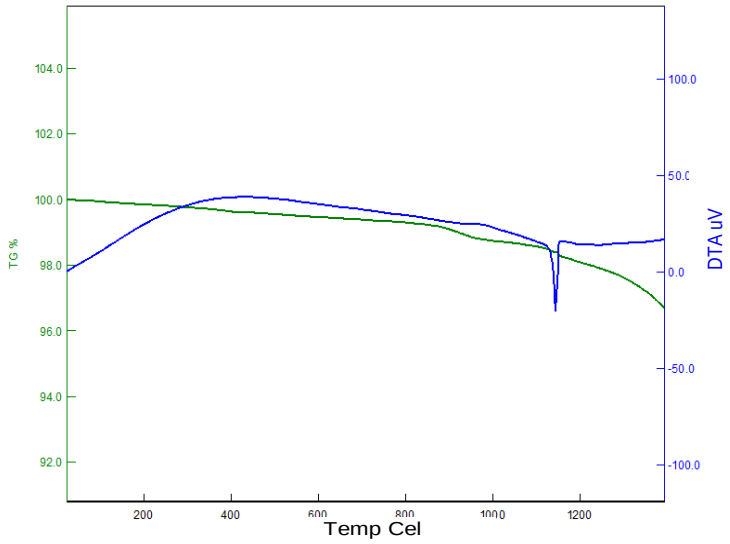

Figure 3.27 DTA/TG of $Co_3(BO_3)_2$

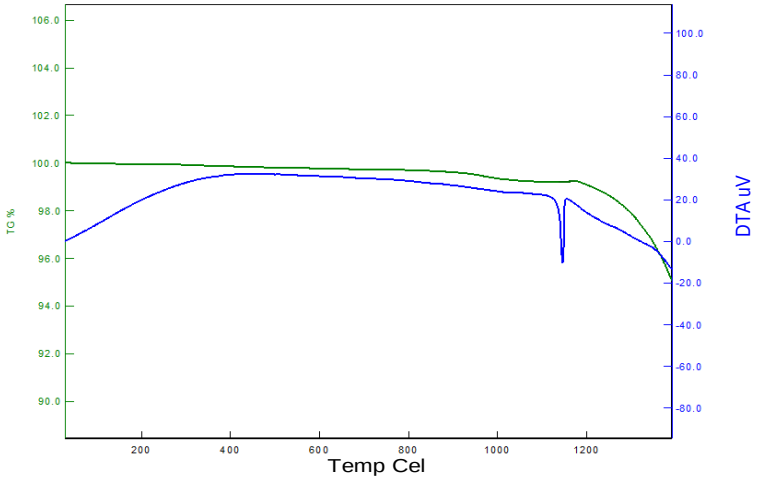

Figure 3.28 DTA/TG of $Co_{2.99}Mn_{0.01}(BO_3)_2$

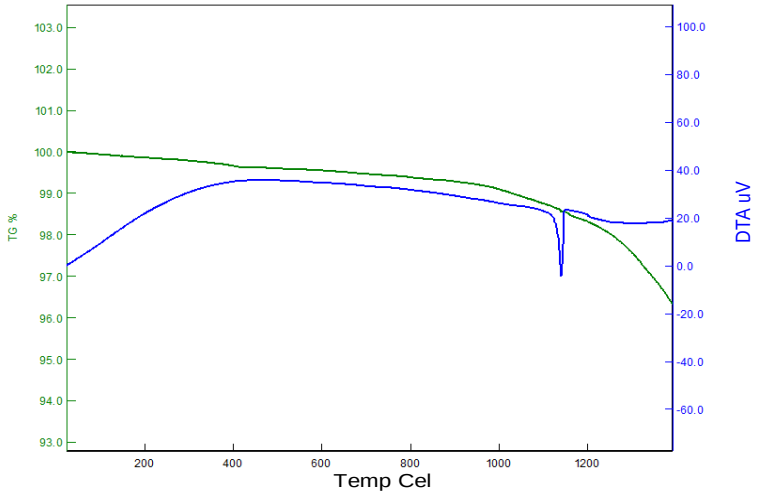

Figure 3.29 DTA/TG of $Co_{2.95}Mn_{0.05}(BO_3)_2$

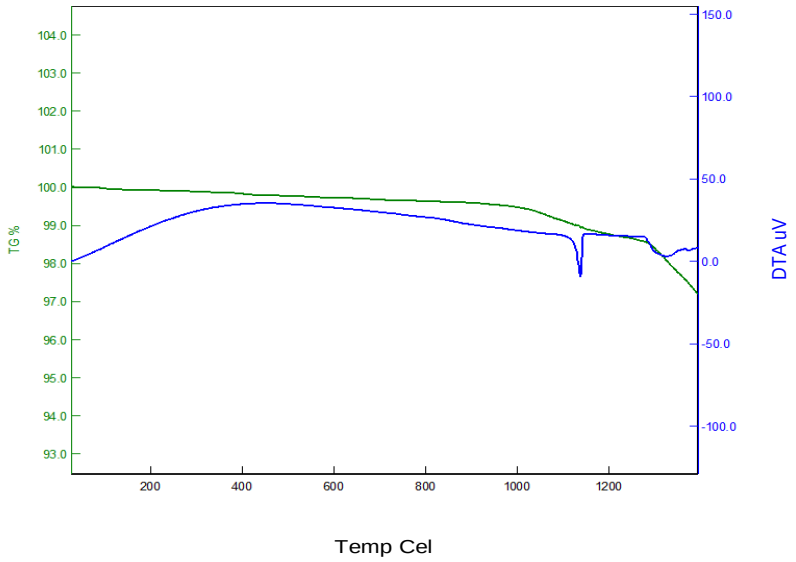

Figure 3.30 DTA/TG of $Co_{2.90}Mn_{0.10}(BO_3)_2$

3.4. Synthesis of $Ni_{3-x}Mn_x(BO_3)_2$ (x = 0, 0.01, 0.05, and 0.10)

$Ni_{3-x}Mn_x(BO_3)_2$ (x = 0, 0.01, 0.05, 0.10) were prepared at 450 ^oC for 4 hours, 600 ^oC for 3 hours, and 4 times at 900 ^oC for 12 hours by using the following scheme:

$$(3\text{-}x)Ni(NO_3)_2.6H_2O_{(s)} + xMnSO_4.H_2O_{(s)} + 2H_3BO_{3(s)} \rightarrow \mathbf{Ni_{(3-x)}Mn_x(BO_3)_{2(s)}} + (18\text{-}6x)NO_{2(g)} + xSO_{2(g)} + (21\text{-}5x)H_2O_{(g)} + 1.5O_{2(g)}$$

(x = 0, 0.01, 0.05, 0.10)

3.4.1. X-ray Power Diffraction (XRD) Studies

The XRD patterns of obtained products, $Ni_{(3-x)}Mn_x(BO_3)_2$, from the reactions of different amount of $MnSO_4.H_2O$ with $Ni(NO_3)_2.6H_2O$ and H_3BO_3 were shown in Figure 3.32. When the powder data of products were compared the XRD data of

kotite type of $Ni_3(BO_3)_2$, ICDD card No. 75-1809, it was found that results are very similar.

The color of products became darker with increasing of doping amount manganese; $Ni_3(BO_3)_2$ (parrot green), $Ni_{2.99}Mn_{0.01}(BO_3)_2$ (peanut green), $Ni_{2.95}Mn_{0.05}(BO_3)_2$ (greenish brown), and $Ni_{2.90}Mn_{0.10}(BO_3)_2$ (dark greenish brown), photos of pruducts were shown in Figure 3.31.

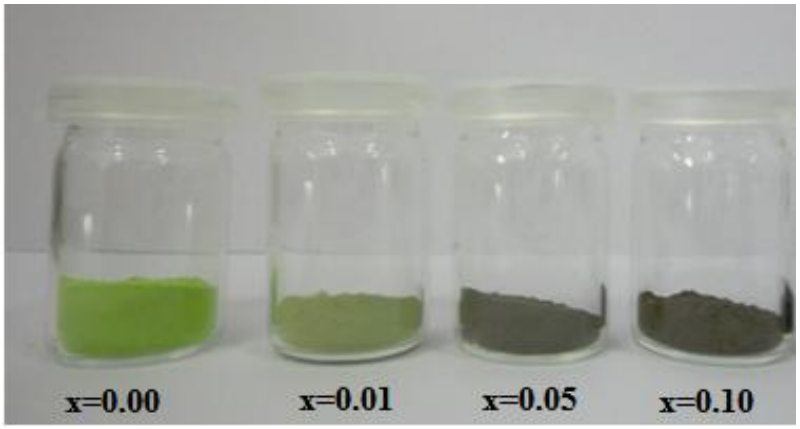

Figure 3.31 Digital photo of $Ni_{3-x}Mn_x(BO_3)_2$ (x= 0, 0.01, 0.05, and 0.10)

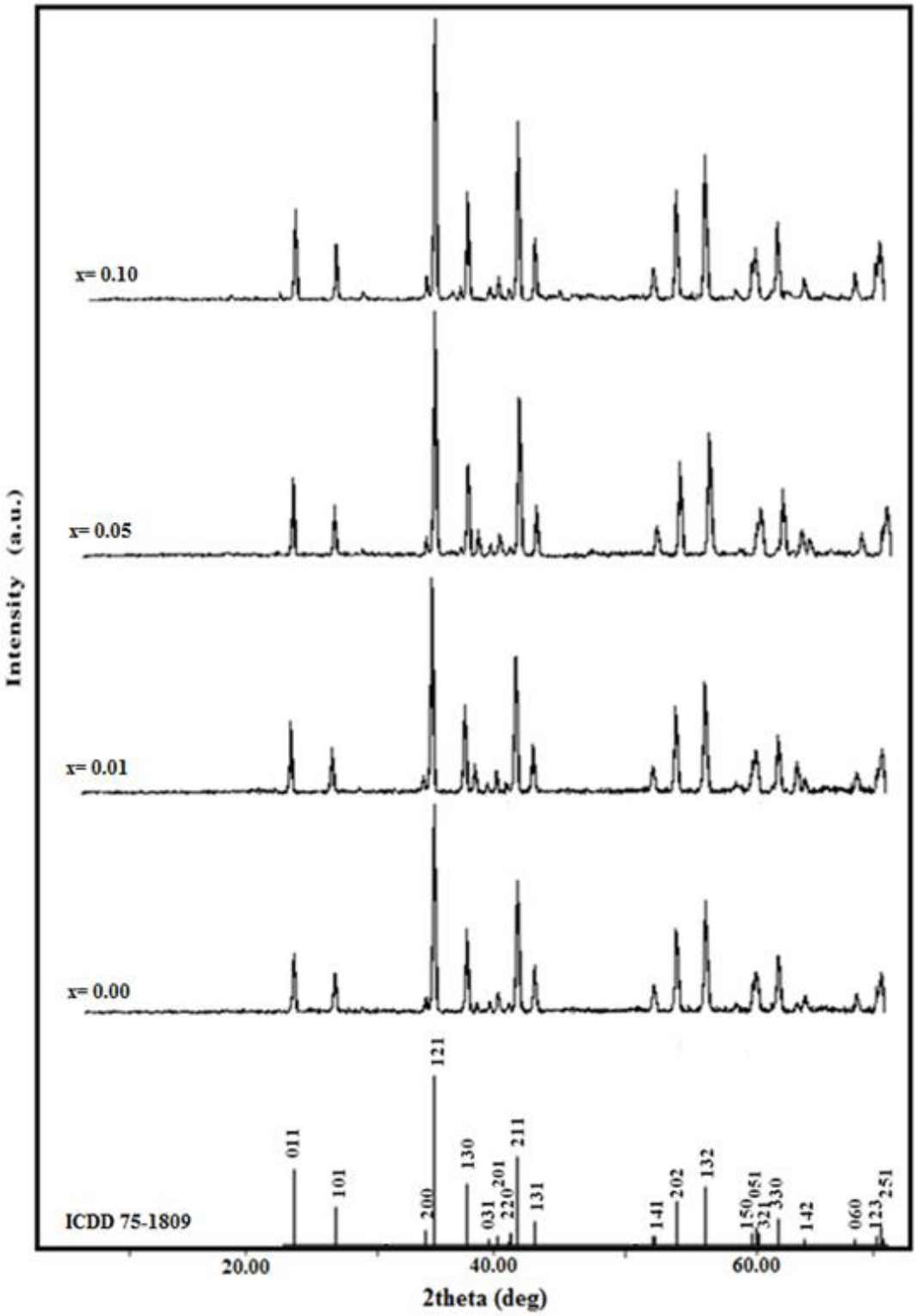

Figure 3.32 XRD Patterns of $Ni_{3-x}Mn_x(BO_3)_2$ (x= 0, 0.01, 0.05, and 0.10) and ICDD 75-1809

Table 3.10 to 3.12 show the details of XRD data of products, $Ni_{2.99}Mn_{0.01}(BO_3)_2$, $Ni_{2.95}Mn_{0.05}(BO_3)_2$, and $Ni_{2.90}Mn_{0.10}(BO_3)_2$, were indexed in the orthorhombic crystal system.

The refined unit cell parameters of $Ni_{3-x}Mn_x(BO_3)_2$ are found as a= 5.397(4), b= 8.301(8), c= 4.458(9) for x=0.01; a= 5.403(6), b= 8.306(6), c= 4.460(3) and for x=0.05 a= 5.404(1), b= 8.310(2), c= 4.463(5) for x= 0.10 using the program Jana2006. These unit cell parameters are close to the reported parameters of the kotoite type, $Ni_3(BO_3)_2$ [42,43]. In addition to these, lattice parameters change with the increasing degree of incorporation of Mn^{2+} ions instead of Ni^{2+} ions place in the crystal lattice (Fig.3.33).

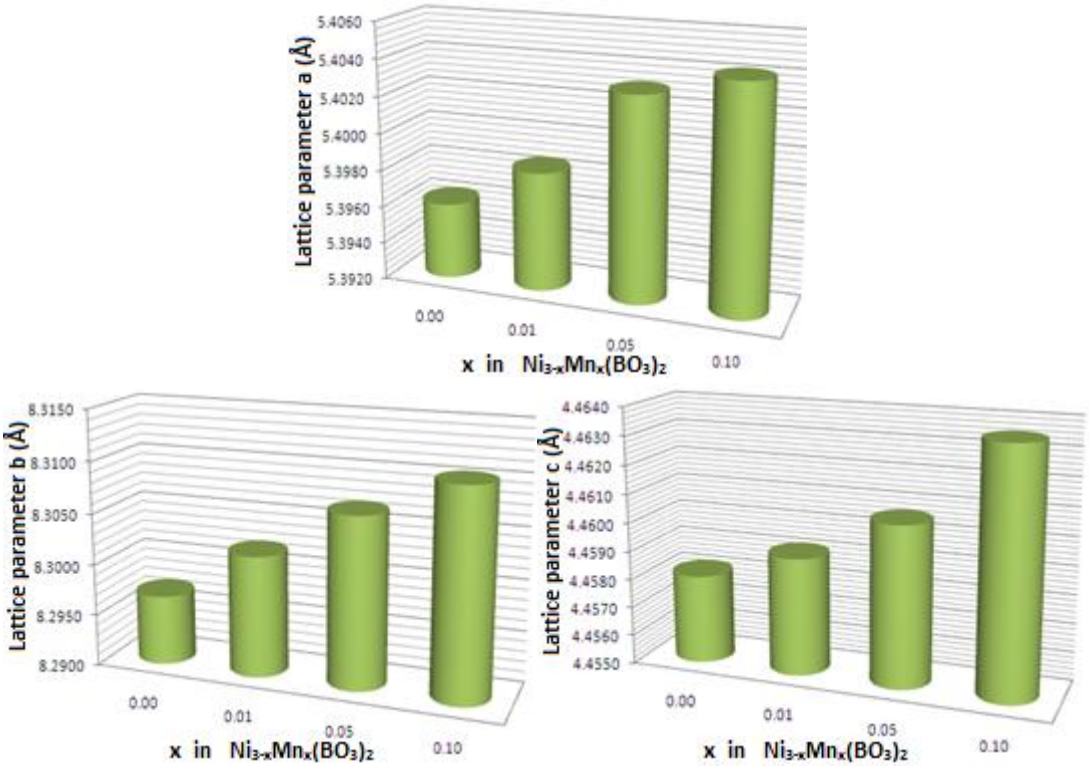

Figure 3.33 Lattice parameters of $Ni_{(3-x)}Mn_x(BO_3)_2$ as a function of substitution Mn content

Table 3.10 The X-ray Powder Diffraction Data of $Ni_{2.99}Mn_{0.01}(BO_3)_2$ with refined cell parameters, a= 5.397(4), b= 8.301(8), c= 4.458(9) Å

No	hkl	I/I_0	$\sin^2(\theta)_{obs}$	$\sin^2(\theta)_{cal}$	d_{obs} (Å)	d_{cal} (Å)	XRD data of $Ni_3(BO_3)_2$ (ICDD 75-1809)	
							d values	I/I_0
1	020	3	0.0345	0.0345	4.145	4.147	4.148	3
2	011	33	0.0386	0.0385	3.917	3.925	3.928	45
3	101	22	0.0504	0.0502	3.429	3.437	3.437	24
4	111	3	0.0591	0.0589	3.168	3.174	3.176	2
5	200	9	0.0817	0.0816	2.695	2.696	2.698	10
6	121	100	0.0848	0.0848	2.644	2.645	2.647	100
7	130	41	0.0982	0.0980	2.458	2.460	2.461	37
8	031	6	0.1078	0.1075	2.346	2.349	2.350	5
9	201	11	0.1116	0.1114	2.305	2.308	2.308	7
10	220	5	0.1160	0.1160	2.262	2.262	2.262	4
11	211	63	0.1201	0.1200	2.222	2.224	2.224	54
12	131	23	0.1278	0.1280	2.154	2.153	2.155	16
13	141	13	0.1886	0.1882	1.774	1.776	1.776	7
14	202	40	0.2010	0.2010	1.718	1.718	1.719	27
15	132	51	0.2174	0.2174	1.652	1.652	1.652	36
16	150	6	0.2359	0.2359	1.586	1.586	1.586	2
17	051	16	0.2453	0.2454	1.555	1.555	1.555	9
18	321	19	0.2476	0.2478	1.548	1.547	1.548	13
19	330	27	0.2608	0.2611	1.508	1.508	1.508	18
20	142	15	0.2725	0.2777	1.476	1.462	1.463	5
21	060	10	0.3102	0.3104	1.383	1.383	1.383	6
22	123	12	0.3233	0.3236	1.355	1.354	1.354	8
23	251	21	0.3262	0.3269	1.349	1.357	1.347	12

Table 3.11 The X-ray Powder Diffraction Data of $Ni_{2.95}Mn_{0.05}(BO_3)_2$ with refined cell parameters, a= 5.403(6), b= 8.306(6), c= 4.460(3) Å

No	hkl	I/I_0	$\sin^2(\theta)_{obs}$	$\sin^2(\theta)_{cal}$	d_{obs} (Å)	d_{cal} (Å)	XRD data of $Ni_3(BO_3)_2$ (ICDD 75-1809)	
							d values	I/I_0
1	020	4	0.0345	0.0345	4.152	4.147	4.148	3
2	011	33	0.0385	0.03855	3.924	3.926	3.928	45
3	101	22	0.0494	0.0498	3.429	3.452	3.437	24
4	111	4	0.0592	0.0589	3.164	3.173	3.176	2
5	200	9	0.0816	0.0816	2.696	2.696	2.698	10
6	121	100	0.0848	0.0847	2.645	2.647	2.647	100
7	130	39	0.0979	0.0980	2.462	2.461	2.461	37
8	031	7	0.1076	0.1074	2.348	2.350	2.350	5
9	201	10	0.1113	0.1114	2.308	2.308	2.308	7
10	220	6	0.1162	0.1161	2.260	2.261	2.262	4
11	211	66	0.1200	0.1200	2.223	2.224	2.224	54
12	131	22	0.1277	0.1277	2.155	2.155	2.155	16
13	141	14	0.1886	0.1882	1.774	1.775	1.776	7
14	202	41	0.2009	0.2009	1.718	1.718	1.719	27
15	132	52	0.2172	0.2173	1.652	1.652	1.652	36
16	150	4	0.2358	0.2359	1.586	1.586	1.586	2
17	051	15	0.2449	0.2453	1.556	1.555	1.555	9
18	321	21	0.2476	0.2475	1.548	1.548	1.548	13
19	330	29	0.2608	0.2610	1.508	1.507	1.508	18
20	142	11	0.2725	0.2777	1.475	1.462	1.463	5
21	060	11	0.3099	0.3103	1.383	1.383	1.383	6
22	123	14	0.3233	0.3235	1.354	1.354	1.354	8
23	251	21	0.3262	0.3268	1.348	1.347	1.347	12

Table 3.12 The X-ray Powder Diffraction Data of $Ni_{2.90}Mn_{0.10}(BO_3)_2$ with refined cell parameters, a= 5.404(1), b= 8.310(2), c= 4.463(5) Å

No	hkl	I/I_0	$\sin^2(\theta)_{obs}$	$\sin^2(\theta)_{cal}$	d_{obs} (Å)	d_{cal} (Å)	XRD data of $Ni_3(BO_3)_2$ (ICDD 75-1809)	
							d values	I/I_0
1	020	4	0.0344	0.0344	4.152	4.153	4.148	3
2	011	33	0.0385	0.0384	3.927	3.931	3.928	45
3	101	22	0.0502	0.0502	3.437	3.438	3.437	24
4	111	4	0.0588	0.0588	3.175	3.177	3.176	2
5	200	10	0.0813	0.0814	2.701	2.699	2.698	10
6	121	100	0.0846	0.0861	2.648	2.648	2.647	100
7	130	39	0.0978	0.0978	2.463	2.463	2.461	37
8	031	7	0.1072	0.1073	2.352	2.352	2.350	5
9	201	10	0.1111	0.1112	2.311	2.310	2.308	7
10	220	4	0.1155	0.1158	2.266	2.264	2.262	4
11	211	66	0.1198	0.1198	2.225	2.225	2.224	54
12	131	23	0.1275	0.1276	2.157	2.156	2.155	16
13	102	5	0.1396	0.1396	2.062	2.062	2.061	3
14	141	14	0.1882	0.1879	1.775	1.777	1.776	7
15	202	40	0.2005	0.2006	1.720	1.720	1.719	27
16	132	52	0.2168	0.2171	1.654	1.653	1.652	36
17	150	7	0.2350	0.2356	1.588	1.587	1.586	2
18	051	15	0.2446	0.2450	1.557	1.556	1.555	9
19	321	20	0.2473	0.2474	1.549	1.549	1.548	13
20	330	29	0.2602	0.2606	1.510	1.509	1.508	18
21	142	10	0.2764	0.2773	1.465	1.463	1.463	5
22	060	12	0.3096	0.3099	1.384	1.383	1.383	6
23	123	14	0.3228	0.3231	1.355	1.355	1.354	8
24	251	21	0.3259	0.3264	1.349	1.348	1.347	12

Refinement patterns of compounds are shown in Figure 3.34 to 3.37 and details of Jana2006 refinement patterns of products and structural parameters such as crystallite size (t), density (d) and specific surface area (S) of products are given Table 3.13. The crystalite size of compounds increased with increasing amount of manganese (II), and it show that these variations are attributed to doped manganese (II).

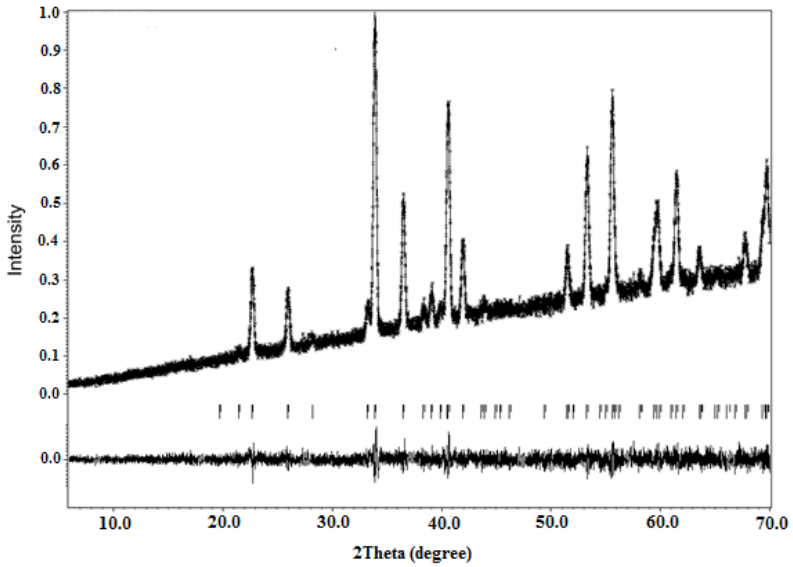

Figure 3.34 Jana2006 refinement pattern of $Ni_3(BO_3)_2$

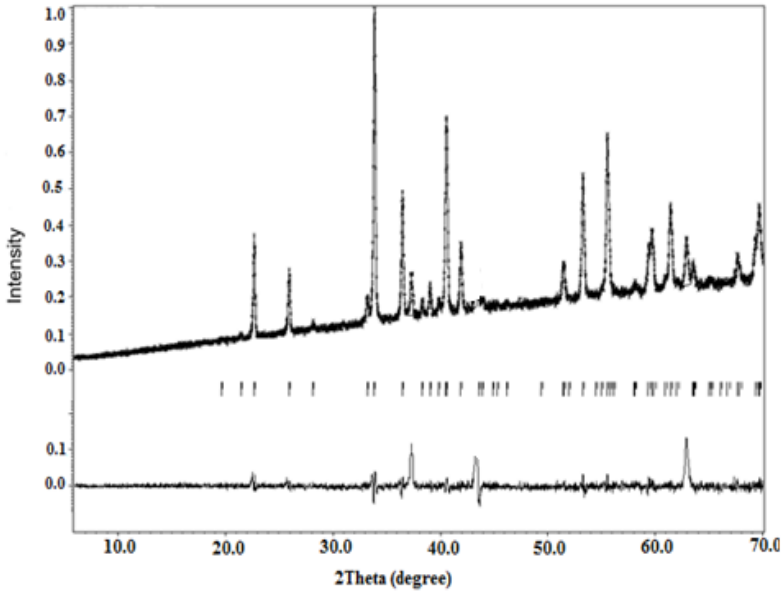

Figure 3.35 Jana2006 refinement pattern of $Ni_{2.99}Mn_{0.01}(BO_3)_2$

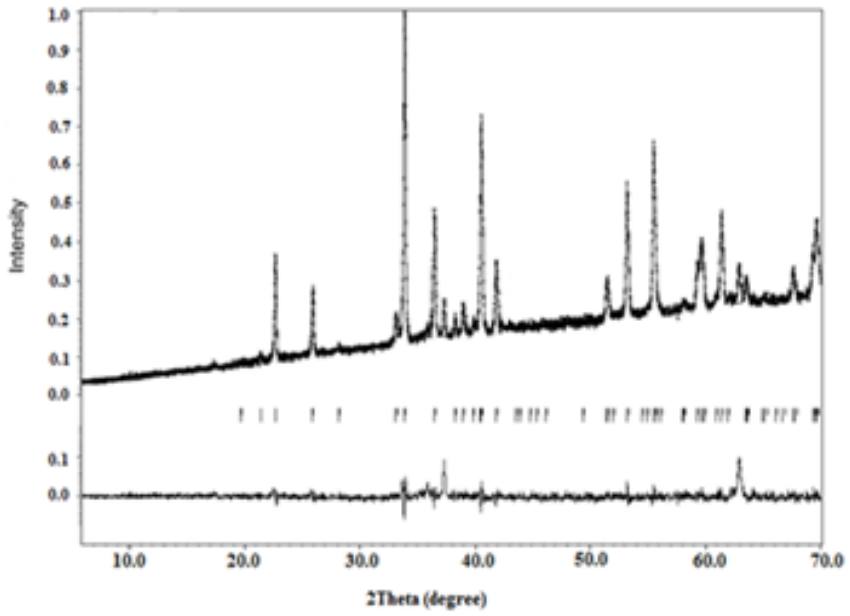

Figure 3.36 Jana2006 refinement pattern of $Ni_{2.95}Mn_{0.05}(BO_3)_2$

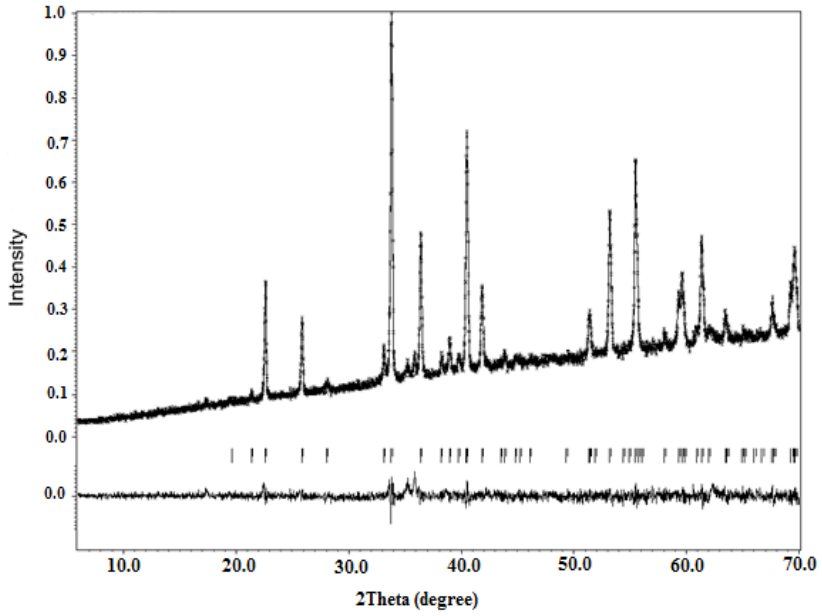

Figure 3.37 Jana2006 refinement pattern of $Ni_{2.90}Mn_{0.10}(BO_3)_2$

Table 3.13 Details of Jana2006 refinement and structural parameters of $Ni_{3-x}Mn_x(BO_3)_2$ (x= 0, 0.01, 0.05, 0.10, and 0.50)

Samples	***x = 0.00***	***x = 0.01***	***x = 0.05***	***x = 0.10***
Diffractometer	Rigaku	Rigaku	Rigaku	Rigaku
Radiation type	Cu Kα	Cu Kα	Cu Kα	Cu Kα
Monochromator	Graphite	Graphite	Graphite	Graphite
Wavelength (Å)	1.5405	1.5405	1.5405	1.5405
Refined profile range(^{o}2θ)	6.00-70.00	6.00-70.00	6.00-70.00	6.00-70.00
Step size (^{o}2θ)	0.02	0.02	0.02	0.02
GOF	1.07	2.25	1.94	1.28
R_P	4.11	3.92	3.89	3.36
R_{WP}	5.39	7.45	6.46	4.53
Symmetry	orthorhombic	Orthorhombic	orthorhombic	orthorhombic
Space Group	Pnnm	Pnnm	Pnnm	Pnnm
a (Å)	5.396(1)	5.397(4)	5.403(6)	5.404(1)
b (Å)	8.296(8)	8.301(8)	8.306(6)	8.310(2)
c (Å)	4.458(5)	4.458(9)	4.460(3)	4.463(5)
α (^{o} degree)	90.000	90.000	90.000	90.000
β (^{o} degree)	90.000	90.000	90.000	90.000
δ (^{o} degree)	90.000	90.000	90.000	90.000
V (Å^3)	196.60	199.80	200.50	200.50
d (g/cm^3)	19.543	19.526	19.451	19.439
t (nm)	24.811	39.468	39.473	41.343
S (m^2/g)	12.376	7.785	7.815	7.466

GOF, R_P, R_{WP}: *agreement factors,* ***a, b, and c:*** *latice constants,* ***V:*** *volume,* ***t:*** *crystallite size,* ***d:*** *density and* ***S:*** *specific surface area*

3.4.2. Infrared Spectoscopy Studies

Figure 3.38 shows the infrared spectra of nickel orthoborate doped with manganese(II), $Ni_{3-x}Mn_x(BO_3)_2$ (x= 0, 0.01, 0.05, and 0.10). In these figures bands are observed in good aggreement with that of the kotoite type nickel orthoborate [30,44].

The characteristic bands are the stretching bands of the highest intensity at around 1178-1298 cm^{-1} may be assigned as the BO_3 antisymmetric stretching vibrations; the bands in the frequency range 628.2–721.4 cm^{-1} caused by the out-of-plane bending vibrations; bands at about 513.0 cm^{-1} due to the in plane bending modes, and those below 500 cm^{-1} attributed to lattice vibrations. Similarly, the absorption band at 3200–3600 cm^{-1} is attributed to water groups [80].

The vibrations and and corresponding assignments of products, $Ni_3(BO_3)_2$, $Ni_{2.99}Mn_{0.01}(BO_3)_2$, $Ni_{2.95}Mn_{0.05}(BO_3)_2$, and $Ni_{2.90}Mn_{0.10}(BO_3)_2$, are summarized in Table 3.14. Obviously, It was seen that $Ni_{3-x}Mn_x(BO_3)_2$ (x= 0, 0.01, 0.05, and 0.10) compounds contains characteristic BO_3^{3-} groups as their basic structural units.

Table 3.14 Infrared band wave numbers (cm^{-1}) and Assigments for $Ni_{2.99}Mn_{0.01}(BO_3)_2$, $Ni_{2.95}Mn_{0.05}(BO_3)_2$, and $Ni_{2.90}Mn_{0.10}(BO_3)_2$

Assignment	$Ni_3(BO_3)_2$	$Ni_{2.99}Mn_{0.01}(BO_3)_2$	$Ni_{2.95}Mn_{0.05}(BO_3)_2$	$Ni_{2.90}Mn_{0.10}(BO_3)_2$
$\nu_2(BO_3)$	603	603	603	604
$\nu_1(BO_3)$	721, 696, 632	721, 696, 631	721, 696, 628	719, 696, 631
$\nu_3(BO_3)$	1294, 1261, 1188	1292, 1257, 1182	1292, 1257, 1178	1298, 1259, 1184
ν_{OH}	3412	3399	3470	3470

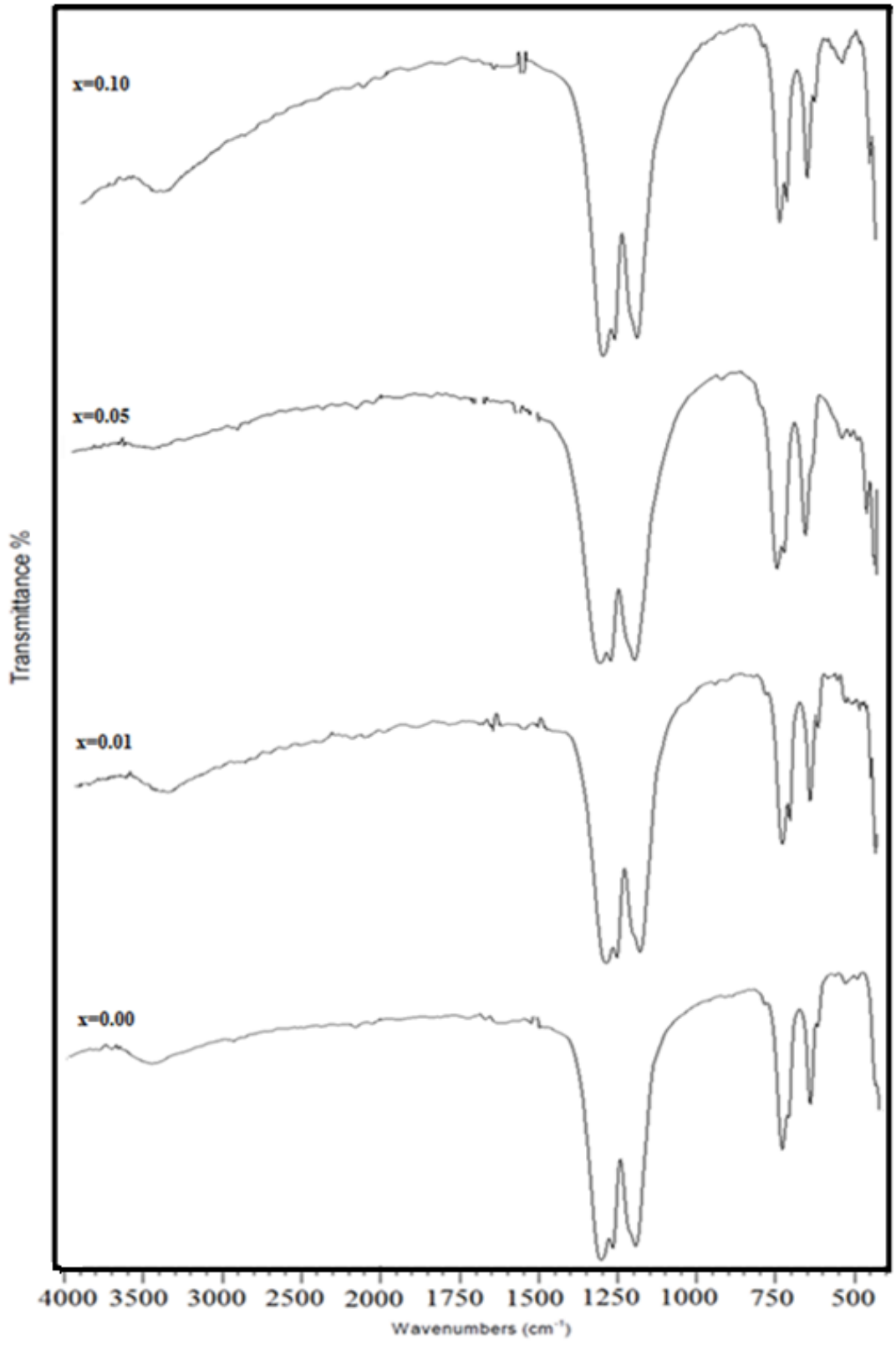

Figure 3.38 IR Spectra of $Ni_{3-x}Mn_x(BO_3)_2$ (x= 0, 0.01, 0.05, 0.10)

3.4.3. SEM and EDX Analysis of $Ni_{3-x}Mn_x(BO_3)_2$

The same morphological feature was also observed in SEM images of the featured surface (Fig 3.39). The image investigations show that the products composition is quite homogeneous and have regularly grained powder. The images of $Ni_{2.99}Mn_{0.01}$ are very similar with that of $Ni_{2.90}Mn_{0.10}(BO_3)_2$.

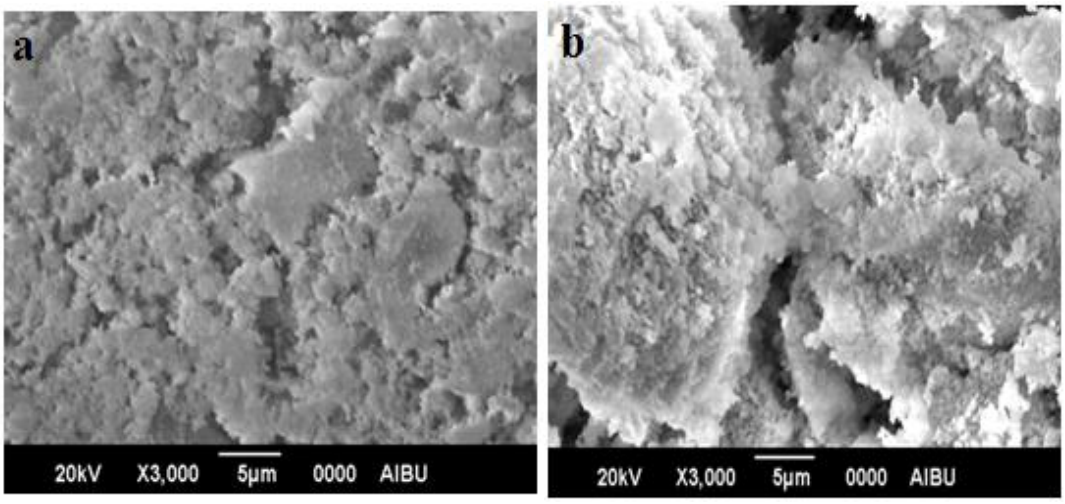

Figure 3.39 SEM images of **a)** $Ni_{2.99}Mn_{0.01}(BO_3)_2$, and **b)** $Ni_{2.90}Mn_{0.10}(BO_3)_2$

The existence of Ni, Mn, B and O elements determined by the EDX analysis of products. The increasing of intensities of peaks attributed to manganese (II) ion is clearly seen in Figures 3.40 to 3.42, when x values increase at formula, $Ni_{(3-x)}Mnx(BO_3)_2$ (x= 0.01, 0.05, 0.10).

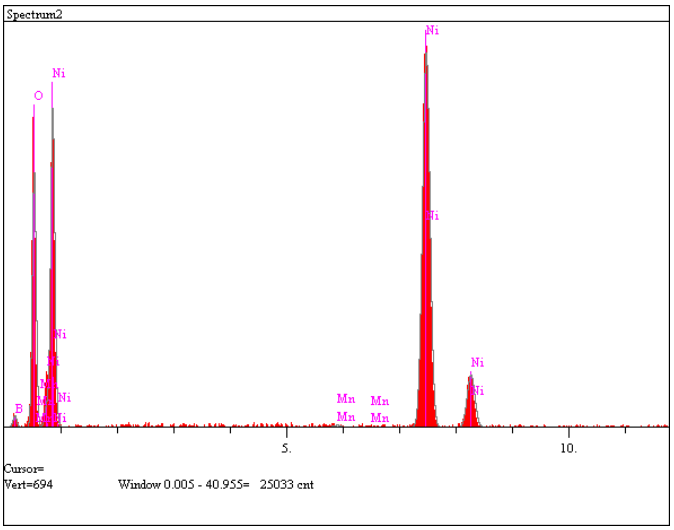

Figure 3.40 EDX Spectrum of $Ni_{2.99}Mn_{0.01}(BO_3)_2$

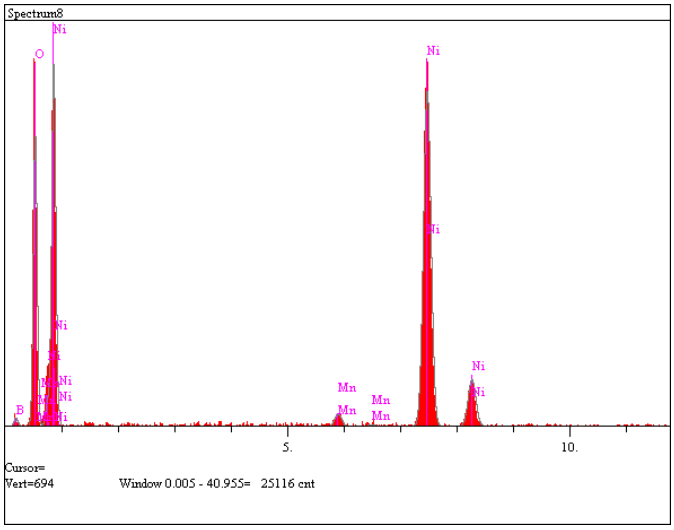

Figure 3.41 EDX Spectrum of $Ni_{2.95}Mn_{0.05}(BO_3)_2$

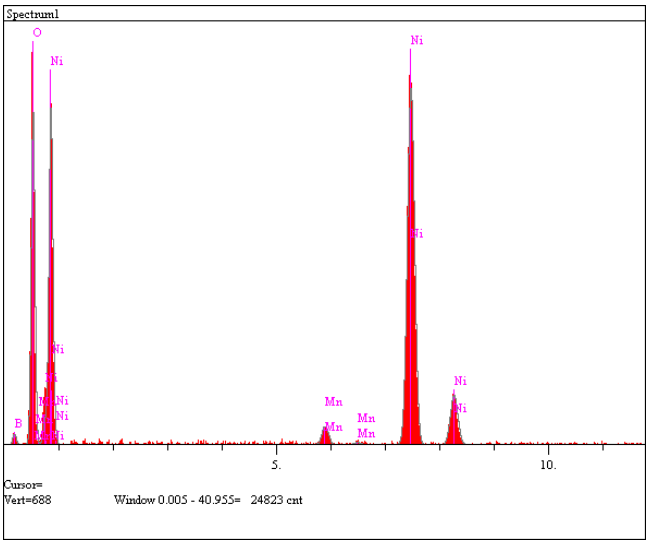

Figure 3.42 EDX Spectrum of $Ni_{2.90}Mn_{0.10}(BO_3)_2$

3.4.4. Thermal Studies (DTA-TG) of $Ni_{3-x}Mn_x(BO_3)_2$ (x = 0, 0.01, 0.05 and 0.10)

The thermal stability of the nickel orthoborate with manganese(II), $Ni_{(3-x)}Mn_x(BO_3)_2$ (x = 0, 0.01, 0.05, and 0.10) was investigated by differential thermal analysis and shown in Figure 3.43 to Figure 3.46, respectively. The DTA analysis indicate that these compounds stabilize as thermal below about 1350^oC to room temperature. In addition to these, as amount of manganase increases, the melting point of products changes. It proves that manganase presences in kotoite type of nickel orthoborate.

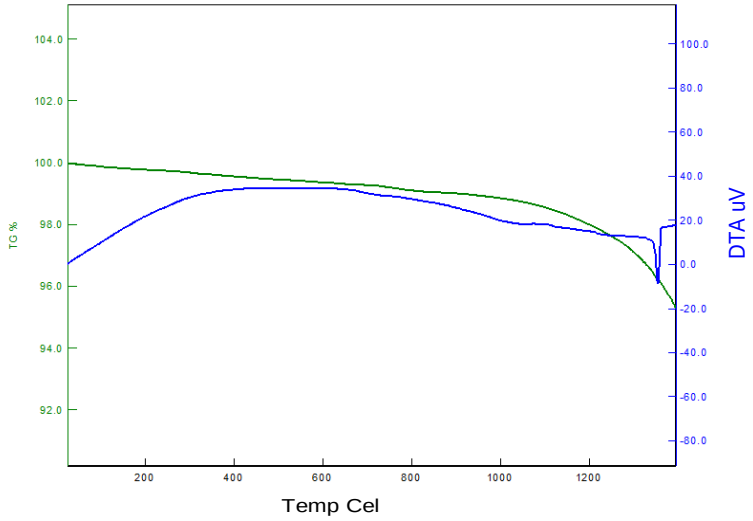

Figure 3.43 DTA/TG of $Ni_3(BO_3)_2$

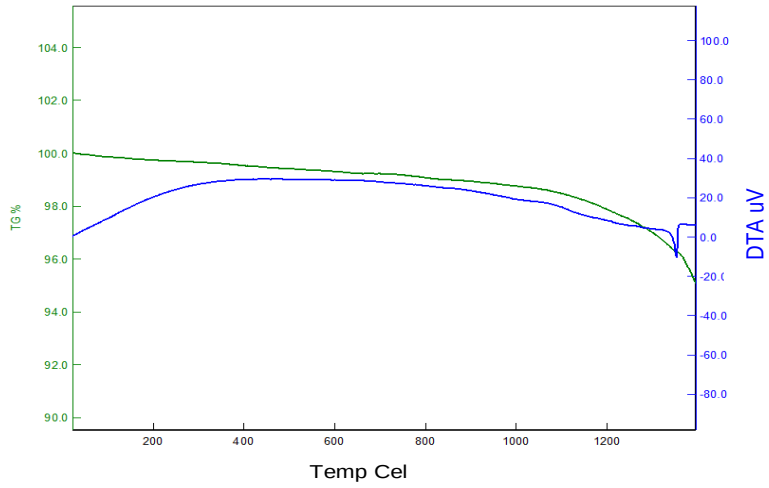

Figure 3.44 DTA/TG of $Ni_{2.99}Mn_{0.01}(BO_3)_2$

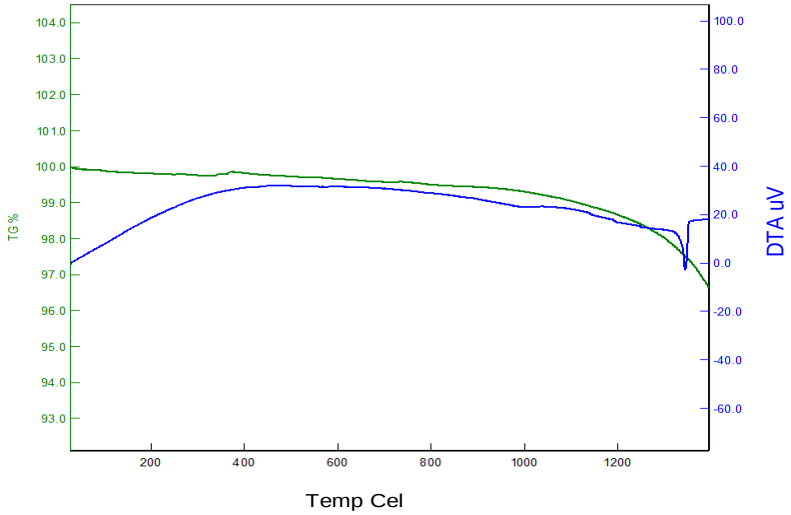

Figure 3.45 DTA/TG of $Ni_{2.95}Mn_{0.05}(BO_3)_2$

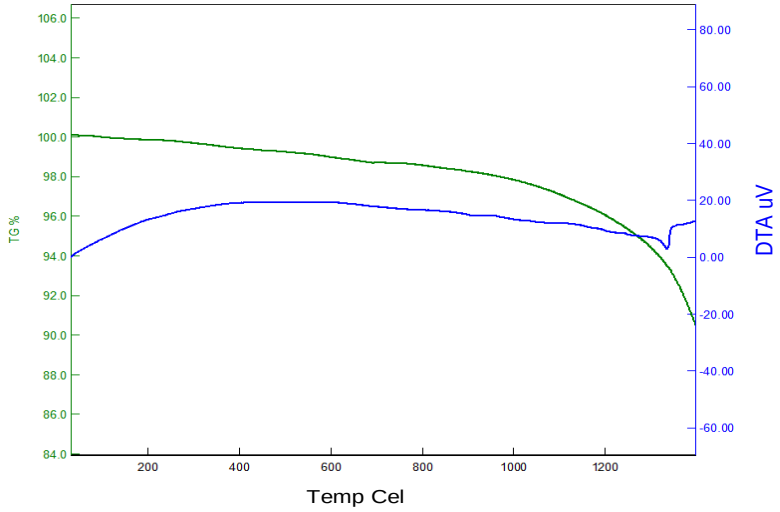

Figure 3.46 DTA/TG of $Ni_{2.90}Mn_{0.10}(BO_3)_2$

CHAPTER 4

GENERAL REVIEW AND CONCLUSION

This work covers firstly the effect of starting materials on the preparation of $Mg_3(BO_3)_2$ and secondly the synthesis of new mixed metal orthoborates $M_{3-x}Mn_x(BO_3)_2$ (M: Mg, Co, and Ni; $0 \leq x \leq 0.10$) via high temperature solid state reactions. Studying of XRD, IR, SEM and TG/DTA of these borates obtained in this thesis led to following conclusions.

In the first part of this study, the effect of starting materials such as MgO, $MgCO_3$ and $MgSO_4$ on synthesis of $Mg_3(BO_3)_2$ was investigated and it was found that very pure magnesium orthoborate was successfully prepared from $MgSO_4$ source through high temperature solid state reactions.

In the second part, Mn^{2+} ion was doped to the kotite type of metal orthoborates to synthesize products, $M_{3-x}Mn_x(BO_3)_2$ (M: Mg, Co, and Ni; $0 \leq x \leq 0.10$), first time by the following reactions;

$$(3-x)MgSO_{4(s)} + xMnSO_4.H_2O_{(s)} + 2H_3BO_{3(s)} \rightarrow Mg_{(3-x)}Mn_x(BO_3)_{2(s)} + 3SO_{2(g)} + (3+x)\,H_2O_{(g)} + 4.5O_{2(g)}$$

(x = 0, 0.01, 0.05, 0.10)

$$(3-x)M(NO_3)_2.6H_2O_{(s)} + xMnSO_4.H_2O_{(s)} + 2H_3BO_{3(s)} \rightarrow M_{(3-x)}Mn_x(BO_3)_{2(s)} + (6-2x)NO_{2(g)} + xSO_{2(g)} + (21-5x)H_2O_{(g)} + 1.5O_{2(g)}$$

(M = Ni, Co; x = 0, 0.01, 0.05, 0.10)

The powder X-ray diffraction studies showed that the synthesized mixed metal orthoborates, $M_{3-x}Mn_x(BO_3)_2$ (M: Mg, Co, and Ni; $0 \leq x \leq 0.10$), were crystallized the orthorhombic crystal system with space group Pnnm given as follows.

- The XRD data of $Mg_{2.99}Mn_{0.01}(BO_3)_2$, $Mg_{2.95}Mn_{0.05}(BO_3)_2$, and $Mg_{2.90}Mn_{0.1}(BO_3)_2$, were indexed and refined with Jana2006. The refined unit cell parameters of these borates were found as a= 5.406(3), b= 8.430(4), c= 4.508(4) Å; a= 5.410(4), b= 8.436(2), c= 4.507(8) Å and a= 5.144(4), b= 8.444(3), c=4.512(0) Å, respectively.
- The refined unit cell parameters of $Co_{2.99}Mn_{0.01}(BO_3)_2$, $Co_{2.95}Mn_{0.05}(BO_3)_2$, and $Co_{2.90}Mn_{0.1}(BO_3)_2$ were calculated as a= 5.469(7), b= 8.451(2), c= 4.533(5) Å; a= 5.469(9), b= 8.452(8), c= 4.533(8) Å and a= 4.483(4), b= 8.476(4), c= 4.538(4) Å, respectively.
- The examination of XRD patterns of $Ni_{2.99}Mn_{0.01}(BO_3)_2$, $Ni_{2.95}Mn_{0.05}(BO_3)_2$, and $Ni_{2.90}Mn_{0.1}(BO_3)_2$ showed that the refined unit cell parameters of a = 5.397(4), b= 8.301(8), c= 4.458(9); a=5.403(6), b= 8.311(6), c= 4.463(3); a=5.404(1), b=8.310(2),c= 4.463(5) and a= 5.405(8),b= 8.313(3), c= 4.465(2) Å, respectively.

The unit cell parameters and hkl values of the magnesium, cobalt and nickel doped with Mn (II) ion are good agreement with kotoite type of $M_3(BO_3)_2$ (M: Mg, Co, and Ni). Therefore, it was concluded that these borates obtained in this work were isomorphous with kotoite type of borates.

The vibrational bands of trigonal planar BO_3 units were clearly observed from the infrared spectra of $Mg_{3-x}Mn_x(BO_3)_2$, $Co_{3-x}Mn_x(BO_3)_2$ and $Ni_{3-x}Mn_x(BO_3)_2$ (x= 0.00, 0.01, 0.05, 0.10) .

The SEM images and surface analysis of the mixed metal orthoborates prepared indicated that these borates have uniform specimens and regularly grained powder.

Crystallite size and volume of magnesium, cobalt and nickel doped with Mn^{2+} ion increased with increasing adding amount Mn(II) ion, whereas their specific surface area decreased. Although these products are structurally and spectroscopically similar to each other, they have different morphologic observations. On the other hand, densities of $Mg_{3-x}Mn_x(BO_3)_2$ increased whereas that of $Co_{3-x}Mn_x(BO_3)_2$ and $Ni_{3-x}Mn_x(BO_3)_2$ decreased with increasing amount of Mn^{2+} ion, (x= 0.00, 0.01, 0.05, 0.10), depending on the order of ionic radii of corresponding metals, Mg > Mn > Co > Ni.

Through TG/DTA method, it was determined that $Mg_{3-x}Mn_x(BO_3)_2$, $Co_{3-x}Mn_x(BO_3)_2$ and $Ni_{3-x}Mn_x(BO_3)_2$ were thermodynamically stable up to 1380, 1170, 1350 ^oC, respectively.

REFERENCES

1. Greenwood, N. N., Earnshaw, A., 1998, Chemistry of The Elements, Butterword Heinemann Pub., Great Bratain.

2. Chatterjee, K. K., 2007, Uses of Metals and Metallic Minerals, New Age International Publishers, New Delhi.

3. Kar, Y., Şen, N., Demirbaş, A., 2006. Boron Minerals in Turkey, Their Application Areas and Importance for the Country's Economy. Minerals & Energy, 3–4, 2–10.

4. Barth, S., 1998. Application of boron isotopes for tracing sources of anthropogenic contamination in ground water. Pergamon, 32, 3, 685-690.

5. Richard, B., 2006, The Elements Boron, Newyork: Marshall Cavendish Benchmark pub., 4-6.

6. Wisniak, J., 2005, Borax, Boric acid, and Boron- From Exotic to Commodity. Indian Journal of Chemical Technology, 12, 488-500.

7. Adair, R., 2007, Understanding the Elements of the Periodic Table: Boron, Rosen Publishing Group, 7-8.

8. Culver, B. D., Smith, R. G., Brotherton, R. J.,Strong, P. .L., Gray, T. M., 1994, Chapter 44:Boron. In: Clayton, G. D., Clayton, F. E. (eds).Patty's industrial hygiene and toxicology, NewYork, John Wiley and Sons, vol 2, part 1.

9. Kıstler R., Helvacı C., Boron and Borates.kisi.deu.edu.tr/cahithelvacı/boron

10. National Boron Research Institute. http://www.boren.gov.tr/en/icerik.php?id=13

11. Roskill, 2006, The Economics of Boron. 11th Edition, Roskill Information Services Ltd., London, England, 516-359.

12. Boron and Borates. http://www.dpi.nsw.gov.au/minerals/geological/industrial-mineral-opportunities.

13. Das, M., Ghatak, S., 2012, Synthesis of boron nitride from boron containing poly(vinyl alcohol) as ceramic precursor. Bulletin of Materials Science, 35,1, 99-102.

14. Şen, İ., Alli, H., Çöl, B., 2012, Boron Contents of Some Wild Growing Mushrooms Collected from the Vicinity of Boron Mines in Balikesir, Turkey. Biological Trace Element Research, 145, 2, 233-239.

15. Kurt R., Mengeloğlu F., 2011, Utilization of boron compounds as synergists with ammonium polyphosphate for flame retardant wood-polymercomposites. Tübitak, 35, 155-163.

16. Soil Fact Sheet, 1991, Boron for Field Crops. British Columbia, Order No. 631.012-1.

17. Sivrikaya, O., Arol, A. İ., 2010, Use of Boron Compounds as Binders in Iron Ore Pelletization. The Open Mineral Processing Journal, 3, 25-35.

18. Blink, J., Farmer, J., Choi, J., and Saw, C., 2009, Applications in the Nuclear Industry for Thermal Spray Amorphous Metal and Ceramic Coatings. Metallurgical and Materials Transactions A, 40, 6, 1344-1354.

19. Gunyaev, G. M., Zhigach, A. F., Perov, B. V., Mitrofanova, E. A., Yartsev, V. A., 1970, Strength of boron fibers. Polymer Mechanics, 6, 6, 988-989

20. Lieberman, S. I., Singh, H., Mao, Y., Sreeranganathan, A., Gokhale, A. M., Tamirisakandala, S., and Miracle, D. B., 2007, The microstructural characterization and simulation of titanium alloys modified with boron. JOM, 59, 1, 59-63.

21. Firlej, L., Kuchta, B., Wexler, C., Pfeifer, P., 2009, Boron substituted graphene: energy landscape for hydrogen adsorption. Adsorption, 15, 3, 312-317.

22. Kabalka, G. W., Tang, C., and Bendel, P., 1997, The role of boron MRI in boron neutron capture therapy. Journal of Neuro-Oncology, 33, 153–161.

23. Firoozjaei, E. A., Koshy, P., Sorrell, C. C., 2012, Effects of Different Boron Compounds on the Corrosion Resistance of Andalusite-Based Low-Cement Castables in Contact with Molten Al Alloy. Metallurgical and Materials Transactions B, 43, 1, 5-13.

24. Önal G., Burat F., 2008, "Boron Mining and Processing in Turkey", World Mining Congress. Poland, pp. 49-59. http://www.minpan.krakow.pl/Wydawnictwa /GSM2443/onal-burat.pdf.

25. Egal, J. E., Trivedi, N. C., Barker, J. M., Krukowski, S. T., 2006, Industrial Minerals & Rocks: Commodities, Markets, and Uses. 7th edition, SME pub., Collerado,USA. Chapter: Boron and Borates, p: 275-283.

26. Bokii, G. B. and Kravchenko, V. B., 1965, Crystal Chemical Classification of Borates. Zhurnal Strukturnoi Khimii, 7, 6, 920-937.

27. Christ, C. L., and Clark, J. R, 1977, A Crystal-Chemical Classification of Borate Structures with Emphasis on Hydrated Borates. Physics and Chemistry of Minerals 2, 59-87.

28. Tekin, B., Güler, H., 2008, synthesis and crystal structure of dicobalt nickel orthoborate, $Co_2Ni(BO_3)_2$. Material Chemistry and Physics, 108, 88-91.

29. Velchuri, R., Kumar, B. V., Devi, V. R., Prasad, G., Prakash, D. J., Vithal, M., 2011, Preparation and characterization of rare earth orthoborates, LnBO3 (Ln = Tb, La, Pr, Nd, Sm, Eu, Gd, Dy, Y) and LaBO3:Gd, Tb, Eu by metathesis reaction: ESR of LaBO3:Gd and luminescence of LaBO3:Tb, Eu. Materials Research Bulletin, 46, 1219–1226.

30. Liu, X., Zhu, W., Cui, X., Liu, T., Zhang, Q., 2012, Facile thermal conversion route synthesis, characterization, and optical properties of rod-like micron nickel borate. Powder Technology, 222, 160–166.

31. Kumari, L., Li, W. Z., Kulkarni, S., Wu, K. H., Chen, W., Wang, C., Vannoy, C. H., Leblanc, R. M., 2010, Effect of Surfactants on the Structure and Morphology of Magnesium Borate Hydroxide Nanowiskers Synthesized by Hydrothermal Route. Nanoscale Res Lett, 5, 149-157.

32. Kusachi, I., Henmi, C., Kobayashi, S., 1995, Takedaite, a new mineral from Fuka, Okayama Prefecture, Japan. Mineralogical Magazine, 59, 549-552.

33. Berger, S. V., 1949, The Crystal Structure Of Isomorphous Orthoborates of Cobalt and Magnesium. Acta Chemica Scandinavica, 3, 660-675.

34. 2001-2005 Mineral Data Publishing, http://www.mindat.orgmin-2262.html

35. Frost, R. L., and Xi, Y. 2012**,** Vibrational spectroscopy of the borate mineral kotoite $Mg_3(BO_3)_2$, Spectrochimica Acta Part A: Molecular and Biomolecular Spectroscopy, 1386-1425 (12) 01127-4.

36. Stewart, D. A., 2009, Oxide layer boron leads to reduced symmetry spin filtering magnetic tunnel junctions. arXiv:0904.4475v1 [cond-mat.mtrl-sci].

37. Zhang, J., Li, Z., and Zhang, B., 2006, Formation and structure of single crystalline magnesium borate ($Mg_3B_2O_6$) nanobelts. Materials Chemistry and Physics, 98, 195–197.

38. Güller, H., Kurtuluş, F., Ay, E., Çelik, G., Doğan, İ., 2009, Solid-State and Microwave-Assisted Synthesis and Characterization of $Mg_2B_2O_5$ and $Mg_3(BO_3)_2$. IV. International Boron Symposium, Eskşehir-Turkey.

39. Doŝler, U., Kržmanc, M. M., and Suvorov, D., 2010, The synthesis and microwave dielectric properties of $Mg_3B_2O_6$ and $Mg_2B_2O_5$ ceramics. Journal of the European Ceramic Society, 30, 413–418.

40. Ağaoğulları, D., Balcı, Ö., Gökçe, H., Duman, İ., Öveçoğlu, M. L., 2012, Synthesis of Magnesium Borates by Mechanically Activated Annealing. Metallurgical and Materials Transactions A-Phsical Metallurgy and Materials Science, 43A**,** 7**,** 2520-2533.

41. Sadanaga, R., Nishimura T., and Watanabe, T., 1965, The Structure of Jimboite, $Mn_3(BO_3)_2$ and Relationship with the Structure of Kotoite. Mineral Journal, 4, 5, 380-388.

42. Pardo, J., Martinez-Ripoll, M. And Garcia-Blanco, S., 1974, The Crystal Structure Of Nickel Orthoborate, $Ni_3(BO_3)_2$. Acta Cryst. B, 30-37.

43. Effenberger, H., and Pertlik, F., 1984,Verfeinerung der Kristallstrukturen der isotypen Verbindungen M3(B03h mit M=Mg, Co und Ni (Strukturtyp : Kotoit), Zeitschrift für Kristallographie, 166, 129-140.

44. Menaka, Lofland, S. E., Ramanujachary, K. V., Ganguli, A. K., 2010, A new low temperature methodology to obtain pure nanocrystalline nickel borate. Journal of Organometallic Chemistry, 695, 1002–1005.

45. Menaka, Sharma, S., Ramanujachary, K. V., Lofland, S. E., Ganguli, A. K., 2011, Controlling the size and morphology of anisotropic nanostructures of nickel borate using microemulsions and their magnetic properties. Journal of Colloid and Interface Science, 360, 393–397.

46. Chen, A. M., Hu, F. C., Gu, P., Ni, Z. M., 2011, Sol-gel Synthesis, Characterization of Nickel Borate Nanorods, Chinese Journal of Inorganic Chemistry, 27, 1, 30-34.

47. Smith, R. W., and Keszler, D. A., 1989, Syntheses and crystal structures of the α- and β-forms of the orthoborate $Sr_2Cu(BO_3)_2$, Journal of Solid State Chemistry, 81, 2, 305–313.

48. Smith, R. W., and Keszler, D. A., 1991, Synthesis, structure, and properties of the orthoborate $SrCu_2(BO_3)_2$. Journal of Solid State Chemistry, 93, 2, 430–435.

49. Smith, R. W., and Keszler, D. A., 1992, The noncentrosymmetric orthoborate $BaZn_2(BO_3)_2$, Journal of Solid State Chemistry, 100, 2, 325–330.

50. Smith, R. W. and Koliha, L. J., 1994, A new noncentrosymmetric orthoborate $[Ba_2Zn(BO_3)_2]$. Materials Research Bulletin. 29, 11, 1203–1210.

51. Utzolino, A., Bluhm, K., 1996, Synthesis and crystal structure of manganese containing pyroborates: $MnCo(B_2O_5)$ and $MnMg(B_2O_5)$. Zeıtschrıft fur Naturforschung Section B-A Journal of Chemical Scıences, 51, 7, 912-916.

52. Fernandes, J. C., Guimaraes, R. B., Continentino, M. A., Rapp, R., Tholence, J. L., Dumas, J., Blancquaert, Y., Yates, S., Paulsen, C., 2004, Low-temperature properties and ESR in the quasi-one-dimensional random compound $MnMgB_2O_5$. Physical Review B, 69, 5, 054418.

53. Pan, S., Smit, J. P., Marvel, M. R., Stern, C. L., Watkins, B., Poeppelmeier, K. R., 2006, Synthesis, structure and properties of $Pb_2CuB_2O_6$. Materials Research Bulletin, 41, 916–924.

54. Güler, H., and Tekin, B., 2009, Synthesis and Crystal Structure $CoNi_2(BO_3)_2$. Inorganic Materials, 45, 5, 538–542.

55. Zhang, M., Pan, S., Han, J., Yang, Y., Cui, L., and Zhou, Z., 2011, Growth, crystal structure and optical properties of layered dibarium cadmium diborate, $Ba_2Cd(BO_3)_2$. Journal of Alloys and Compounds, 509, 6696–6699.

56. Ardiçoğlu, B., Özbayoğlu, G., Özdemir, Z., and Yılmaz, A., 2006, production and identification of rare-earth doped lithium triborate. Journal of Alloys and Compounds, 418, 77-79.

57. Akella, A., and Keszler, D. A., 1995, Structure and Eu3+ Luminescence of Dibarium Magnesium Orthoborate. Materials Research Bulletin, 30, 1, 105-111.

58. Liu, L. Y., Zhang, Y. L., Hao, J. Q., Li, C. Y., Tang, Q., Zhang, C. X., Su, Q., 2006, Thermoluminescence studies of rare earth doped $Sr_2Mg(BO_3)_2$ phosphor. Materials Letters, 60, 639–642.

59. Wang, H., Jia, G., Wang, Y., You, Z., Li, J., Zhu, Z., Yang, F., Wei, Y., Tu, C., 2007, Crystal growth and spectral properties of pure and Co^{2+}doped $Mg_3B_2O_6$ crystal. Optical Materials, 29, 1635–1639.

60. Yao, S., Xue, L., Yan, Y., 2011, Concentration quenching of Eu^{2+} in $Ba_2Mg(BO_3)_2$: Eu2+ phosphor. Current Applied Physics, 11, 639-642.

61. Zhang, X., 2011, Thermally stable luminescence and energy transfer in Ce^{3+}, Mn^{2+} doped $Sr_2Mg(BO_3)_2$ phosphor. Optical Materials, 33, 1704–1709.

62. Lin, H., Liang, H., Tian, Z., Han, B., Wang, J., Su, Q., and Zhang, G., 2009, Luminescence of $Ba_2Ca(BO_3)_2$:Ce^{3+} influence of charge compensator, energy transfer and LED application. Journal of Physics D: Applied Physics, 42, 165409, 9.

63. Lin, H., Liang, H., Zhang, G., Su, Q., 2011, The luminescence of Eu3+ activated $Ba_2Mg(BO_3)_2$ phosphors. Applied Physics A, 105, 143–147.

64. Zhang, X., Fei, L., Shi, J., Gong, M., 2011, Eu^{2+} activated $Ba_2Mg(BO_3)_2$ yellow-emitting phosphorsfor near ultraviolet basedlight emitting diodes. Physica B, 406, 2616–2620.

65. Lin, H. H., Liang, H. B., Su, Q., Zhang, G. B., Luminescence of $Sr_2Mg(BO_3)_2:Tb^{3+}$ under Vacuum Ultraviolet Excitation. Spectroscopy and Spectral Analysis, 31, 7, 1743-1746.

66. Liang, H., Lin, H., Zhang, G., Dorenbos, P., Su, Q., 2011, Luminescence of Ce^{3+} and Pr^{3+} doped $Sr_2Mg(BO_3)_2$ under VUV–UV and X-ray excitation. Journal of Luminescence 131, 194–198.

67. Lin, H., Liang, H., Zhang, G., Tao, Y., 2012, A comparison of Ce^{3+} luminescence in $X_2Z(BO_3)_2$ (X=Ba, Sr; Z=Ca, Mg) with relevant composition and structure. Journal of Rare Earths, 30, 1, 1.

68. Anantharamulu, N., Kumar, B. V., Devi, V. R., Sarojini, T., Anjaneyulu, C. H., and Vithal, M., 2009, Preparation and characterization studies of metaborates, $Cu_{1-x}M_xB_2O_4$ (M = Ni, Co and Mn; x = 0, 0.1 and 0.5). Bull. Mater. Sci., 32, 4, 421–430.

69. Kawano, T., Suehiro, T., Sato, T., Yamane, H., 2010, Preparation, crystal structure and photoluminescence of Mn^{2+} -doped magnesium pyroborates solidsolutions, $(Mg_{1-x}Mn_x)_2B_2O_5$. Journal of Luminescence, 130, 2161–2165.

70. Yamane, H., Kawanoa, T., Fukudab, K., Suehiroa, T., Sato, T., 2012, Preparation, crystal structure and photoluminescence of lithium magnesium manganese borate solid solutions, $LiMg1{-}xMnxBO_3$. Journal of Alloys and Compounds, 512, 223– 229.

71. Rahaman, M. N., 2003, Ceramic Processing and Sintering. 2nd edution, CRC press, USA. Chapter 2, 61-92.

72. West, R. A., 1990, Solid State Chemistry and Its Applications. 5th edution, John Willey & Sons press, USA. Chapter 2, p.5,6.

73. Rao, C. N. R., Gopalakrishnan, J., 1997, New Directions in Solid State Chemistry. 2nd edution, Cambridge University press, USA. Chapter 3, p.125.

74. Smart, L. E., Moore, E. A., 2005, Solid State Chemistry, 3th edution, CRC press Taylor & Francis Group, England. Chapther 3, p. 148-152.

75. Segal, D., 1997, Chemical synthesis of ceramic materials. http://pubs.rsc.org | doi:10.1039/A700881C

76. Capelle, R., 1961, Spectrophotometry Determination of Boron with an Azomethine H Derivative. Anal. Chim. Acta., 24, 555–572.

77. Zaijun, L., Yuling, Y., Jiaomai, P., and Jan, T., 2001, 1-(2- hydroxy-3-methoxybenzylideneamino)-8 hydroxynaphthalene- 3,6 Disulfonic Acid as a Reagent for the Spectrophotometric Determination of Boron in Ceramic Materials. The Analyst., 126, 1160–1163.

78. Akhamanova, M. V., 1961, Investigation of The Structure of Native Borates by Infrared Absorption Spectroscopy. Zhurnal Strukturnoi Khimii, 3, 1, 28-34.

79. Ternane, R., Cohen-Adad, M. T., Panczer, G., Goutaudier, C., Kbir-Ariguib, N., Trabelsi-Ayedi, M., Florian, P., and Massiot, D., 2002, Introduction of boron in hydroxyapatite: synthesis and structural characterization. Journal of Alloys and Compounds, 333, 62–71.

80. Lakshminarayana, G., and Buddhudu, S., 2005, Spectral analysis of Cu^{2+}: B_2O_3–ZnO–PbO glasses. Spectrochimica Acta Part A, 62, 364–371.

81. Tukia, M., Hölsä, J., Lastusaari, M., Niittykoski, J., 2005, Eu^{3+} doped rare earth orthoborates, RBO_3 (R = Y, La and Gd), obtained by combustion synthesis. Optical Materials, 27, 1516–1522.

82. Chen, X., Yin, H., Chang, X., Zang, H., Xiao, W., 2010, Synthesis, crystalstructure,spectrumproperties,andelectronicstructureof a novelnon - centro symmetric borate, $BiCd_3(AlO)_3(BO_3)_4$. Journal of Solid State Chemistry, 183, 2910–2916.

83. Altuntas Öztas, N., and Erdoğan, H., 2009, Synthesis and Characterization of Magnesium Pyroborate by Solution Combustion and Conventional Ceramic Methods: A Comparative Study. Z. Anorg. Allg. Chem., 1626–1632, DOI: 10.1002/zaac.200900026

84. Üçyıldız, A., Girgin, İ., 2010, Controlled synthesis, characterization and thermal properties of $Mg_2B_2O_5$. Central European Journal of Chemistry, 8, 4, 758–765.

85. Shannon, R., D., 1976, Revised Effective Ionic Radii and Systematic Studies of Interatomie Distances in Halides and Chaleogenides. Acta Cryst., A32, 751-767.